2008-07-28

Predicting the Response of Powder Metallurgy Steel Components to Heat Treatment.

Virendra S. Warke
Worcester Polytechnic Institute

Predicting the Response of Powder Metallurgy Steel Components to Heat Treatment

by

Virendra S. Warke

A thesis

Submitted to the faculty of the

Worcester Polytechnic Institute

in partial fulfillment of the requirements for the degree of

Doctor of Philosophy

in

Materials Science and Engineering

July 2008

Professor M.M. Makhlouf, Advisor
Director, Advanced Casting Research Center

Professor R.D. Sisson, Jr., Co-Advisor
Director and Head of Manufacturing and Materials Engineering Program

ABSTRACT

The goal of heat treating manufactured steel components is to enhance the characteristics of the metal so that the components meet pre-specified quality assurance criteria. However, the heat treatment process often creates considerable distortion, dimensional change, and residual stresses in the components. These are caused mainly by thermal stresses generated by a non-uniform temperature distribution in the part, and/or by transformation stresses due to the volume mismatch between the parent phase and product phases that may form by phase transformation. With the increasing demand for tighter dimensional tolerances and better mechanical properties from heat treated components, it is important for the manufacturer to be able to predict the ability of a component to be heat treated to a desired hardness and strength without undergoing cracking, distortion, and excessive dimensional change. Several commercial softwares are available to accurately predict the heat treatment response of wrought steel components. However, these softwares cannot be used to predict the heat treatment response of steel components that are made by powder metallurgy (PM) processes since these components generally contain pores which affect the mechanical, thermal, and transformation behavior of the material. Accordingly, the primary objective of this research is to adapt commercially available simulation software, namely DANTE, so that it can accurately predict the response of PM steel components to heat treatment. Additional objectives of the research are to characterize the effect of porosity on (1) the mechanical properties, (2) the heat transfer characteristics, and (3) the kinetics of phase transformation during heat treatment of PM steels.

ACKNOWLEDGMENTS

I am profoundly grateful to my advisor, Prof. Makhlouf M. Makhlouf, for his energetic support and encouragement, and his valuable guidance and day to day advice throughout this research project. I would also like to express my appreciation to him for providing me the opportunity to carry out this research work.

I would like to extend my deepest gratitude to my co-advisor, Prof. Richard D. Sisson, Jr., for his valuable advice and guidance throughout this research program. I would also like to specially thank Prof. Diran Apelian, Dr. Lynn Ferguson, Prof. Mohammed Maniruzzaman, and Dr. Stephen Mashl for their valuable support and for being part of my PhD dissertation committee.

I would like to thank the Boorkey family for providing me with financial support through the Morris Boorkey fellowship. I would like to gratefully acknowledge all the member companies of the Powder Metallurgy Research Center of the Metal Processing Institute at WPI for the financial support and help during this research work, Deformation Control Technology Inc., Cleveland OH, for their assistance on data analysis, High Temperature Materials Laboratory at Oak Ridge National Laboratory, Oak Ridge TN, for their assistance during dilatometry testing, Welding Engineering Department at The Ohio State University, Columbus OH, for providing their facility for mechanical testing, and PANalytical Inc., Natick MA, for assisting with XRD measurements.

I am also grateful to my colleagues and friends in the Materials Science and Engineering Department and the Metal Processing Institute, who made my academic journey memorable, and enjoyable.

Last, but not least, I simply could not have come this far without love, understanding, patience, and inspiration from my wife, Paurnima, and my parents, Sitaram and Sunita.

TABLE OF CONTENTS

CHAPTER 1

INTRODUCTION

BACKGROUND

Powder metallurgy (PM) components experience considerable change during heat treatment including changes in their mechanical properties, dimensions, magnitude and sense of residual stresses, and metallurgical phase composition. Since the quality assurance criteria that heat-treated PM components must meet include prescribed minimum mechanical properties and compliance with dimensional tolerances, it is necessary for heat treaters to be able to accurately predict these changes in order to take appropriate measures to prevent their harmful effects and insure the production of good quality parts. Satisfactory response to heat treatment is often gauged by the ability of the component to be heat-treated to a desired microstructure, hardness, and strength level without undergoing cracking, distortion, or excessive dimensional changes.

In addition to reversible changes that are caused by thermal expansion and contraction, metallic components experience permanent dimensional changes during heat treatment. These permanent changes can be broadly classified into two groups based on their origin. These groups are: (1) Dimensional changes with mechanical origins, which include dimensional changes caused by stresses developed by external forces, dimensional changes that arise from thermally induced stresses, and dimensional changes that are caused by relaxation of residual stresses. (2) Dimensional changes with metallurgical origins, which include dimensional changes that are caused by recrystallization, solution and precipitation of alloying elements, and phase transformations.

Residual stresses often adversely affect the mechanical properties of PM components. They are caused by thermal gradients in the parts during quenching and depend on the cooling rates, section thickness, and material strength. Decreasing the severity of the quench results in a lower level of residual stresses but with a correspondingly decrease in the strength of heat-treated materials. Residual stresses may also arise from phase transformations during heat treatment that result from volumetric changes inherently associated with the crystal structure of parent and product phases during the phase transformations in the material [1].

Several software packages that are capable of predicting the response of wrought steels to heat treatment are available commercially. These include HEARTS [1], TRAST [2], SYSWELD [3], and DANTE [4]. In this work, a finite element-based model and the necessary database to predict the response of powder metallurgy steels to heat treatment are presented and discussed. The model is based on a modification of the commercially available software DANTE* coupled to the finite element analysis software ABAQUS†. The model requires an extensive database, which includes temperature and porosity dependent phase transformation kinetics, and temperature and porosity dependent phase-specific mechanical, physical, and thermal properties of the steel. This data was developed for FL-4605 PM steel and is used in the model to predict dimensional change, distortion, residual stresses, and type and quantity of metallurgical phases present in the microstructure of a typical PM component after the component is subjected to a specified heat treatment schedule. Finally, these characteristics were measured for a commercially produced FL-4605 PM steel component and compared to their model-predicted counterparts.

DANTE is comprised of a set of user-defined subroutines that are linked to the finite element solver ABAQUS-standard. The DANTE subroutines contain a mechanics subroutine and

* DANTE is marketed by Deformation Control Technology, Inc., Ohio, USA.
† ABAQUS is marketed by Simulia, Inc., Rhode Island, USA.

database, a phase transformation subroutine and database, and a mass diffusion subroutine and database that are coupled to a stress/displacement solver, a thermal solver, and a mass diffusion solver, respectively. This modeling approach is schematically shown in Figure 1.

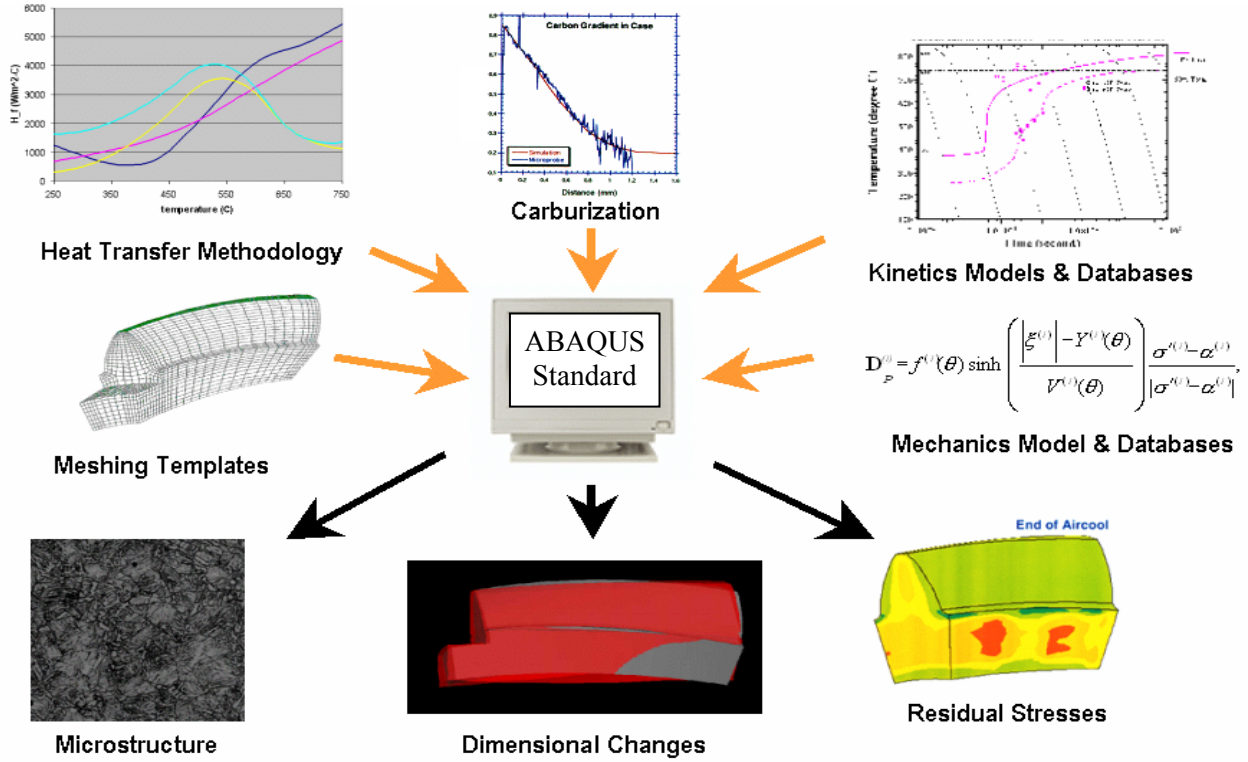

Figure 1: Structure of the DANTE- ABAQUS model.

The phase transformation subroutine is based on an internal state variable framework in which the volume fraction of metallurgical phases is tracked with changing time and temperature. In this subroutine, formation of ferrite, pearlite, and bainite is assumed to follow diffusive transformation kinetics. The martensitic transformation is assumed to be athermal; however, the kinetics equations, which are written in the form of rate equations, have an explicit dependency on cooling rate [6]. Material data for the phase transformation kinetics subroutine is derived

from heating and cooling dilatometer measurements on specimens with three significantly different levels of porosity. The details of the mathematical model and the procedures used to obtain the model parameters for the phase transformation kinetics of each phase at the three levels of porosity are presented in detail in Appendix A.

The mechanics subroutine is based on internal state variables and describes the mechanical behavior of each metallurgical phase over a wide range of temperature, extent of deformation, and deformation rate. The mechanics subroutine can reflect the effect of phase transformations as well as transformation-induced plasticity in the various metallurgical phases during heat-treating [5]. In this research, extensive testing was performed in order to characterize the porosity dependent mechanics and transformation plasticity parameters for FL-4605 PM steel. Material data for the mechanics subroutine was obtained from temperature and rate-dependent tension and compression measurements on specimens with the three levels of porosity. The details of the mathematical model and the procedures used to obtain the model parameters for the mechanics model and transformation plasticity model are presented in detail in Appendix B and Appendix C, respectively.

Thermal boundary conditions, i.e. heat transfer coefficients as a function of temperature for different porosity levels were obtained by quenching CHTE probes [8] made from FL-4605 PM steel. The other necessary thermal properties of FL-4605 PM steel, such as its thermal conductivity and heat capacity were obtained from the available literature and were implemented in the subroutines as functions of temperature and porosity [7]. The procedure used to obtain the heat transfer coefficient is presented in detail in Appendix D.

The effect of porosity on the various mechanical and thermal properties of the material was accounted for in the model by datasets that include mechanical and thermal properties, and

phase transformation characteristics of the alloy at each porosity level and interpolating these parameters at the node level.

A block diagram of the combined DANTE/ABAQUS model is shown in Figure 2. It consists of a geometry and mesh generators, a post processor, the thermal subroutine, and the mechanics subroutine. The thermal subroutine is setup to solve the heat transfer problem for each one of the steps of the heat-treating process, i.e., the furnace heating step, the immersion into the quench tank step, and the quenching step. The output file generated by the thermal subroutine contains the thermal history of the part during the various process steps. The mechanics subroutine accesses this output file and calculates the residual stresses, the displacements, the volume fraction of metallurgical phases, and the hardness of the material for the entire temperature history of the part.

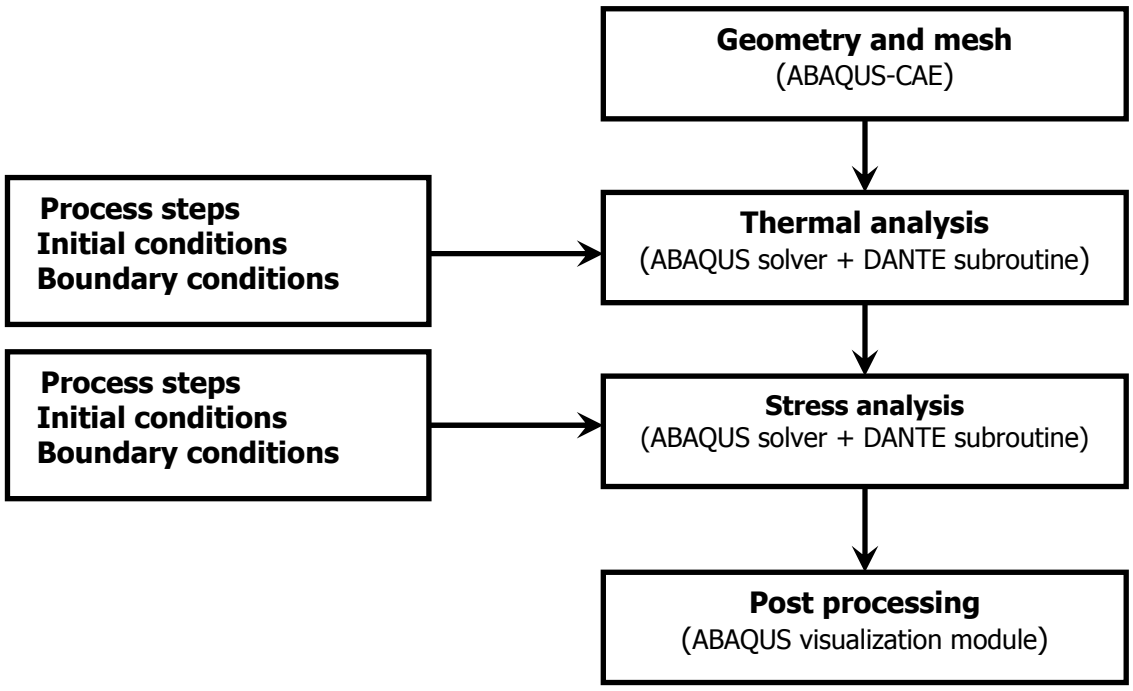

Figure 2: Solution procedure for the DANTE/ABAQUS combined model.

RESEARCH OBJECTIVES

The primary objective of this research is to adapt the commercially available simulation software DANTE so that it can accurately predict the response of PM steel components to heat treatment. Simulations with the modified model should accurately predict dimensional changes and distortion, residual stresses, type and quantity of metallurgical phases in the microstructure, and the hardness of PM steel components upon heat treatment.

Additional objectives of the research are to characterize the effect of porosity on

(1) The mechanical properties,

(2) The heat transfer characteristics, and

(3) The kinetics of phase transformation during heat treatment of PM steels.

THESIS ORGANIZATION

The remainder of this document is a series of manuscripts to be submitted to various journals each representing a chapter of the dissertation as follows:

Chapter II contains a journal article titled “A Model for Predicting the Response of Powder Metallurgy Steel Components to Heat Treatment”.

Chapter III contains a journal article titled “The Effect of Porosity on the Austenite to Ferrite Transformation in Powder Metallurgy Steels”.

Chapter IV contains a journal article titled “The Effect of Porosity on the Austenite to Bainite Transformation in Powder Metallurgy Steels”.

Chapter V contains a journal article titled “A Model for Converting Dilatometric Strain Measurements to the Fraction of Phase Formed during the Transformation of Austenite to Martensite in Powder Metallurgy Steels”.

Chapter VI contains a journal article titled “Effect of Porosity on the Quenching Heat Transfer Characteristics of Powder Metallurgy Steels”.

The measurement procedures, for determining the phase transformation kinetics, the phase specific - temperature and porosity dependent mechanical properties, the transformation induced plasticity, and the quenching heat transfer coefficient of PM steels are presented in Appendixes A, B, C, and D, respectively.

REFERENCES

1. Inoue T. and Arimoto K, *Quenching and Distortion Control Conference Proceedings*, ASM International, 1992, pp. 205-212.
2. Jarvstrat N., and Sjostrom S., *ABAQUS Users' Conference Proceedings*, 1993, pp. 273-287.
3. Southwest Research Institute and Farmatome, *Presentation at the National Center for Manufacturing Sciences*, April 14, 1992.
4. Dowling W., *Second International Conference on Quenching and Control of Distortion*, 1996, pp. 367-375.
5. Bammann D.J., Chiesa M.L., and Johnson G.C., *Proceedings of the Nineteenth International Congress on Theoretical and Applied Mechanics,* 1996, pp. 359-376.
6. Lusk M.T. , and Lee Y.K., *Proceedings of the Seventh International Seminar on Heat Treatment and Surface Engineering of Light Alloys,* 1999, pp. 273-282.
7. Ferguson B.L., Petrus G.J., and Pattok T., *Proceedings of the Third International Conference on Quenching and Control of Distortion*, 1999, pp. 188-200.
8. Maniruzzaman M., Chaves C., McGee C., Ma S., and Sisson, Jr. R. D., Proceedings of the Fifth International Conference on Frontiers of Design and Manufacturing (ICFDM 2002), Vol. 1, 2002, pp. 619-625.

Chapter 2

A Model for Predicting the Response of Powder Metallurgy Steel Components to Heat Treatment

Virendra S. Warke, Richard D. Sisson Jr., and Makhlouf M. Makhlouf

ABSTRACT

A model and the necessary database for predicting the response of powder metallurgy steels to heat treatment are presented and discussed. The model is based on a modification of the commercially available software DANTE coupled to the finite element analysis software ABAQUS. The model requires an extensive database that includes temperature and porosity-dependent phase transformation kinetics, and temperature and porosity-dependent phase-specific mechanical, physical, and thermal properties of the steel. This data is developed for FL-4065 PM alloy and is used in the model to predict dimensional change, distortion, residual stresses, and type and quantity of metallurgical phases present in the microstructure of a typical PM component after the component is subjected to a specified heat treatment schedule. The model predictions are found to be in very good agreement with measured values.

2.1 INTRODUCTION

Powder metallurgy (PM) components experience considerable changes during heat treatment that include changes in their mechanical properties, dimensions, magnitude and sense of residual stresses, and metallurgical phase composition. Since the quality assurance criteria that heat-treated PM components must meet include prescribed minimum mechanical properties and compliance with dimensional tolerances, it is necessary for PM producers to be able to

accurately predict these changes in order to take appropriate measures to prevent their harmful effects and insure the production of good quality parts. Satisfactory response to heat treatment is often gauged by the ability of the component to be heat-treated to a desired microstructure, and hardness and strength levels without undergoing cracking, distortion, or excessive dimensional changes.

In addition to reversible changes that are caused by thermal expansion and contraction, metallic components experience permanent dimensional changes during heat treatment. These permanent changes can be broadly classified into three groups based on their origin. These groups are: (1) Dimensional changes with mechanical origins, which include dimensional changes caused by stresses developed by external forces, dimensional changes that arise from thermally induced stresses, and dimensional changes that are caused by relaxation of residual stresses. (2) Dimensional changes with metallurgical origins, which include dimensional changes that are caused by recrystallization, solution and precipitation of alloying elements, and phase transformations.

Several software packages that are capable of predicting the response of wrought steels to heat treatment are commercially available. These include HEARTS [1], TRAST [2], SYSWELD [3], and DANTE [4]. In this work, a finite element-based model and the necessary database to predict the response of powder metallurgy steels to heat treatment are presented and discussed. The model is based on a modification of the commercially available software DANTE[*] coupled to the finite element analysis software ABAQUS[†]. The model requires an extensive database, which includes temperature and porosity dependent phase transformation kinetics, and temperature and porosity dependent phase-specific mechanical, physical, and thermal properties of the steel. This

[*] DANTE is marketed by Deformation Control Technology, Inc., Ohio, USA.
[†] ABAQUS is marketed by Simulia, Inc., Rhode Island, USA.

data is developed for FL-4605 PM steel and is used in the model to predict dimensional change, distortion, residual stresses, and type and quantity of metallurgical phases present in the microstructure of a typical PM component after the component is subjected to a specified heat treatment schedule. Finally, these characteristics were measured for the commercially produced FL-4605 PM steel component and compared to their model-predicted counterparts.

2.2 BACKGROUND

DANTE is comprised of a set of user-defined subroutines and can be linked to the finite element solver ABAQUS-standard. The DANTE subroutines contain a mechanics module, a phase transformation module, and a diffusion module that are coupled to a stress/displacement solver, a thermal solver, and a mass diffusion solver, respectively.

The mechanics module is based on internal state variables and describes the mechanical behavior of each metallurgical phase over a wide range of temperature, extent of deformation, and deformation rate. The mechanics module can reflect the effect of phase transformations as well as transformation-induced plasticity in the various metallurgical phases during heat-treating on the component's response to heat treatment [5].

The phase transformation module is also based on an internal state variable framework in which the volume fraction of metallurgical phases is tracked with changing time and temperature. In this module, formation of ferrite, pearlite, and bainite is assumed to follow diffusive transformation kinetics. The martensitic transformation is assumed to be athermal; however, the kinetics equations, which are written in the form of rate equations, have an explicit dependency on cooling rate [6].

Material data for the mechanics module is obtained from temperature and rate-dependent tension and compression measurements, and data for the phase transformation module is derived from heating and cooling dilatometry measurements. Other mechanical and thermal properties of the material are extracted from the available literature and are implemented in the modules as functions of temperature [7]. The effect of porosity on the various mechanical and thermal properties of the material is accounted for by introducing the relative density of the part as a state variable in the various subroutines. The effect of porosity on the various mechanical and thermal properties of the material is accounted for by introducing datasets representing mechanical, thermal, and phase transformation of the alloy at each level of the density and interpolating the these properties for intermediate range of densities.

A block diagram of the combined DANTE/ABAQUS model is shown in Figure1. It consists of a geometry and mesh generators, a post processor, the thermal module, and the mechanics module. The thermal module is setup to solve a heat transfer problem for each one of the steps of the heat-treating process, i.e., the furnace heating step, the immersion into the quench tank step, and the quenching step. The output file generated by the thermal module contains the thermal history of the part during the various process steps. The mechanics module accesses this output file and calculates the residual stresses, the displacements, the volume fraction of metallurgical phases, and the hardness for the entire temperature history of the part.

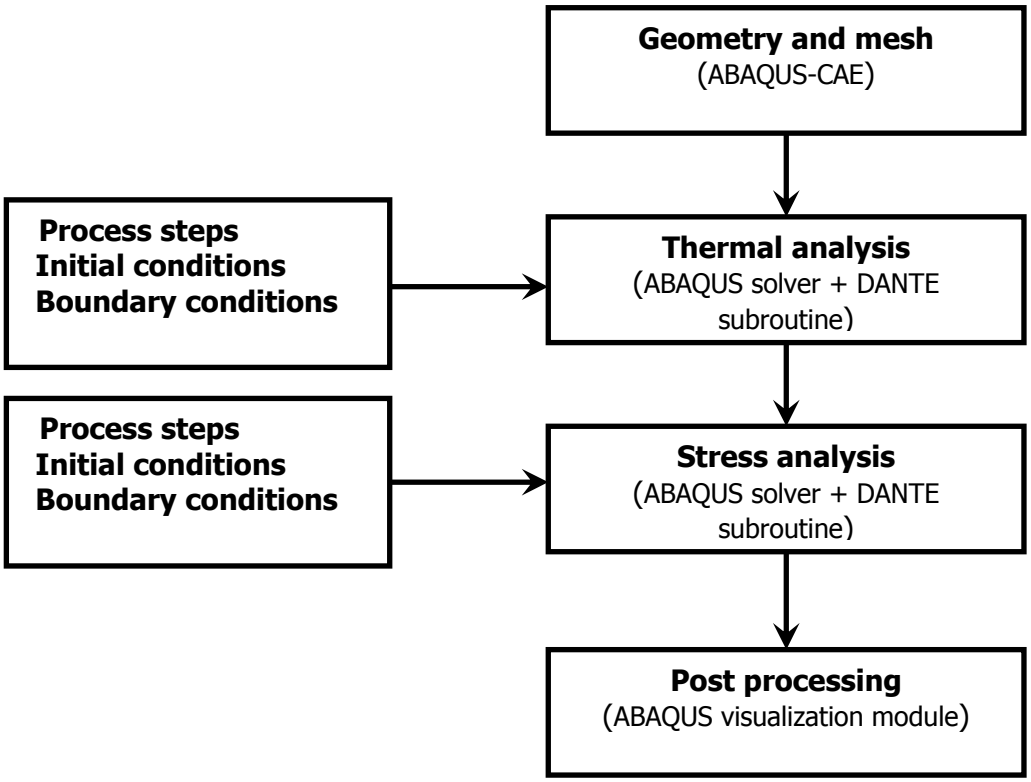

Figure 1: Solution procedure for the DANTE/ABAQUS combined model.

2.3 DATABASE GENERATION - PROCEDURES AND MEASUREMENTS

Production of the Bulk Material

AUTOMET 4601 steel powder* was admixed with powdered graphite to yield 0.5 wt. pct. carbon in the final product. Table I shows the chemical composition of the resultant powder.

Table I: Composition of the alloy (in wt.%) powder after admix of Graphite powder

Carbon	Oxygen	Sulfur	Manganese	Molybdenum	Nickel	Iron
0.5	0.11	0.0093	0.196	0.549	1.812	Remainder

* AUTOMET 4601 steel powder is manufactured by Quebec Metal Powders, Ltd., Quebec, Canada.

Bulk material was produced from this powder in three different densities corresponding to 90%, 95%, and 100% of theoretical density. In order to produce the 90% dense material, the powder was cold-compacted using 690 MPa pressure in a hydraulic press to produce green compacts that were then sintered at 1120°C for 30 minutes under a controlled atmosphere. In order to produce the 95% dense material, the powder was cold-compacted using 690 MPa pressure, but the green compacts were first pre-sintered at 850°C for 30 minutes and then they were re-pressed using 690 MPa pressure and re-sintered at 1120°C for an additional 30 minutes. The 100% dense material was produced by warm-compacting the powder using 690 MPa pressure, heating the resulting compacts to 1150°C, and then forging them in a press using 760 MPa pressure for 10 seconds. Cylindrically shaped specimens for quench dilatometry measurements were machined from specific locations in these bulk materials using an electric discharge machine (EDM). The specimens were 8mm long and 3mm in diameter.

Measurement of the Heat Transfer Coefficient

The method employed for measuring the heat transfer coefficient involves quenching a heated cylindrical probe that is machined from the material to be tested into the quenching medium and acquiring the temperature-time profile. The apparatus used for this purpose is shown in Figure 2 and consists of an electric box furnace for heating the probe, a connecting rod that joins the probe to a pneumatic cylinder that allows automatic quenching of the probe into a beaker that contains the quenching oil, and a computer connected to a fast data acquisition system. A k-type thermocouple inserted at the geometrical center of the probe continuously measures the temperature of the probe [8-10]. The probe dimensions are chosen such that the Biot number for the quenching process is < 0.1. This requirement insures that significant thermal gradients will

not be present in the radial direction of the probe. Accordingly, a simple heat balance analysis (usually referred to as a lumped parameter analysis) can be performed on the system (probe + quenching medium) to yield the heat transfer coefficient. With Bi < 0.1, the error associated with such calculations of the heat transfer coefficient is less than 5%. A heat balance applied to the probe results in Equation 1, which is used to calculate the heat transfer coefficient at the surface of the probe [11].

$$h = -\frac{\rho V C_p}{A_s\left(T_s - T_f\right)}\frac{dT}{dt} \tag{1}$$

In Equation (1), h is the heat transfer coefficient at the surface of the probe, ρ, V, C_p, and A_s are the density, volume, specific heat, and surface area of the steel probe, respectively. T_s is the temperature at the surface of the probe, which, due to the geometry of the probe, is approximately equal to the measured temperature at the center of the probe, and T_f is the bulk temperature of the quenching medium. Figure 3 shows the heat transfer coefficient obtained by this method for FL- 4605 PM steel probes pressed and sintered to different levels of porosity.

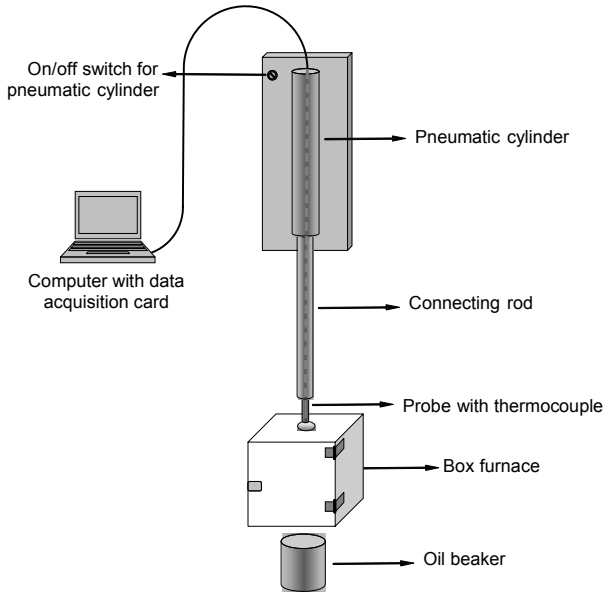

Figure 2: Apparatus used to measure the heat transfer coefficient during quenching.

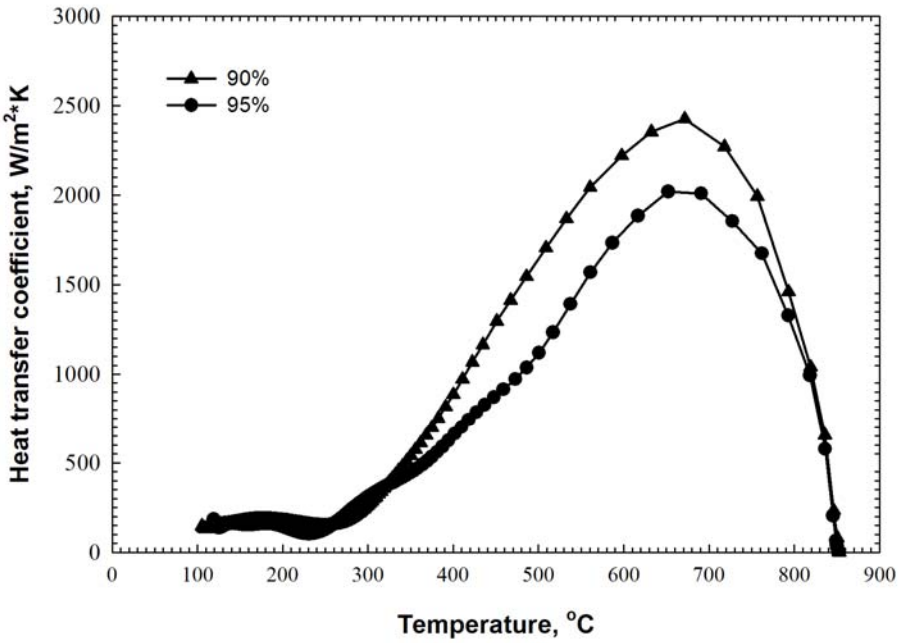

Figure 3: Variation of the heat transfer coefficient with temperature and part density [12].

Determination of the Phase Transformation Kinetics Parameters

The phase transformation kinetics parameters were obtained by quench dilatometry. Dilatometry is based on the principle that during heating and cooling dimensional changes occur in materials as a consequence of both thermal expansions associated with temperature change, and phase transformations. Sensitive, high-speed dilatometers are used to measure these changes as a function of time and temperature. The resulting data is then converted to discrete values of strain for specific values of time and temperature during the thermal cycle. Strain as a function of time and temperature is then used to determine the start and completion of phase transformations [12]. Two types of dilatometry measurements were performed on the specimens. These are (1) isothermal transformation measurements, and (2) continuous cooling transformation measurements. Data from the isothermal transformation measurements provided the kinetics parameters for diffusive transformations such as the austenite to bainite, and the austenite to ferrite/pearlite transformation. On the other hand, data from the continuous cooling

transformation measurements provided the transformation kinetics parameters for the austenite to martensite transformation. The following sections detail the procedures that were used to perform these measurements.

Specimen conditioning – Each specimen was subjected to a conditioning run before testing in order to remove residual stresses and stabilize the position of the test specimen within the apparatus. This treatment consisted of heating the specimen to 850°C±5°C at a nominal rate of 10°C/s, holding the specimen at 850°C for 5 minutes and then cooling it to room temperature with cooling rate 100°C/s. The specimen was not removed from the apparatus prior to conducting the dimensional measurements. This conditioning cycle is designed such that each specimen has the same starting microstructure (martensite in this case) before characterizing the transformation behavior.

Determination of the critical temperatures – The critical temperatures, Ac_1 and Ac_3, were determined from specimens that are separate from those that were used for transformation measurements. The specimen were heated to 600±5°C at a nominal rate of 10°C/s. Heating was then continued at a nominal rate of 28°C/hr while strain was continuously measured until the Ac_1 and Ac_3 temperatures were identified.

Generation of the isothermal transformation data sets – Each isothermal transformation thermal cycle consisted of heating a specimen to an austenitizing temperature of 850°C ± 5°C at a nominal rate of 10°C/s. The specimen was held at this austenitizing temperature for 5 minutes

and then quenched to the isothermal hold temperature. A cooling rate of at least 175°C/s was employed. During the quench, the temperature of the specimen did not undershoot the isothermal hold temperature by more than 20°C and stabilized at the isothermal hold temperature within 2 seconds. The temperature of the specimen was maintained within ±5°C of the isothermal hold temperature during dimension measurement. The specimen was held at the isothermal hold temperature and its dimensions continuously measured until the transformation was 100% complete[*]. The specimen was then quenched to room temperature. Data was sampled and recorded at a rate of at least 5 dimension measurements per second, and a different specimen was used for each thermal cycle. The data collected from these measurements for specimens with 100% density as they underwent the austenite to bainite transformation at different transformation temperatures is shown in Figure 4.

Generation of the continuous cooling transformation data sets – Each continuous cooling transformation thermal cycle consisted of heating a specimen to an austenitizing temperature of 850±5°C at a nominal rate of 10°C/s. The specimen was held at the austenitizing temperature for 5 minutes and then cooled to room temperature at different cooling rates. Data was sampled and recorded at the rate of one dimension measurement per degree Celsius. Linear cooling rates were used to the maximum cooling rate possible. For cooling rates where linear control was not possible, the rate at 700°C was reported along with the cooling time between 800°C and 500°C. A different specimen was used for each thermal cycle. The data collected during these measurements for specimens with 100% density is shown in Figure 5.

[*] Complete transformation is defined as the time at which maximum dimensional change has occurred.

Data generated from the isothermal and continuous cooling measurements was used to generate the kinetics parameters for the austenite to ferrite, austenite to pearlite, austenite to bainite, and austenite to martensite transformations. The procedure shown in Figure 6 was used to fit this data to mathematical equations that were then used to create a database of transformation kinetics and a Time-Temperature-Transformation (TTT) diagram for the PM steel. Figure 7 shows the TTT diagram for FL-4605 PM steel with two levels of porosity.

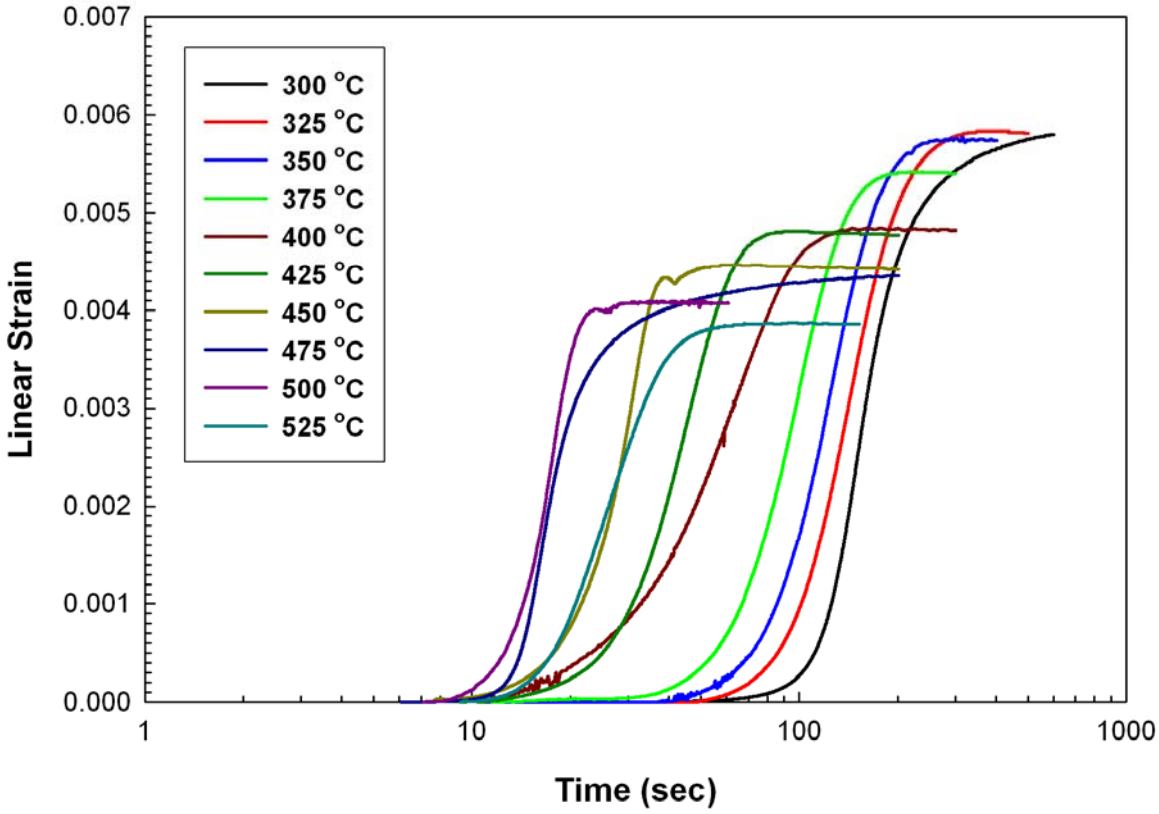

Figure 4: Measured strain vs. time data for bainite transformation at different isothermal holding temperatures.

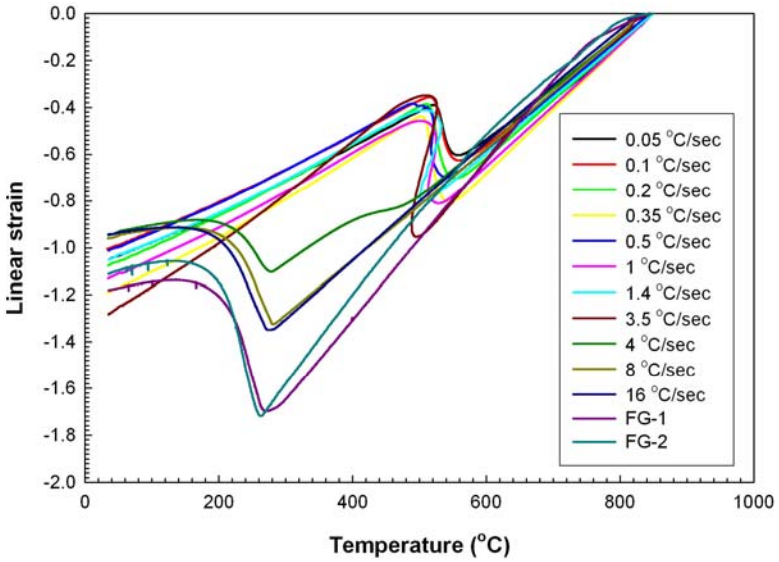

Figure 5: Measured strain vs. temperature data at different cooling rates during continuous cooling transformation tests.

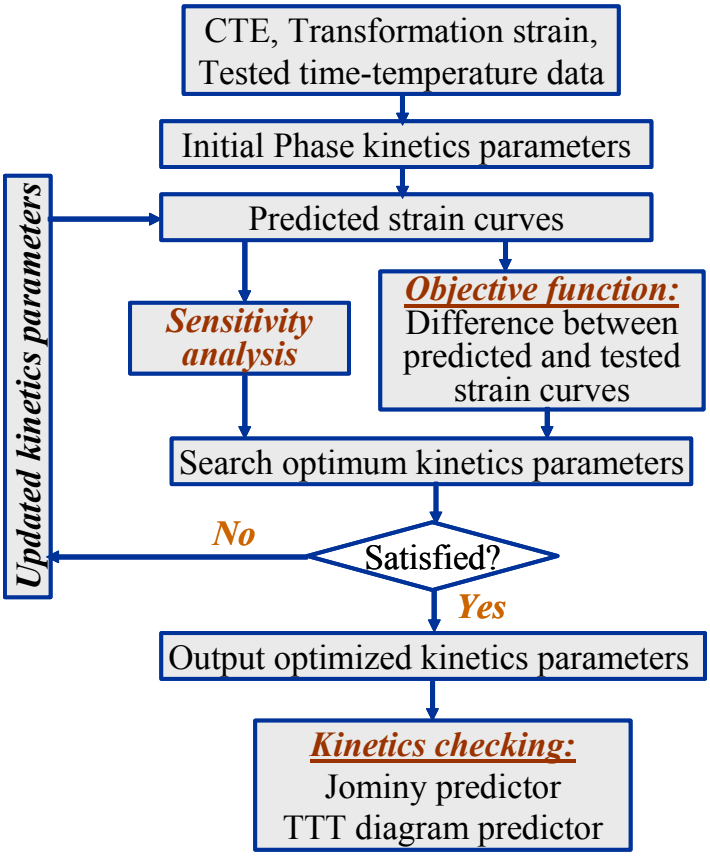

Figure 6: Flow chart for fitting the kinetics parameters (developed by DCT).

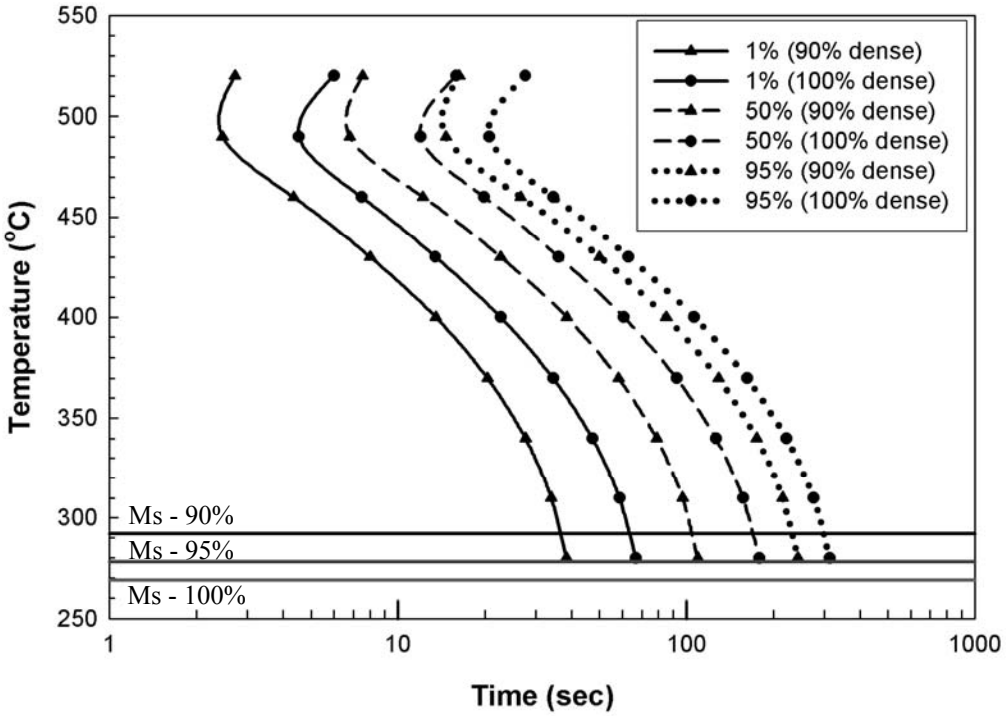

Figure 7: TTT diagram for 90% and 100% density material plotted for the austenite to bainite and the austenite to martensite transformations.

Determination of the Mechanical Properties and Transformation Plasticity

These measurements were performed using a Gleeble machine with both heating and cooling capabilities. The following sections describe the procedures that were employed on specimens that were conditioned using the procedure described earlier in order to generate stress vs. strain curves.

Measurement of the mechanical properties – The specimen was austenitized at 850°C±5°C and then cooled to the required test temperature. If austenite was being characterized, the test was conducted as soon as the specified temperature has been reached. On the other hand, if a diffusive phase was being characterized, the specimen was held at temperature until the phase transformation at that temperature was complete, and then the specimen was tested.

In the case of martensite, compression tests as opposed to tensile tests were used because of the brittle nature of as-quenched martensite. Test specimens for martensite testing were heated and quenched using a box furnace and a small quench bath. The as-quenched specimens were then compressed at room temperature or soon after heating to a low temperature.

Figure 8 shows the data collected during tensile testing of 90% density austenite specimens at three different temperatures. Curves similar to those in Fig. 8 were obtained for specimens of each metallurgical phase with each of 3 density levels (90%, 95% and 100%) as functions of temperature and strain rate, and a fitting routine was used to fit this data to mathematical equations that were then used to create a mechanical property database.

The plastic behavior of steels during phase transformation can be divided into two parts: (1) *Classical plasticity*, i.e., plastic flow caused by changes in the applied stress or by temperature cycling, and (2) *Transformation plasticity,* i.e., plastic flow caused by changes in the relative amounts of the metallurgical phases due to phase transformation. That is to say, the progress of a transformation happening in the metal under an external stress induces plastic deformation in the metal even when the applied stress and the transformation temperature are kept constant. Low Stress Dilatometry was used to characterize the transformation-induced plasticity in FL-4605 PM steel. The procedure entailed applying an external compressive static load to a standard specimen in a Gleeble machine just before the start of the transformation. The magnitude of the applied load was chosen such that the magnitude of the resulting stress was less than the flow stress of austenite at the temperature of application of the load. Transformation induced plasticity measurements were performed on specimens that were conditioned following the conditioning procedure described earlier. The specimens were of three density levels (90%, 95%, and 100%), and the measurements were performed for the austenite to martensite and the austenite to bainite

transformations. The following paragraphs detail the procedures that were followed in performing these measurements.

Austenite to martensite transformation – Each measurement consisted of heating a specimen to an austenitizing temperature of 850°C ±5°C at a nominal rate of 10°C/s. The test specimen was held at the austenitizing temperature for 5 minutes and then it was cooled to room temperature at a rate of 80°C/s under the applied compressive stress. The stress was applied on the specimen just before the start of the transformation (at about 300°C), and was kept constant until the specimen cooled to room temperature. Dilatation data from the specimen was recorded at the rate of one dimension measurement per degree Celsius.

Austenite to bainite transformation – Each measurement consisted of heating a specimen to an austenitizing temperature of 850°C±5°C at a nominal rate of 10°C/s. The specimen was held at the austenitizing temperature for 5 minutes, and then it was cooled to the isothermal hold temperature (480°C). A cooling rate of at least 80°C/s was employed. The temperature of the specimen was maintained within ±5°C of the isothermal hold temperature during dimension measurement. The uni-axial compressive stress was applied just before the start of the transformation and was kept constant until the measurement was complete. The specimen was then quenched to room temperature. Dilatation data from the specimen was recorded at the rate of at least 5 dimension measurements per second.

Figures 9(a) and (b) show the measured dilatation for 90% density specimens at three levels of applied stress during the austenite to bainite and the austenite to martensite transformations,

respectively. Similar measurements were performed on specimens with 95 % and 100% density, and a fitting routine was used to fit this data to mathematical equations that were then used to create a transformation induced plasticity database.

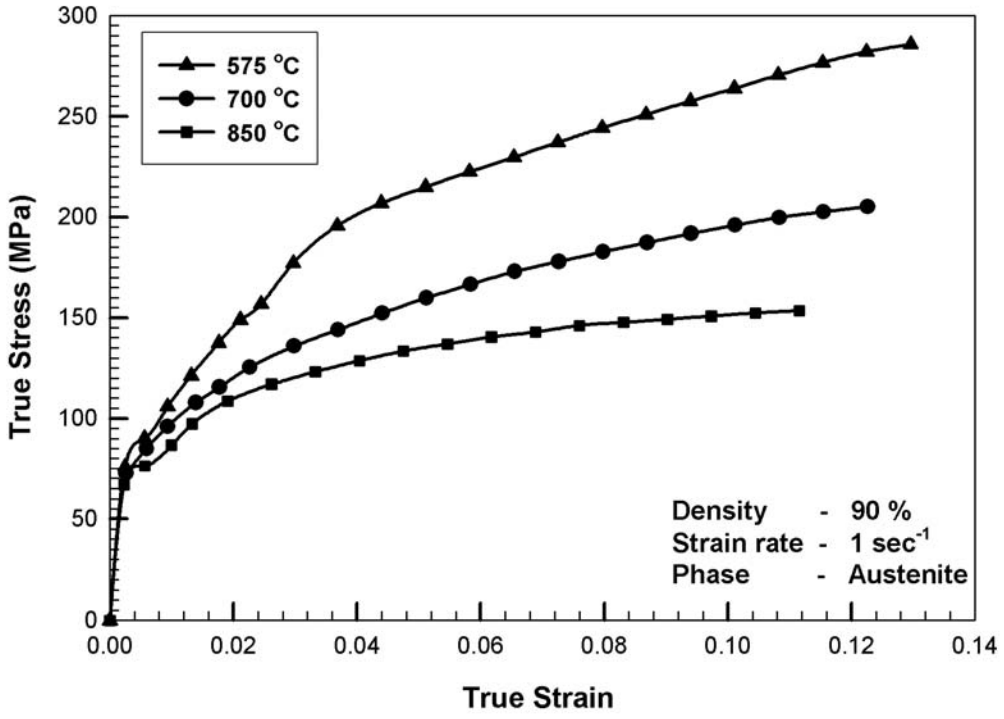

Figure 8: True stress vs. true strain curve for austenite at three different temperatures measured for the samples with 90% density at 1 sec^{-1} strain rate.

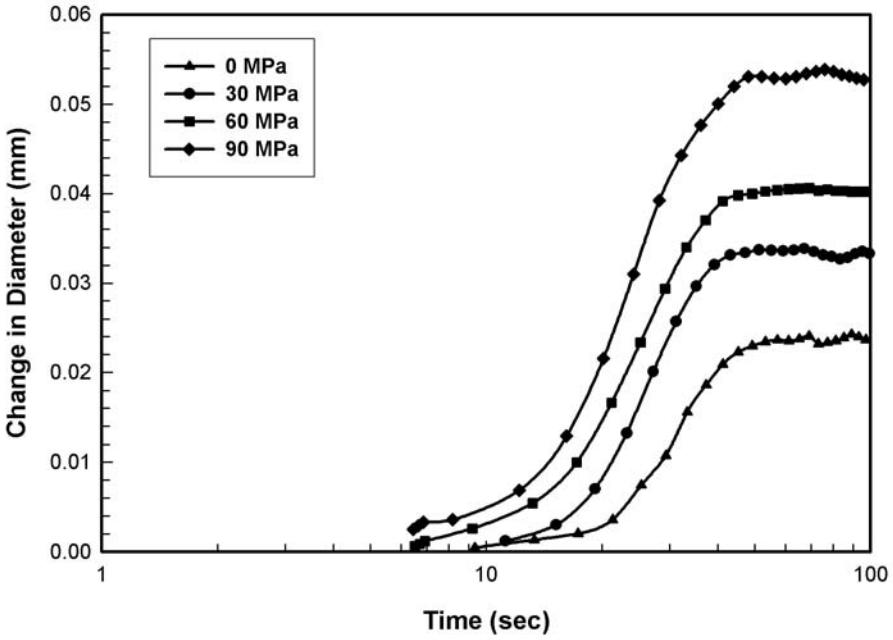

(a)

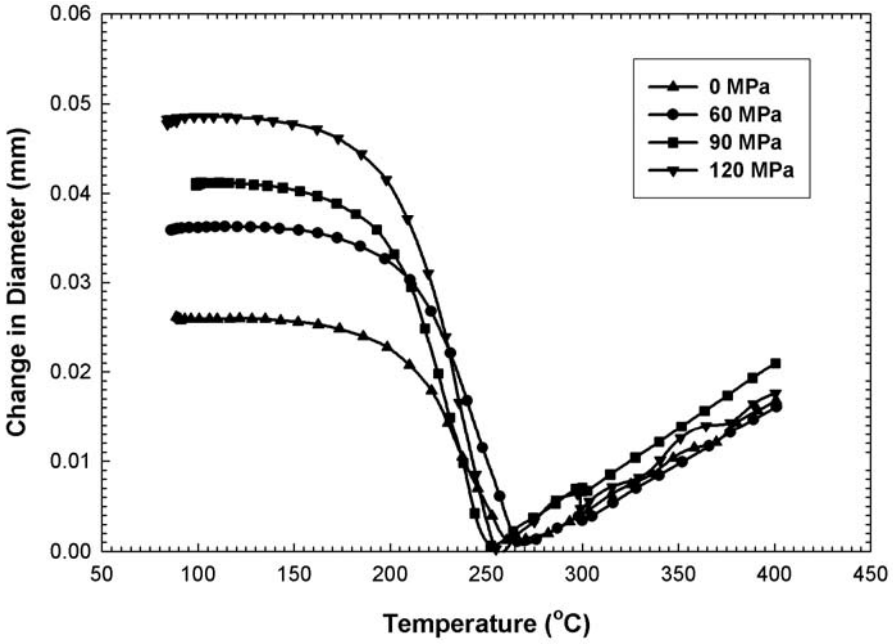

(b)

Figure 9: Measured dilatation data on samples with 90% density at three stress levels for, (a) austenite to bainite transformation, and (b) austenite to martensite transformation.

2.4 MODELING

The capabilities of the model are demonstrated using the part shown in Figure 10. The dimensions of the test part are summarized in Table II. Because of symmetry, only one half of the part is modeled. Figure 10 shows the 3-D part geometry created and meshed by the ABAQUS pre-processor. The meshed geometry contains 13,720 hexahedral elements and 15,975 nodes. In order to capture the steep temperature gradient caused by quenching, the mesh was generated such that the density of nodes is higher near the surface of the part than in the interior.

Table II: Dimensions of the part.

Dimension	Magnitude
Outer diameter	110.5 mm
Inner diameter	92.9 mm
Center offset	4.8 mm
thickness	12.7 mm

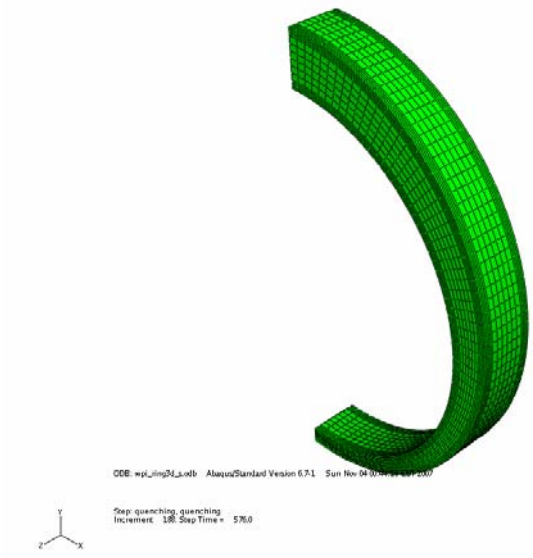

Figure 10: Geometry and mesh used in the model.

Solution Procedure and Boundary Conditions

Details of modeling the part are described in the following paragraphs.

The thermal module – The part was heat treated according to the following schedule: Furnace heating to 850°C, followed by immersion into a quench tank with a velocity of 40 mm/sec, followed by quenching in oil to room temperature.

The initial conditions needed by the thermal module are the carbon content of the part, the temperature of the part before heat-treating (room temperature in this case), and the heat treatment mode. The heat treatment mode is used to select the appropriate kinetics input from the different kinetics modules in DANTE to match each of the process steps as they change from furnace heating to specimen immersion in the quenching fluid to quenching.

The boundary conditions relevant to each of the heat treatment process steps are as follows:

For the furnace-heating step: A convective boundary condition was specified at the surface of the part by providing the measured heat transfer coefficient for heating the part to the austenitizing temperature of 850°C.

For the immersion step: The direction and velocity of immersion of the part into the quench tank was defined. This step is important in order to capture the temperature gradient along the immersion length of the part. In this simulation, the part was immersed along its length with a velocity of 40 mm/s, and the process time for this step is 2.75 seconds.

For the quenching step: A convective boundary condition was specified at the surface of the part by providing the measured heat transfer coefficient for quenching the part in oil down to the room temperature.

The stress module – This module uses mainly the time-temperature history of the part, which is generated by the thermal module, in order to calculate the nodal displacements, stresses, and volume fraction of metallurgical phases.

For the initial condition, the stress at all nodes was set to zero. If an initial stress state existed, appropriate values could have been easily used.

Nodal constraints are required in order to prevent rigid body displacement and rotation. This requirement applies to all the process steps, and is defined only once in the model input file. Referring to the 3-D geometry in Figure 10, all the nodes in the two symmetry faces were constrained from moving in the *x* direction. In addition, one node at the center of the top symmetry face was constrained from moving in the *y* and *z* directions, and one node at the center of the bottom symmetry face was constrained from moving in the *z* direction.

2.5 MODEL RESULTS AND COMPARISON TO MEASUREMENTS

In order to verify the accuracy of the model, the model predictions were compared to measurements performed on a FL-4605 PM steel part of configuration and dimensions similar to those used in the model.

Production of the Part

AUTOMET 4601 steel powder with the chemical composition shown in Table I was admixed with Asbury 1651 graphite powder to yield 0.5 wt. pct. carbon in the final product. Zinc sterate was added to the powder to serve as a lubricant, and the admixed powder was then placed in a die and pressed using 216 tons of pressure. The green part was sintered at 1100°C for 30 minutes

in a continuous sintering furnace under controlled atmosphere and then air cooled to room temperature. The average measured density of the parts was found to be 95% of theoretical density with negligible variation within each part and from part to part.

Heat Treatment of the Part

The heat treatment cycle for the sintered parts consisted of furnace heating to 850°C, holding at this temperature for 20 minutes, and then quenching in oil with the parts in an upright position and with their thinner section pointing down. Twenty parts were heat treated in an internal quench batch furnace under an endothermic atmosphere with carbon potential of 0.5 wt. %.

Characterization of the Part

In order to characterize the amount of distortion in the parts caused by the heat treatment, a fixture was designed to hold the parts at the same location in a coordinate measurement machine (CMM) before and after heat treatment. The fixture consisted of an aluminum block with pins that fits the holes on the part to hold it in an upright position with the thinnest section of the part on the top as shown schematically in Figure 11. The circular hole was measured before and after heat treating at locations around the periphery in 5° increments. Measurements were repeated at four depths along the thickness of the part. The XY data from the CMM measurements was converted into a radius, r, and an angle θ at each data point. The radius was then normalized by dividing it by the average radius before heat treatment. Figures 12 and 13 compare the measured and model-predicted changes in dimensions of the central hole due to heat treatment.

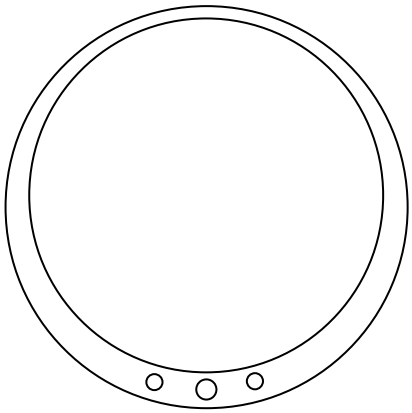

Figure 11: Orientation of the part in CMM machine for measuring the dimensions of the circular hole.

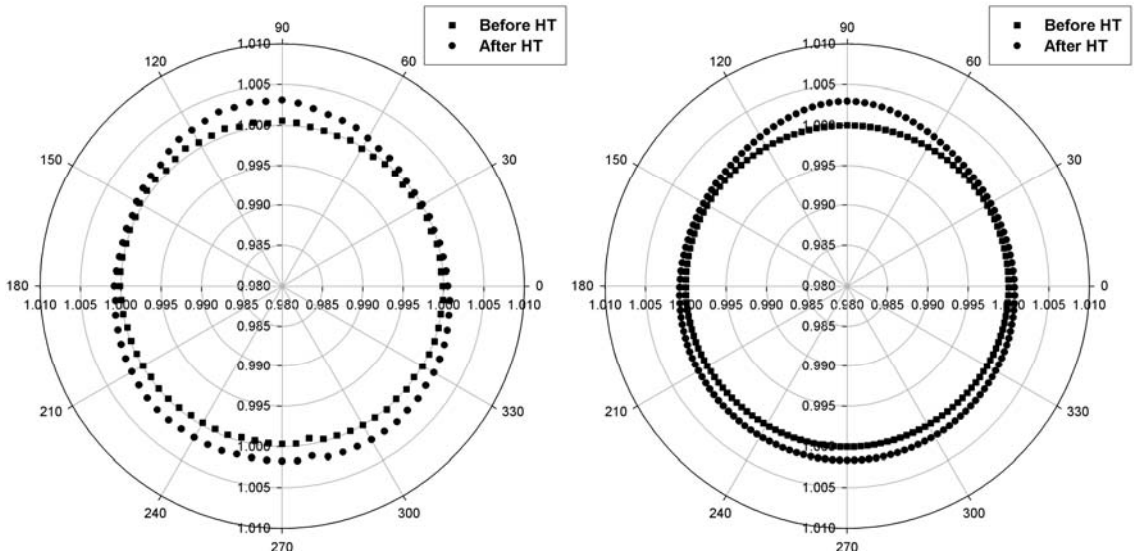

(a) (b)

Figure 12: Coordinates of the circular hole before and after heat treatment, (a) Measured using CMM, and (b) predicted by the model.

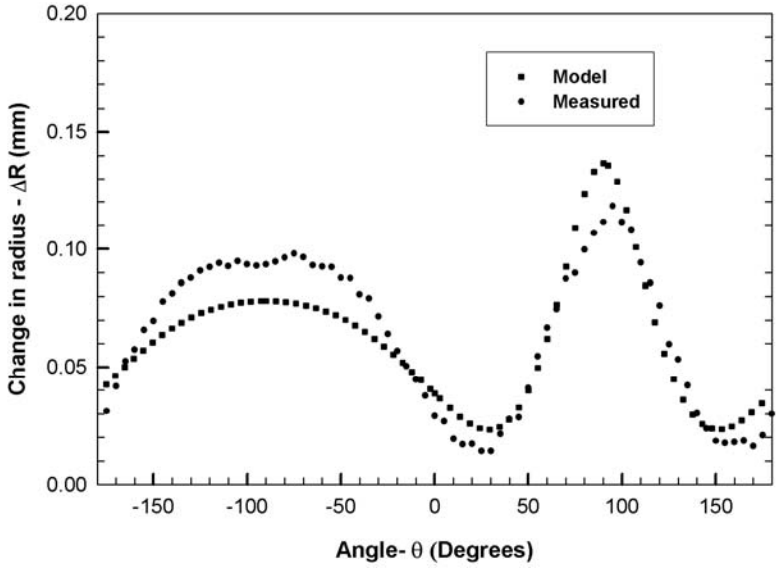

Figure 13: Comparison of model-predicted changes in radius of the circular hole vs. angle.

In order to characterize the fraction of metallurgical phases that are formed in the part during heat treatment, the amount of retained austenite in the heat treated parts was measured using X-ray diffraction. The parts were cut along the dotted line shown in Figure 14(a). These parts were wet-ground and polished using standard metallographic techniques and then they were ultrasonically cleaned. X-ray diffraction was performed on the parts according to ASTM E975 standard practice using a "θ- θ" type diffractometer*. Measurements were performed at 3 different locations on each of three different parts using chromium K_α radiation. Figure 14(b) shows the X-ray peaks from the collected data. Integrated intensities for the 200 martensite peak and the 200 austenite peak were estimated by calculating the area under the measured peaks, and the amount of retained austenite was calculated by solving Equations 2 and 3 simultaneously.

$$\frac{I_\gamma}{I_\alpha} = \frac{R_\gamma c_\gamma}{R_\alpha c_\alpha} \tag{2}$$

* Model : X'Pert Pro Diffractometer manufactured by PANalytical, Inc., Natick, MA, USA.

$$c_\alpha + c_\gamma = 1 \tag{3}$$

In Equations (2) and (3), I_γ and I_α are the measured intensities of the austenite and martensite peaks respectively, R_γ and R_α are constants calculated from knowledge of the lattice parameters, crystal structure, and carbon content of each phase, and c_γ and c_α are the concentrations of austenite and martensite in the part. There was no significant change in the amount of retained austenite along the cross-section of the part; hence, the average of the results was obtained over the entire section plane. Figure 15 shows the model-predicted and the measured amount of retained austenite. It is clear that the model prediction is in excellent agreement with the measured data.

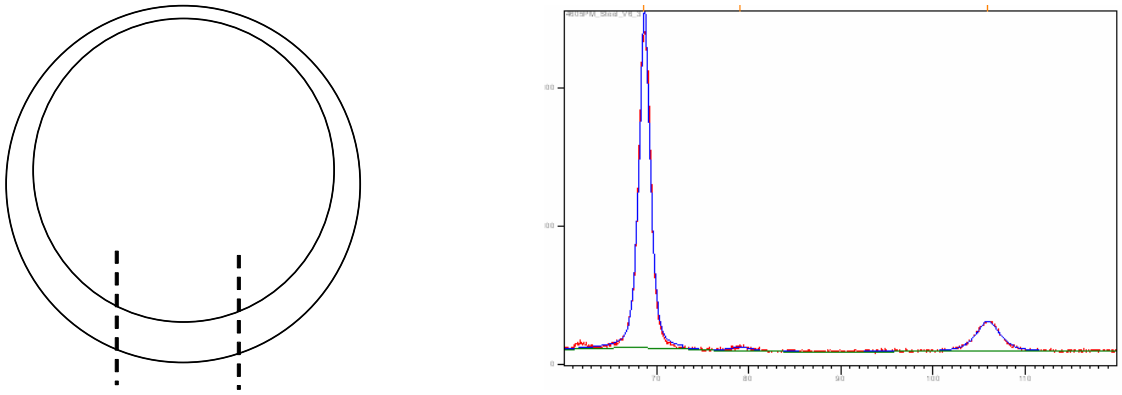

(a) (b)

Figure 14: (a) Section lines showing cuts for measuring retained austenite.
(b) Diffraction data showing the 110 martensite, 200 austenite, and 200 martensite peaks.

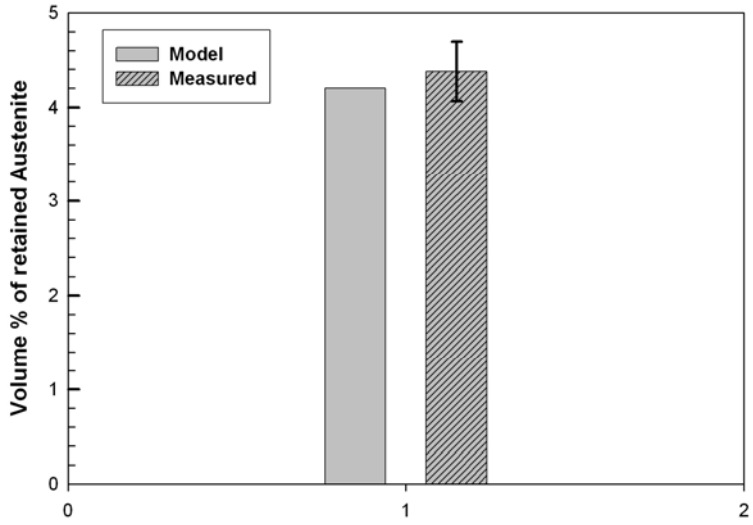

Figure 15: Amount of retained austenite as predicted by the model and as measured by X-ray diffraction.

In order to characterize the magnitude and sense of the residual stresses that develop in the part during heat treatment, the residual stresses in the heat treated parts were measured using x-ray diffraction. Fig. 16 shows the apparatus that was used where "1" indicates the location on the part where the measurements were made. This particular location was chosen because it was expected to have the highest residual stresses since it exhibited the highest distortion. In order to measure the bi-axial stresses, the $\sin^2\psi$ method [13, 14] was used at 3 different sample orientations. A typical plot of $\sin^2\psi$ vs. the inter-planar spacing (d) for the 211 peak at 45º sample orientation is shown in Figure 17. Similar plots were generated for the other two sample orientations. Figure 18 shows the model-predicted and the measured values of the two principal stresses. It is to be noted that phase-specific temperature dependent mechanical property data for martensite in AISI 4340 steel were used in place of their un-available counterparts for FL-4605 PM steel to produce Figure 18. Despite of that, the model-predicted and the measured values of residual stress are in good agreement.

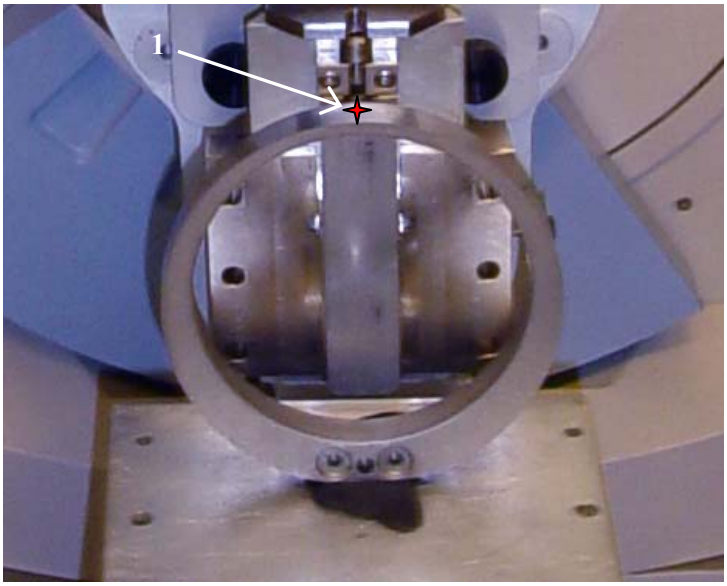

Figure 16: Part location (position 1) where the residual stress measurements are performed.

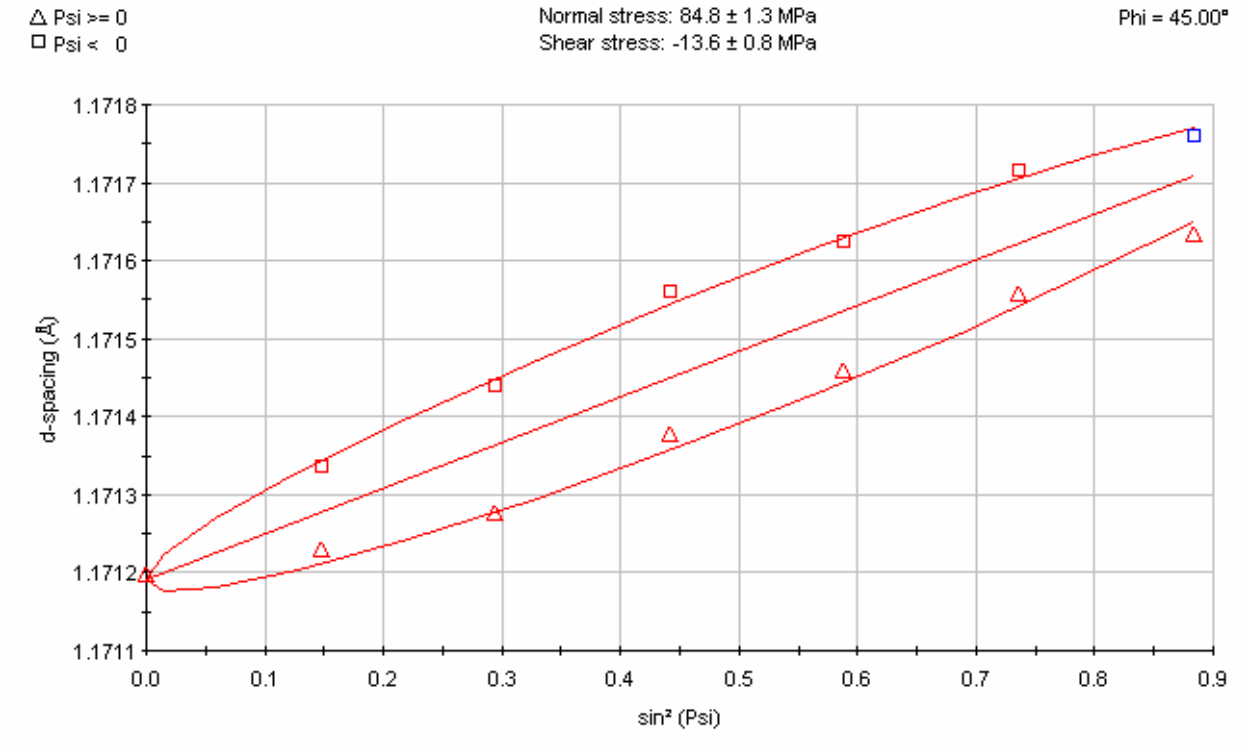

Figure 17: plot for $\sin^2 \Psi$ vs. d spacing for 45º part orientations.

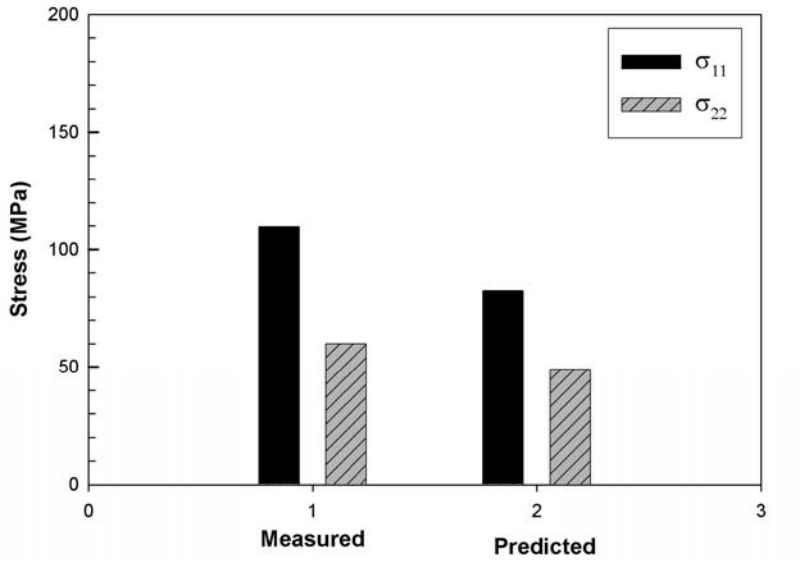

Figure 18: Comparison of residual stresses as predicted by the model and as measured by X-ray diffraction.

2.6 SUMMARY AND CONCLUSIONS

The finite element-based commercial code DANTE for predicting the response of wrought steels to heat treatment was modified to enable it to predict the response of PM steels to heat treatment by introducing porosity as a state variable of the model.

An extensive database was developed for FL-4605 PM steel and contains information on phase transformation kinetics, elevated temperature mechanical properties, and heat transfer characteristics - all as functions of temperature and porosity for all the phases that can be present in the steel, i.e., austenite, ferrite/pearlite, bainite, and martenisite. A side-product of developing the database was creating, for the first time, a Time - Temperature - Porosity - Transformation (TTPT) diagram for the PM steel. These diagrams are necessary for understanding and accounting for the effect of porosity that invariably exists in PM steels on the kinetics of phase transformations in these steels.

The response of a typical FL-4605 PM steel part to heat treatment was simulated using the model and the model predictions were compared to measurements made on similar parts that were commercially produced and commercially heat treated. The model-predicted dimensional changes, residual stresses, and amount of retained austenite after heat treatment were found to be in very good agreement with their measured counterparts.

ACKNOWLEDGEMENTS

The authors gratefully acknowledge the member companies of the Particulate Materials Research Center of Worcester Polytechnic Institute for their support of this work. In addition, the authors gratefully acknowledge Deformation Control Technology, Inc. for providing the Dante Software. Finally, the authors gratefully acknowledge the High Temperature Materials Laboratory User Program, Oak Ridge National Laboratory managed by UT-Battelle, LLC for the U.S. Department of Energy under contract number DE-AC05-00OR22725 for providing assistance with the dilatometry measurements.

REFERENCES

1. Inoue T. and Arimoto K, *Quenching and Distortion Control Conference Proceedings*, ASM International, 1992, pp. 205-212.
2. Jarvstrat N., and Sjostrom S., *ABAQUS Users' Conference Proceedings*, 1993, pp. 273-287.
3. Southwest Research Institute and Farmatome, "SYSWELD - A Predictive Model for Heat Treat Distortion," *Presentation at the National Center for Manufacturing Sciences*, April 14, 1992.
4. Dawling W., *Second International Conference on Quenching and Control of Distortion*, 1996, pp. 367-375.

5. Bammann D.J., Chiesa M.L., and Johnson G.C., *Proceedings of the Nineteenth International Congress on Theoretical and Applied Mechanics,* 1996, pp. 359-376.
6. Lusk M.T. , and Lee Y.K., *Proceedings of the Seventh International Seminar on Heat Treatment and Surface Engineering of Light Alloys,* 1999, pp. 273-282.
7. Ferguson B.L., Petrus G.J., and Pattok T., *Proceedings of the Third International Conference on Quenching and Control of Distortion*, 1999, pp. 188-200.
8. Maniruzzaman M., Chaves C., McGee C., Ma S., and Sisson, Jr. R. D., *Proceedings of the Fifth International Conference on Frontiers of Design and Manufacturing (ICFDM 2002)*, Vol. 1, 2002, pp. 619-625.
9. Chaves J.C., "The Effect of Surface Condition and High Temperature Oxidation on Quenching Performance of 4140 Steel in Mineral Oil," Ph.D. Dissertation, Worcester Polytechnic Institute, Worcester, MA, 2001, p.133.
10. Ma S., Maniruzzaman M., and Sisson, Jr. R.D., *Proceedings of the First International Surface Engineering Congress*, ASM International, Columbus, Ohio, 2002, pp. 281-289.
11. Warke V., Yuan J., Maniruzzaman M., Makhlouf M., and Sisson, Jr. R.D., *Proceedings of the 2004 International Conference on Powder Metallurgy & Particulate Materials*, 2004, pp. 39-53.
12. "Recommended Practice for the Quantitative Measurement and Reporting of Hypo- Eutectoid Carbon and Low-Alloy Steel Phase Transformations," *ASTM Standard*, A1033-04.
13. Cullity B.D., and Stock S.R, "Elements of X-Ray Diffraction", *3rd edition, Princeton Hall Publications,* 2004, pp. 435-468.
14. "Residual Stress Measurement by X-Ray Diffraction", *SAE Standard,* J784a, August 1971.

CHAPTER 3

The Effect of Porosity on the Austenite to Ferrite Transformation in Powder Metallurgy Steels

Virendra S. Warke, Richard D. Sisson, Jr., and Makhlouf M. Makhlouf

ABSTRACT

The effect of porosity on the kinetics of the austenite to ferrite isothermal transformation in powder metallurgy steels was characterized using high-speed quench dilatometery. The measurements reveal that the presence of porosity in these steels reduces the stability of austenite and hence shortens the incubation time of the transformation. An Avrami-type equation was fitted to the measured data in order to quantify the effect of porosity on the Avrami constants. In addition, samples with varying levels of porosity were interruptedly quenched after holding them at 650°C for 900 seconds. Quantitative microscopic measurements performed on these samples showed an increase in the number and a decrease in the average diameter of the ferrite grains with increasing porosity. It is hypothesized that pores in powder metallurgy steels increase the rate of nucleation of ferrite from austenite by providing high diffusivity paths for carbon atoms that help accelerate their partitioning during the transformation.

Keywords: Phase transformations; kinetics; Ferrite; dilatometry.

3.1 INTRODUCTION

Despite numerous investigations, the effect of porosity on phase transformations in powder metallurgy steels is not yet certain [1-3]. Indeed there is agreement that the presence of porosity in sintered steels causes a decrease in the Ac1 temperature, an increase in the Ar1 temperature,

and, under isothermal conditions, shortening of the incubation time and the overall reaction time [1-3], yet a detailed quantitative understanding of the role that porosity plays in the kinetics of the transformations is still unclear.

In this work, the isothermal transformation of austenite to ferrite in powder metallurgy steels is characterized using quench dilatometry performed on FL-4605 PM steel alloy with three levels of porosity. The fraction of ferrite formed during the isothermal transformation is measured by quantitative metallography and the measured values are used to convert dilatational strain to volume fraction of ferrite formed during the transformation. The isothermal kinetics of the austenite to ferrite transformation is described using Avrami parameters by fitting the Avrami equation to the measured data. The effect of porosity on these constants is characterized and a hypothesis is presented to describe the formation of ferrite in the presence of porosity. The proposed hypothesis is supported by metallographic evidence.

3.2 MATERIALS AND PROCEDURES

AUTOMET 4601 steel powder* was admixed with powdered graphite to yield 0.5-wt% carbon in the final product. Table I shows the chemical composition of the resultant powder.

Table I: Composition of the alloy (in wt.%).

Carbon	Oxygen	Sulfur	Manganese	Molybdenum	Nickel	Iron
0.5	0.11	0.0093	0.196	0.549	1.812	Remainder

Bulk material was produced from this powder in three different densities corresponding to 90%, 95%, and 100% of theoretical density. Except for special products, commercial components

* Manufactured by Quebec Metal Powder Ltd., Quebec, Canada.

manufactured by powder metallurgy methods are rarely less than 90% dense. Only three significantly different density levels are achievable in the density range between 90 and 100%.

In order to produce the 90% dense material, the powder was cold-compacted using 690 MPa pressure in a hydraulic press to produce green compacts that were then sintered at 1120°C for 30 minutes under a controlled atmosphere. In order to produce the 95% dense material, the powder was cold-compacted using 690 MPa pressure, but the green compacts were first pre-sintered at 850°C for 30 minutes and then they were re-pressed using 690 MPa pressure and re-sintered at 1120°C for an additional 30 minutes. The 100% dense material was produced by warm-compacting the powder using 690 MPa pressure, heating the resulting compacts to 1150°C, and then forging them in a press using 760 MPa pressure for 10 seconds. Cylindrically shaped specimens for quench dilatometry were machined from specific locations in these bulk materials using an electric discharge machine (EDM). The specimens were 8mm long and 3 mm in diameter.

Quench dilatometry was performed in an MMC high-speed quenching dilatometer* in which the cylindrical specimen is suspended and heated in an induction-heating coil that is enclosed in a vacuum chamber. Measurements were performed at 1×10^{-5} torr and specimen cooling was accomplished by a combination of controlled reduction in the heating current and injection of an inert gas onto the specimen. Dimensional change was measured along the longitudinal axis of the specimen and temperature was measured by means of a Type R thermocouple that was welded to the surface of the specimen midway along its length. Prior to attaching the thermocouple to the specimen, the specimen was de-greased using ethanol and was lightly sanded by means of a 600 grit silicon carbide paper at the point of thermocouple attachment in order to remove any surface

* Manufactured by Avenel Inc., NY, USA.

oxide and ensure proper connection of the thermocouple to the specimen. The length and diameter of the specimen were measured with a micrometer prior to and after thermal cycling. These measurements were used to verify dimensional changes that occur during thermal cycling. For maximum accuracy, the length change measuring device, i.e., the linear variable differential transformer (LVDT) was adjusted so that it did not pass through its natural zero point during thermal cycling.

Each specimen was subjected to a conditioning run before measurements were performed in order to stabilize its position within the apparatus, remove residual stresses, and ensure that each specimen has the same starting microstructure (martensite in this case) before characterizing its transformation behavior. This conditioning treatment consisted of heating the specimen to 850°C ±5°C at a nominal rate of 10°C/s, holding the specimen at 850°C for 5 minutes, and then cooling it to room temperature at a cooling rate of 100°C/s.

Each isothermal transformation cycle consisted of heating a specimen to an austenitizing temperature of 850°C ±5°C at a nominal rate of 10°C/s, holding it at this temperature for 5 minutes, and then quenching it to a pre-determined isothermal holding temperature. A cooling rate of at least 80°C/s was used. During quenching, the temperature of the specimen did not undershoot the pre-determined isothermal holding temperature by more than 20°C and it stabilized at the isothermal holding temperature within 2 seconds. The temperature of the specimen was maintained within ±5°C of the isothermal holding temperature while its dimensions were continuously measured until transformation was complete[*]. The specimen was then quenched to room temperature. Data was sampled and recorded at a rate of 50 dimension

[*] Complete transformation is defined as the time at which maximum dimensional change has occurred.

measurements per second and a different specimen was used for each thermal cycle. Table II shows the design of experiments.

Table II: Design of experiments.

Density levels	Isothermal holding temperature (°C)	Isothermal holding time (hrs)	Number of repetitions
3	600	18	3
3	650	4	3
3	675	24	3

Additional specimens were machined from the bulk material and pre-conditioned in a manner similar to that used in the isothermal transformation measurements, namely heating the specimen to 850°C ±5°C at a rate of 10°C/s, holding at this temperature for 5 minutes, and then quenching to the isothermal holding temperature (in this case 650°C) at a cooling rate of 80°C/s, and holding at 650°C for 900 seconds before quenching the specimen to room temperature. These specimens were used for examining the microstructure and so they were sectioned, mounted and polished using standard metallurgical procedures, and etched with a 2% Nital solution.

3.3 RESULTS AND DISCUSSION

Figure 1 shows typical data obtained from quench dilatometry. It is a plot of the measured linear strain and the measured temperature as functions of time. The measured linear strain was normalized such that zero strain corresponds to the start of the isothermal hold after quenching the specimen from 850°C and the transformation time was normalized such that zero time corresponds to the start of the cooling of the specimen from 850°C. These procedures produced Figure 2. Curves similar to the one shown in Figure 2 were obtained for all the conditions

depicted in Table II. After quench dilatometry measurements, samples were sectioned from each specimen and mounted, polished, and etched with 2 % Nital. Figure 3 shows the microstructure after isothermal transformation at 600°C for 18 hours. Similar micrographs were obtained for all the conditions depicted in Table II. Image analysis was performed on 10 micrographs representing each sample and the average volume fraction of ferrite (ϕ_{F_M}) formed at each temperature and density level was computed. The results are shown in Table III.

Close examination of the dilatometry curves (e.g., Figure 2) shows that two transformation events occur during the dilatometry measurement. These are: (1) the austenite to ferrite transformation, and (2) the austenite to pearlite transformation. Hence, the volume fraction of ferrite that formed during the transformation (ϕ_{F_D}) was determined by dividing the strain caused by formation of ferrite (e_F) by the total strain at the end of the measurement (e_T) as shown in Eq. (1).

$$\phi_{F_D} = \frac{e_F}{e_T} \qquad (1)$$

Results obtained from Eq. (1) are compared with the volume fraction of ferrite estimated from image analysis (ϕ_{F_M}). Table III shows both ϕ_{F_D} and ϕ_{F_M} and it is clear that they are within 1- 2% of each other with ϕ_{F_M} being always larger than ϕ_{F_D}. This may be attributed to the fact that the end of the ferrite transformation in the dilatation curve is always masked by the onset of the pearlite transformation which makes pin pointing it somewhat difficult..

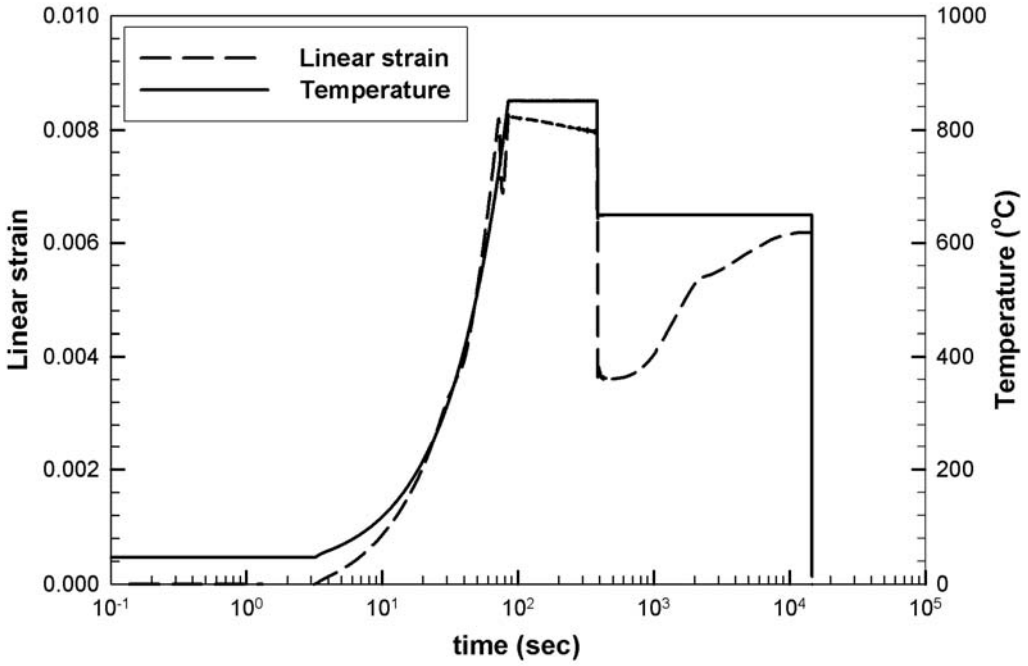

Figure 1: Measured linear strain and temperature as functions of time for the austenite to ferrite transformation at 650°C in a 95 % dense steel specimen.

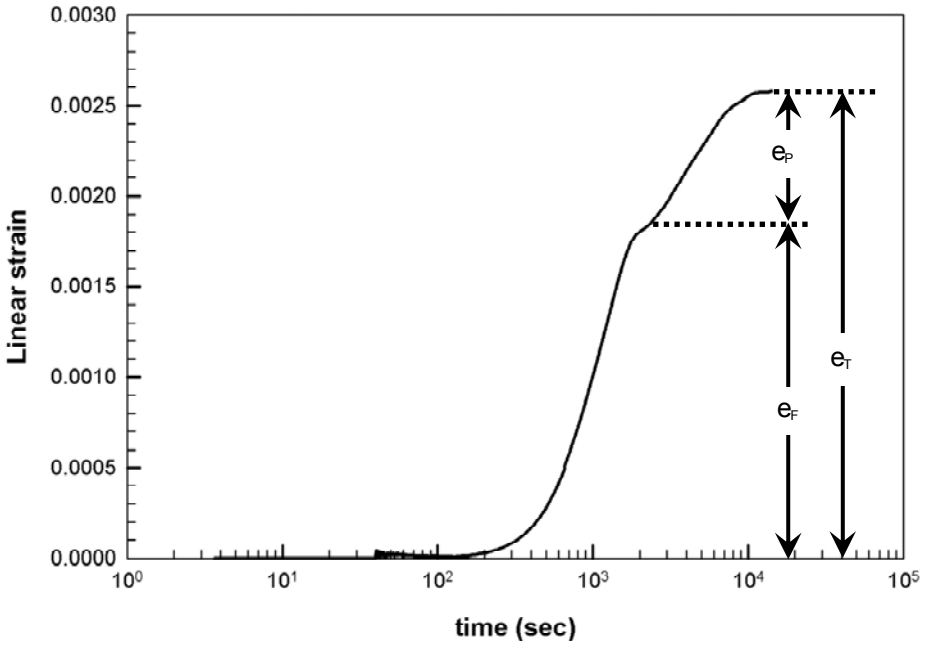

Figure 2: Normalized linear strain vs. time from isothermal transformation measurements performed at 650°C on a 95% dense specimen.

Table III. Average fraction of ferrite, ϕ_{F_D} calculated from dilatation using Eq. 1, ϕ_{F_M} estimated from image analysis, at each testing condition.

Temperature (°C)	90 % density		95 % density		100 % density	
	ϕ_{F_D}	ϕ_{F_M}	ϕ_{F_D}	ϕ_{F_M}	ϕ_{F_D}	ϕ_{F_M}
600	0.74	0.75	0.73	0.75	0.73	0.75
650	0.75	0.78	0.76	0.78	0.76	0.77
675	0.94	0.95	0.94	0.96	0.93	0.95

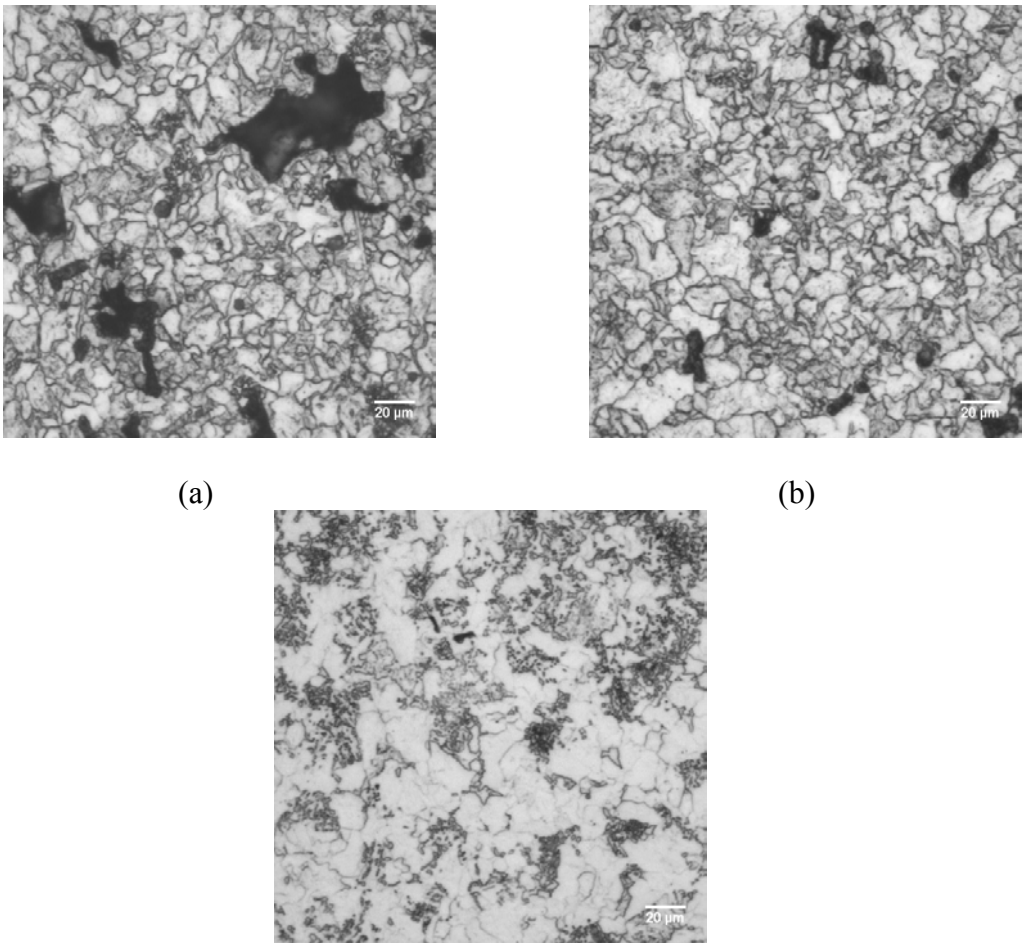

(a) (b)

(c)

Figure 3: Optical micrographs of samples isothermally transformed at 600ºC showing ferrite (in white) and pearlite (in grey). (400 X , 2 % Nital)(a) 90% dense specimen, (b) 95% dense specimen, and (c) 100% dense specimen.

The normalization method first proposed by Hawbolt et al. [4] was used to convert the dilatation data into volume fraction of ferrite. In this method, the instantaneous fraction of ferrite is normalized such that the maximum ferrite fraction at each temperature corresponds to ϕ_{F_M} keeping in mind that as time t $\rightarrow \infty$, $\phi_F(t) \rightarrow 1$ as shown in Eq. 2.

$$\phi_F(t) = \frac{\phi_{F_D}(t)}{\phi_{F_M}} \tag{2}$$

Figure 4 shows the normalized volume fraction of ferrite as a function of time. It is clear that at all the tested temperatures, the incubation time for formation of ferrite decreases with increasing porosity in the steel.

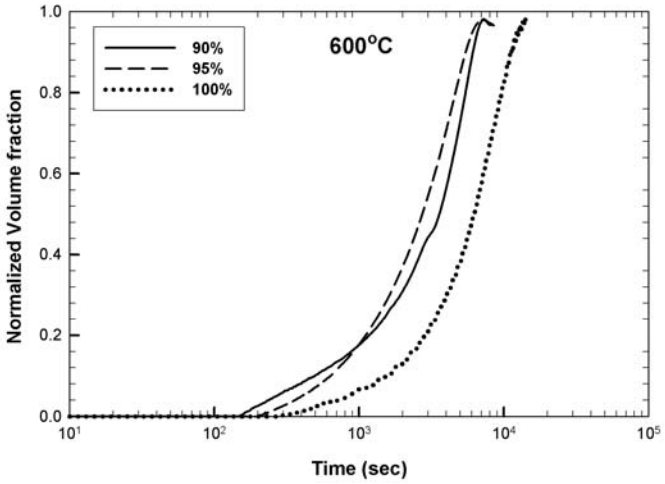

(a)

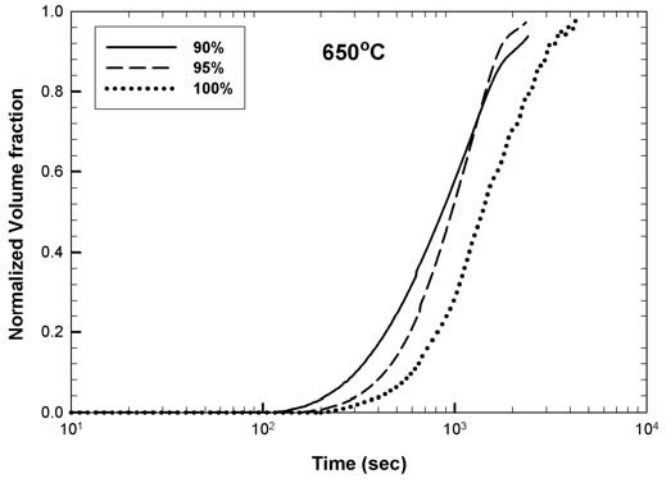

(b)

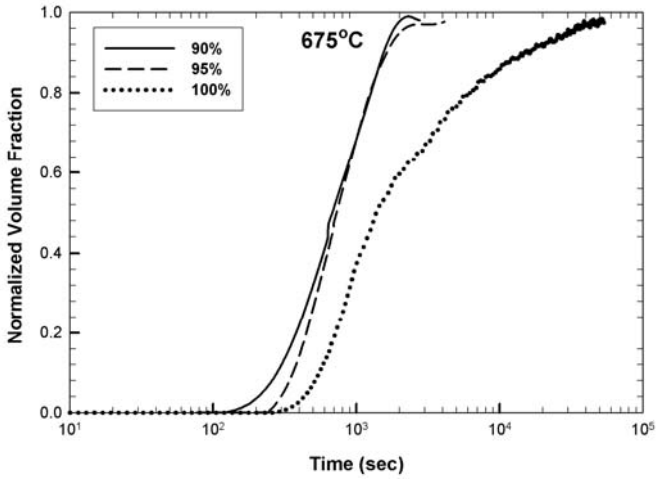

(c)

Figure 4: Normalized volume fraction of ferrite as a function of isothermal holding time (a) Specimen held at 600°C, (b) Specimen held at 650°C, and (c) Specimen held at 675°C.

Assuming that the isothermal transformation of austenite to ferrite follows diffusive kinetics, an Avrami-type equation, Eq. 3 was applied to the data presented in Figure 4.

$$\phi_F(t) = 1 - \exp\left[-b(T)\left(t - t_o\right)^n\right] \qquad (3)$$

In Equation (3), $\phi_F(t)$ is the volume fraction of ferrite, n is the transformation mechanism exponent, $b(T)$ is a temperature-dependent parameter whose magnitude depends on the combined nucleation and growth characteristics of the material, and t_o is the incubation time [4,5]. The data from all the measurements depicted in Table II was converted to normalized volume fraction of ferrite as a function of time using Eq. 2 and Eq. 3 was fitted to the normalized volume fraction vs. time data using regression analysis. Variation of the parameters n, b, and t_o with temperature and porosity is shown graphically in Figures 5, 6, and 7, respectively. Figure 5 shows that n, the Avrami exponent is independent of temperature and porosity. The average value of n was found to be 1.45, which suggests a nucleation event with early site saturation in which mass diffusion is rate limiting [4]. On the other hand, Figure 6 shows that b, the Avrami

constant is a function of both temperature and porosity, and the magnitude of *b* increases with increasing porosity at all the temperatures tested. Recalling that *b* is directly proportional to the product of the nucleation rate and the growth rate during the phase transformation, it becomes clear from Figure 6 that an increase in porosity increases nucleation rate and/or growth rate of the formation of ferrite from austenite. This proposition is supported by the results of optical microscopy and image analysis. Figure 8 shows micrographs of ferrite that formed in 90%, 95%, and 100% dense samples that were held at 650°C for 900 seconds. The micrographs clearly show that the number of ferrite particles decreases with decreasing porosity which implies that the nucleation rate of ferrite decreases with decreasing porosity. Moreover, Table IV shows that the average equivalent diameter of the ferrite particles decreases with increasing porosity.

Table IV: Average Equivalent diameter of ferrite particles grown in 900 seconds at 650 °C.

	90 % density	95 % density	100 % density
Average Equivalent Diameter (μm)	4.51	5.09	5.48
Standard deviation (%)	0.64	1.08	0.71
Standard error (%)	2.1	3.5	1.8

Also, from the data presented in Figure 4 (a)-(c), it can be seen that rate of transformation in 95 % density samples supersedes the rate of transformation in 90 % density sample after certain fraction of ferrite has formed. From both observations it is evident that growth rate in 90 % samples has reduced due to impingement of ferrite particles after certain fraction of ferrite has formed. However, from Figure 9, showing rate of transformation as a function of volume fraction of ferrite formed, it is apparent that initial growth rate is higher in lower density specimen.

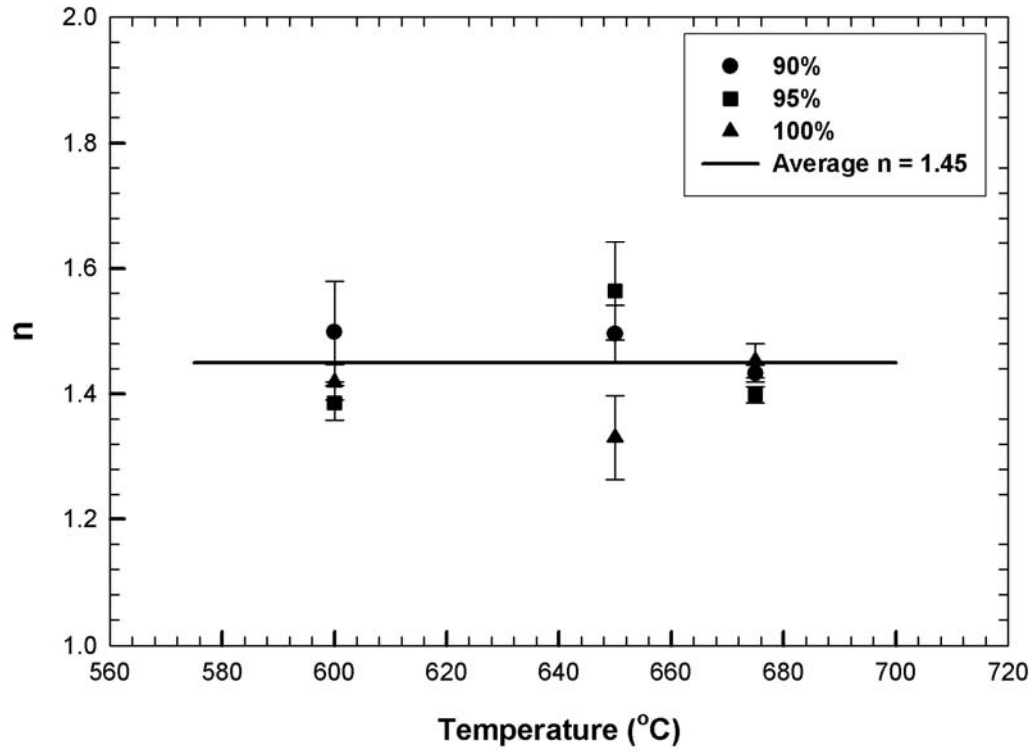

Figure 5: Variation of the Avrami exponent *n* with transformation temperature.

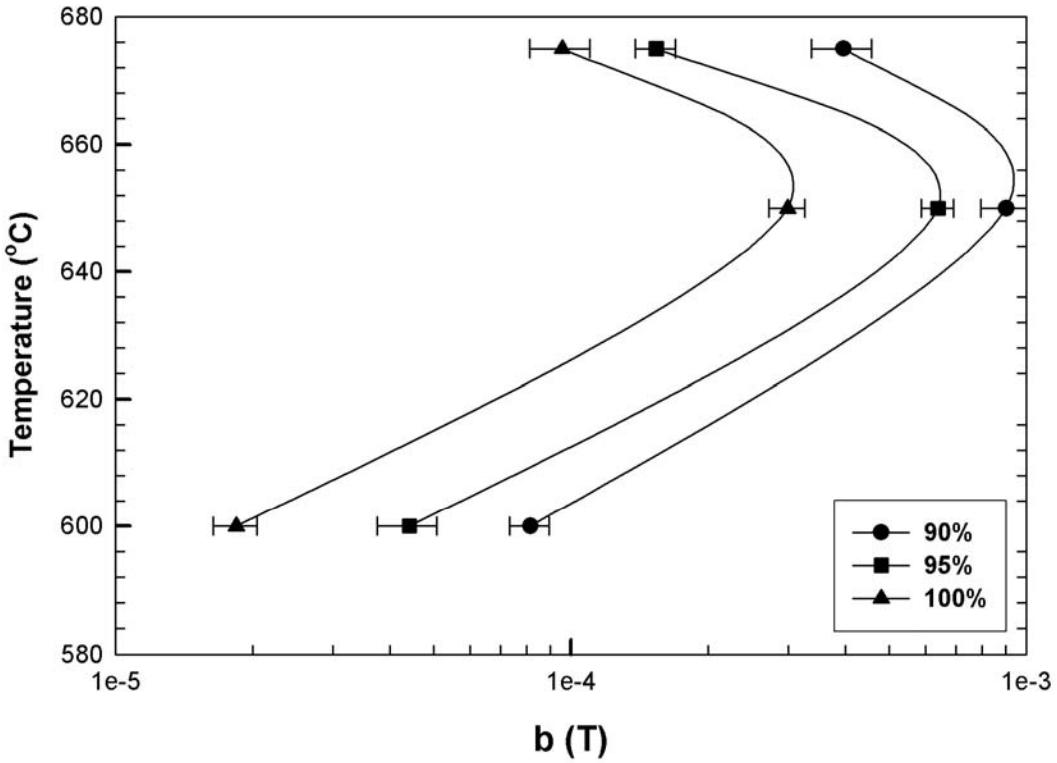

Figure 6: Variation of the Avrami constant *b* with transformation temperature.

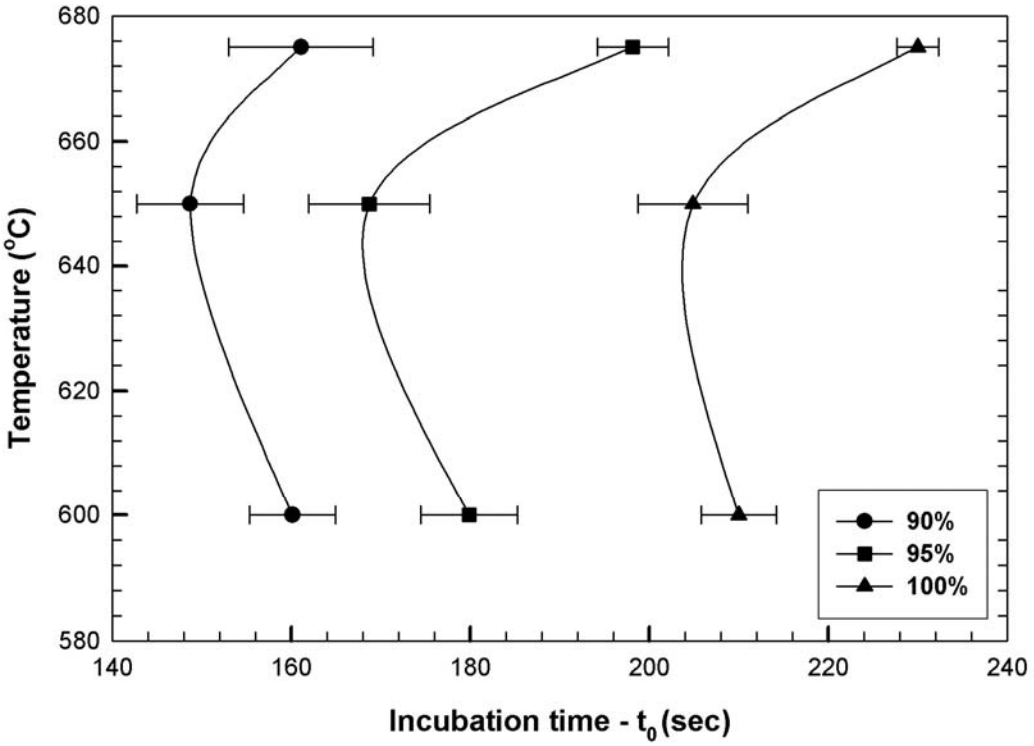

Figure 7: Variation of the incubation time with transformation temperature.

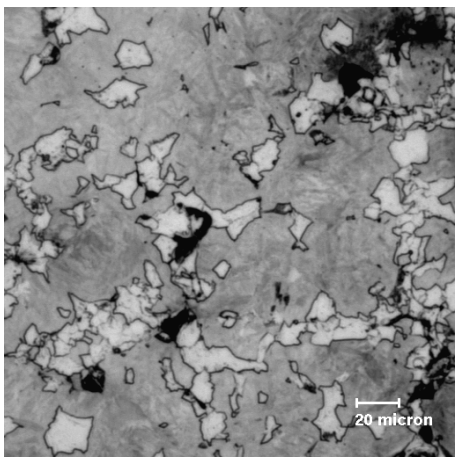

(a)

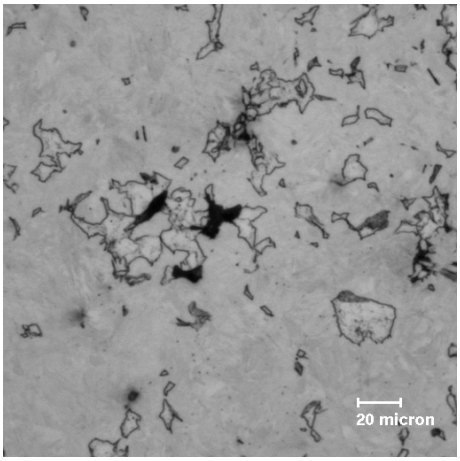

(b)

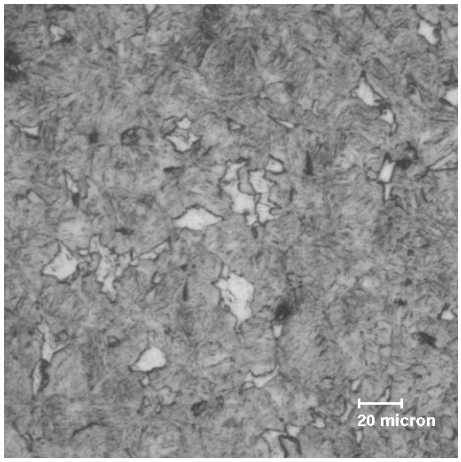

(c)

Figure 8: Optical micrographs from specimens interruptedly quenched from 650ºC after 900 seconds showing ferrite particles (white) in a martensitic background. (a) 90% dense specimen, (b) 95% dense specimen, and (c) 100% dense specimen.

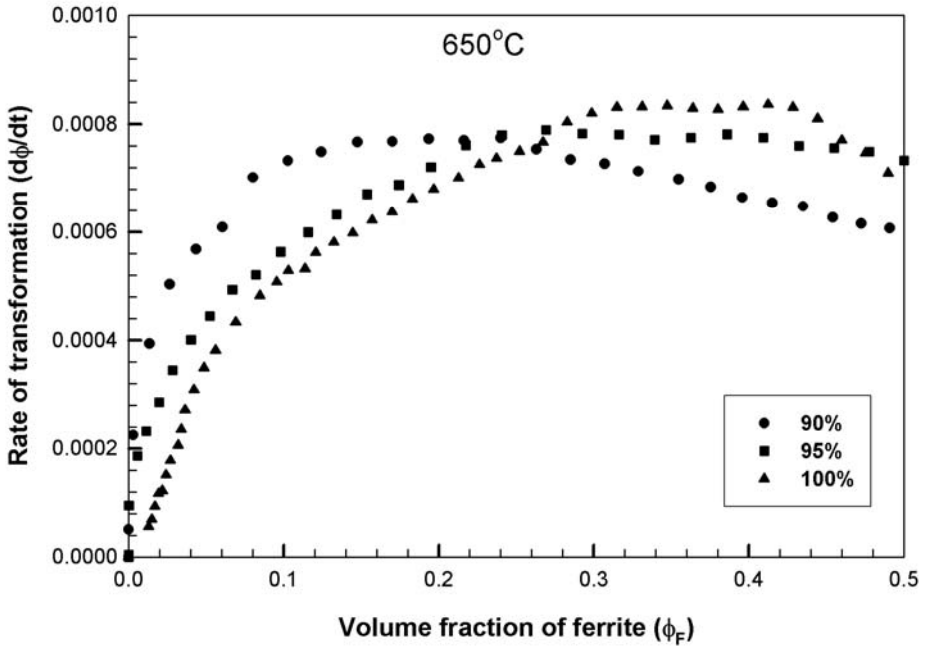

Figure 9: Variation of the austenite to ferrite transformation rate with volume fraction of ferrite at 650ºC.

3.4 SUMMARY AND CONCLUSIONS

The effect of porosity on the kinetics of the austenite to ferrite transformation in powder metallurgy steels was experimentally investigated using a high-speed quenching dilatometer. The measurements showed a reduction in the incubation time of the transformation with increased porosity.

Within the explored range of porosity, the dilatometry data nicely fits an Avrami-type equation with average value of $n = 1.45$ independent of temperature and pore fraction of the sample suggesting early site saturation during nucleation, and diffusion controlled growth. Moreover, the Avrami constant, $b(T)$, found to be increasing with increasing porosity implying important role of porosity in the nucleation and/or growth of ferrite. Metallographic measurements on interrupted quench specimens showed that the number of ferrite particles have increased with increasing porosity. Hence, it is most certain that nucleation rate of ferrite has increased due to presence of pores.

Although, average equivalent diameters of ferrite particles were found to be increasing with decreasing porosity in the sample, rate of transformation vs. fraction transformed plot revealed highest initial growth rate in the samples with 90% density.

Findings from this article suggest that, presence of pore in the sample reduces overall stability of the austenite phase, hence reducing the incubation time for the transformation. It was also found that nucleation rate of porosity increases due to presence of the pores, mostly by providing high diffusivity path and nucleation sites. Growth rate of ferrite transformation, before impingement, also increases with porosity naturally implying higher rate of diffusion due to presence of pores.

ACKNOWLEDGEMENTS

The authors gratefully acknowledge the member companies of the Powder Metallurgy Research Center of Worcester Polytechnic Institute for their support of this work. In addition, the authors gratefully acknowledge the High Temperature Materials Laboratory User Program, Oak Ridge National Laboratory managed by UT-Battelle, LLC for the U.S. Department of Energy under contract number DE-AC05-00OR22725 for providing assistance with the dilatometry measurements.

REFERNCES

1. Pustovoit V.N., Churyukin Yu. N., and Blinovskij V.A., *Izv AN SSSR Met*, 1991, **2**, 90.
2. Ermakov S.S., Kukushkin N.N., and Reznikov G.T., *Powder metallurgy materials (journal,)* Kiev: IPM AN USSR, 1976, 56.
3. Ermakov S.S., *Powder metallurgy materials*, Kiev: IPM AN USSR, 1980, 150.
4. Hawbolt E.B., Chau B. and Brimacombe J.K., *Metall. Trans.,* 1985, **16A**, 565.
5. Porter, D.A. and Easterling K.E., *Phase Transformations in Metals and Alloys*, CRC press, 2nd edition, 2001.

CHAPTER 4

The Effect of Porosity on the Austenite to Bainite Transformation in Powder Metallurgy Steels

Virendra S. Warke, Richard D. Sisson, Jr., and Makhlouf M. Makhlouf

ABSTRACT

The effect of porosity on the kinetics of the austenite to bainite isothermal transformation in powder metallurgy steels was characterized using a high-speed quenching dilatometer. The measurements revealed that the presence of porosity shortens the incubation time as well as the overall isothermal transformation time. An Avrami-type equation was fitted to the measured data and the effect of porosity on the nucleation rate of bainite was quantified. In addition, the activation energy for diffusion of carbon atoms during nucleation of bainite was calculated and was found to decrease with increasing porosity.

Keywords: Phase transformations; kinetics; nucleation and growth; Bainite; dilatometry.

4.1 INTRODUCTION

Despite numerous investigations, the effect of porosity on phase transformations in powder metallurgy steels is not yet certain. Indeed there is agreement that the presence of porosity in sintered steels causes a decrease in the Ac1 temperature, an increase in the Ar1 temperature, and, under isothermal conditions, shortening of the incubation time and the overall reaction time [1-3], yet a detailed quantitative understanding of the role that porosity plays in the kinetics of the transformations is still lacking.

The present work focuses on the kinetics of the austenite to bainite transformation in powder metallurgy steels. In these experiments, typical powder metallurgy steel specimens of controlled porosity are austenitized and quenched at very high rates to various isothermal transformation temperatures in a high-speed quenching dilatometer. From the measured specimen dilatation, information on the bainite fraction formed over time is obtained and conclusions regarding the kinetics and the prevailing driving force for the austenite to bainite transformation are drawn. Particular focus of the work is placed on exploring the role that porosity plays in the transformation mechanism. Finally, the transformation kinetics is analyzed quantitatively and the effect of porosity on the activation energy of diffusion of carbon atoms in austenite during the transformation is calculated.

4.2 MATERIALS AND PROCEDURES

AUTOMET 4601 steel powder* was admixed with powdered graphite to yield 0.5-wt% carbon in the final product. Table I shows the chemical composition of the resultant powder.

Table I: Composition of the alloy (in wt.%).

Carbon	Oxygen	Sulfur	Manganese	Molybdenum	Nickel	Iron
0.5	0.11	0.0093	0.196	0.549	1.812	Remainder

Bulk material was produced from this powder in three different densities corresponding to 90%, 95%, and 100% of theoretical density. In order to produce the 90% dense material, the powder was cold-compacted using 690 MPa pressure in a hydraulic press to produce green compacts that

* Manufactured by Quebec Metal Powder Ltd., Quebec, Canada.

were then sintered at 1120°C for 30 minutes under a controlled atmosphere. In order to produce the 95% dense material, the powder was cold-compacted using 690 MPa pressure, but the green compacts were first pre-sintered at 850°C for 30 minutes and then they were re-pressed using 690 MPa pressure and re-sintered at 1120°C for an additional 30 minutes. The 100% dense material was produced by warm-compacting the powder using 690 MPa pressure, heating the resulting compacts to 1150°C, and then forging them in a press using 760 MPa pressure for 10 seconds. Cylindrically shaped specimens for quench dilatometry were machined from specific locations in these bulk materials using an electric discharge machine (EDM). The specimens were 8mm long and 3 mm in diameter.

Quench dilatometry was performed in an MMC high-speed quenching dilatometer* in which the cylindrical specimen is suspended and heated in an induction-heating coil that is enclosed in a vacuum chamber. Measurements were performed at 1×10^{-5} torr and specimen cooling was accomplished by a combination of controlled reduction in the heating current and injection of an inert gas onto the specimen. Dimensional change was measured along the longitudinal axis of the specimen and temperature was measured by means of a Type R thermocouple that was welded to the surface of the specimen midway along its length. Prior to attaching the thermocouple to the specimen, the specimen was de-greased using ethanol and was lightly sanded by means of a 600 grit silicon carbide paper at the point of thermocouple attachment in order to remove any surface oxide and ensure proper connection of the thermocouple to the specimen. The length and diameter of the specimen were measured with a micrometer prior to and after thermal cycling. These measurements were used to verify dimensional changes that occur during thermal cycling. For maximum accuracy, the length change measuring device, i.e., the linear variable differential

* Manufactured by Avenel Inc., NY, USA.

transformer (LVDT), was adjusted so that it did not pass through its natural zero point during thermal cycling.

Each specimen was subjected to a conditioning run before measurements were performed in order to stabilize its position within the apparatus, remove residual stresses, and ensure that each specimen has the same starting microstructure (100% martensite in this case) before characterizing its transformation behavior. This conditioning treatment consisted of heating the specimen to 850°C ±5°C at a nominal rate of 10°C/s, holding the specimen at 850°C for 5 minutes, and then cooling it to room temperature at a cooling rate of 100°C/s.

Each isothermal transformation cycle consisted of heating a specimen to an austenitizing temperature of 850°C ±5°C at a nominal rate of 10°C/s, holding it at this temperature for 5 minutes, and then quenching it to a pre-determined isothermal holding temperature. A cooling rate of at least 80°C/s was used. During quenching, the temperature of the specimen did not undershoot the pre-determined isothermal holding temperature by more than 20°C and it stabilized at the isothermal holding temperature within 2 seconds. The temperature of the specimen was maintained within ±5°C of the isothermal holding temperature while its dimensions were continuously measured until transformation was complete[*]. The specimen was then quenched to room temperature. Data was sampled and recorded at a rate of 50 dimension measurements per second and a different specimen was used for each thermal cycle. Table II shows the design of experiments.

[*] Complete transformation is defined as the time at which maximum dimensional change has occurred.

Table II: Design of experiments.

Density levels	Isothermal holding temperature (°C)	Number of repetitions
3	525	3
3	500	3
3	475	2
3	450	3
3	425	2
3	400	2
3	350	2
3	300	2

Additional specimens were machined from the bulk material and pre-conditioned in a manner similar to that used in the isothermal transformation measurements, namely heating the specimen to 850°C ±5°C at a rate of 10°C/s, holding at this temperature for 5 minutes, and then quenching to the isothermal holding temperature (in this case 350°C) at a cooling rate of 80°C/s, and holding at 350°C for 60 seconds before quenching the specimen to room temperature. These specimens were used for examining the microstructure and so they were sectioned, mounted and polished using standard metallurgical procedures, and etched with a 2% Nital solution.

4.3 RESULTS AND DISCUSSION

Figure 1 shows the typical data collected from dilatometry measurements performed on a 100% dense specimen and it shows the measured linear strain and the measured temperature as functions of time. The measured linear strain was normalized such that zero strain corresponds to the start of the isothermal hold after quenching the specimen from 850°C and the transformation time was normalized such that zero time corresponds to the start of the cooling of the specimen from 850°C. These procedures produced Figure 2. Curves similar to the one shown in Figure 2

were obtained for all conditions depicted in Table II. The linear strain vs. transformation time data was then converted to volume fraction of bainite $\phi(t)$ using Equation (1) [4].

$$\phi(t) = \frac{e(t)}{e_{total}} \tag{1}$$

In Equation (1), $e(t)$ and e_{total} are the instantaneous linear strain at time t and the total linear strain, respectively. Figure 3 shows the change in volume fraction of bainite with isothermal holding time for specimens with 90%, 95%, and 100% of theoretical density.

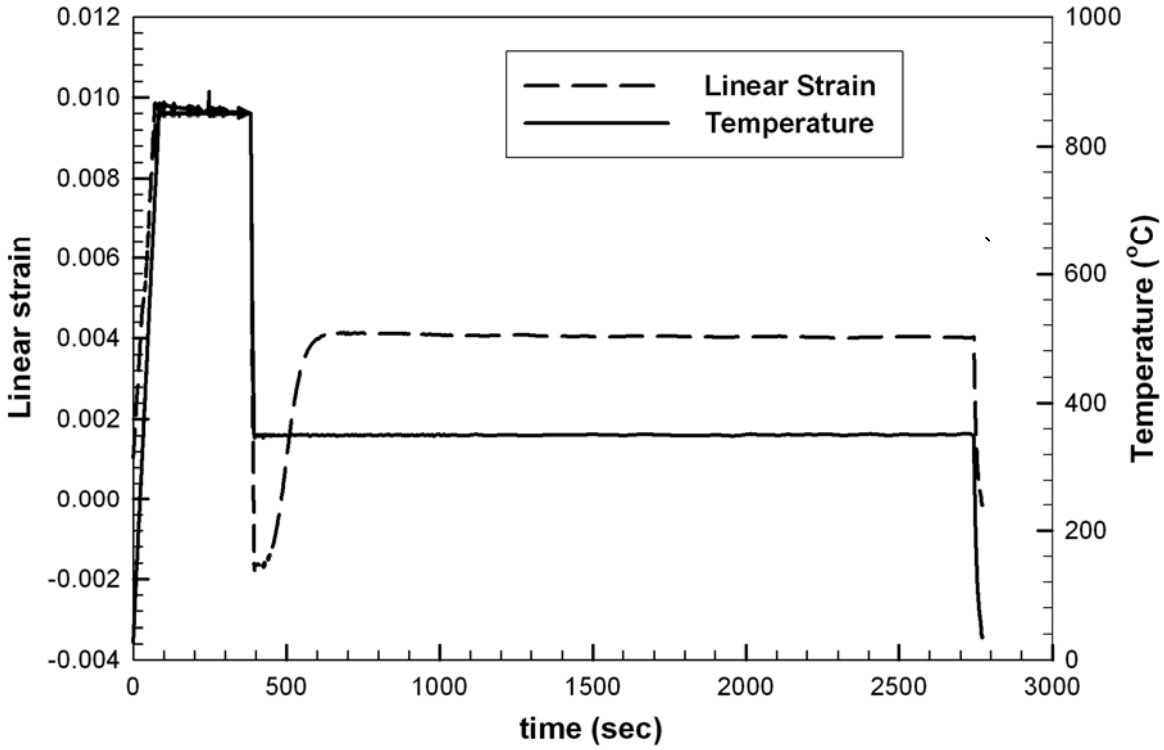

Figure 1: Measured linear strain and temperature as functions of transformation time for the austenite to bainite transformation at 350°C in a 100% dense specimen.

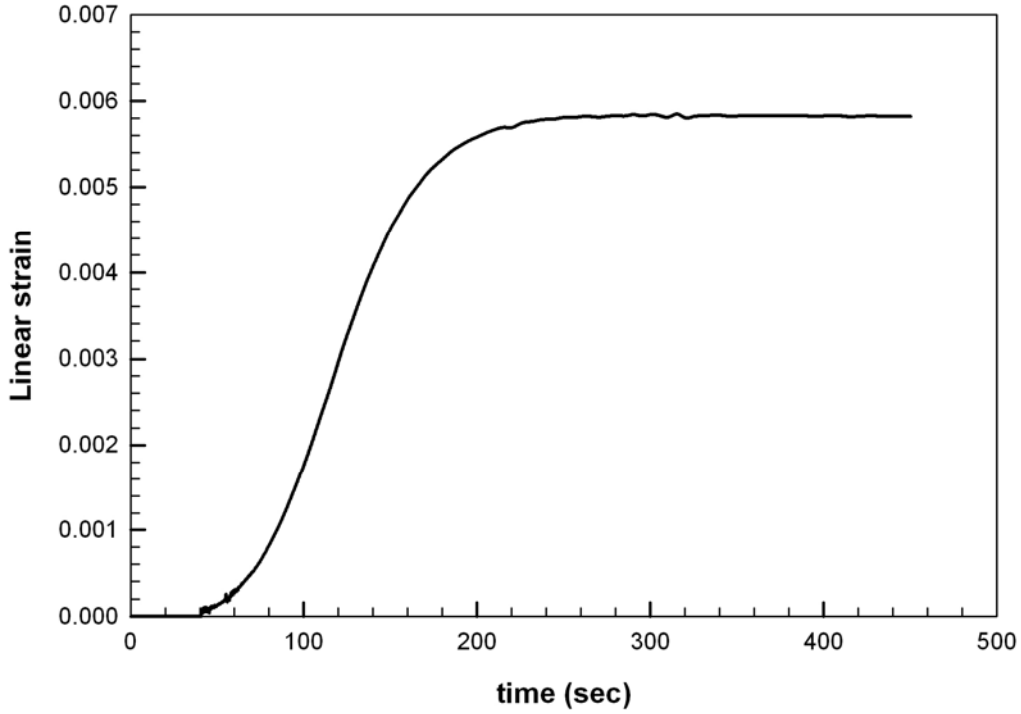

Figure 2: Normalized linear strain vs. time from isothermal transformation measurements performed at 350°C on a 100% dense specimen.

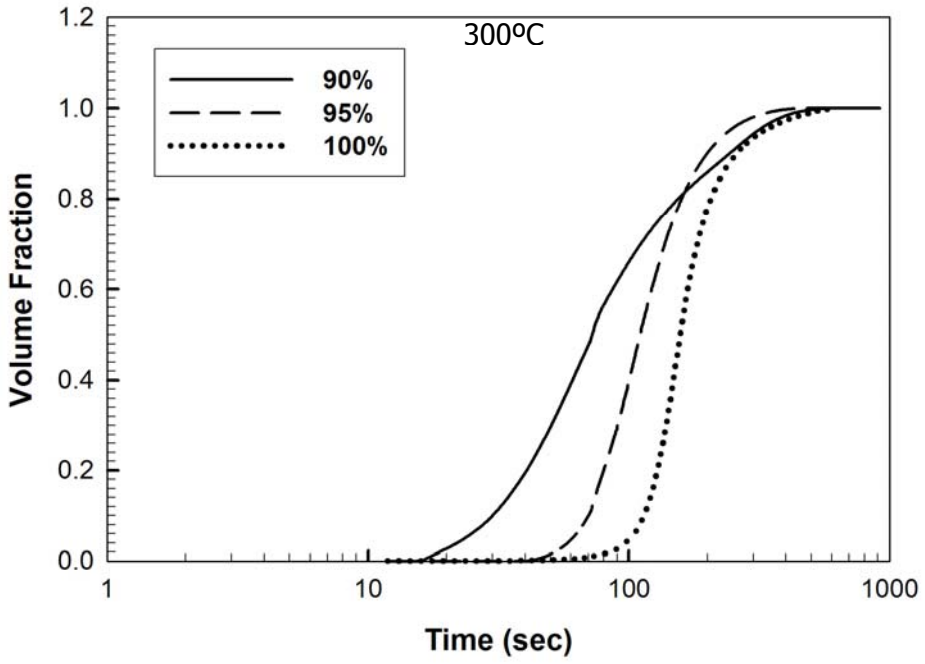

(a)

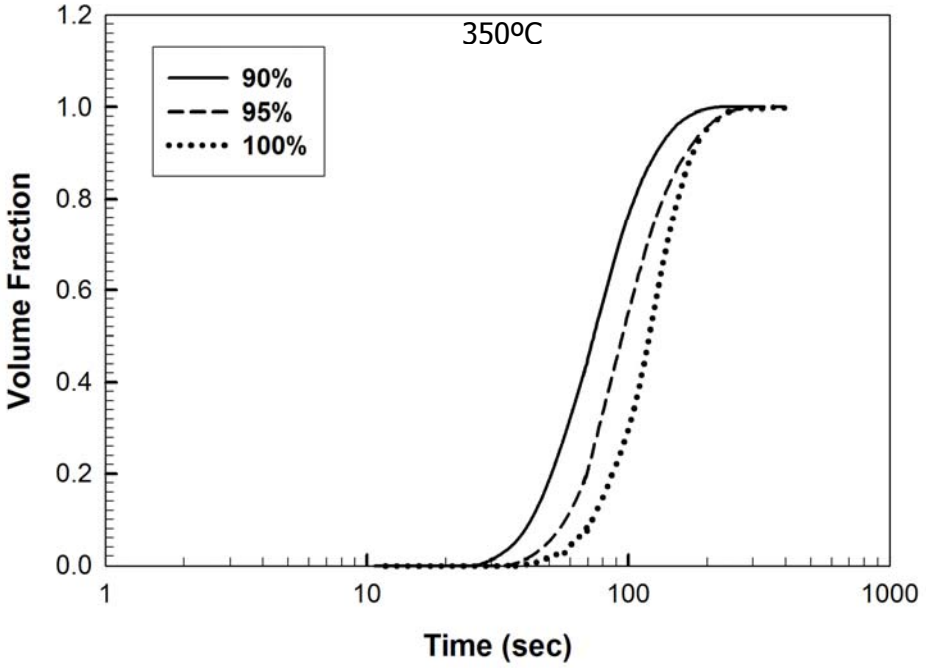
350ºC
90%
95%
100%
Volume Fraction
Time (sec)
0.0
0.2
0.4
0.6
0.8
1.0
1.2
1
10
100
1000

(b)

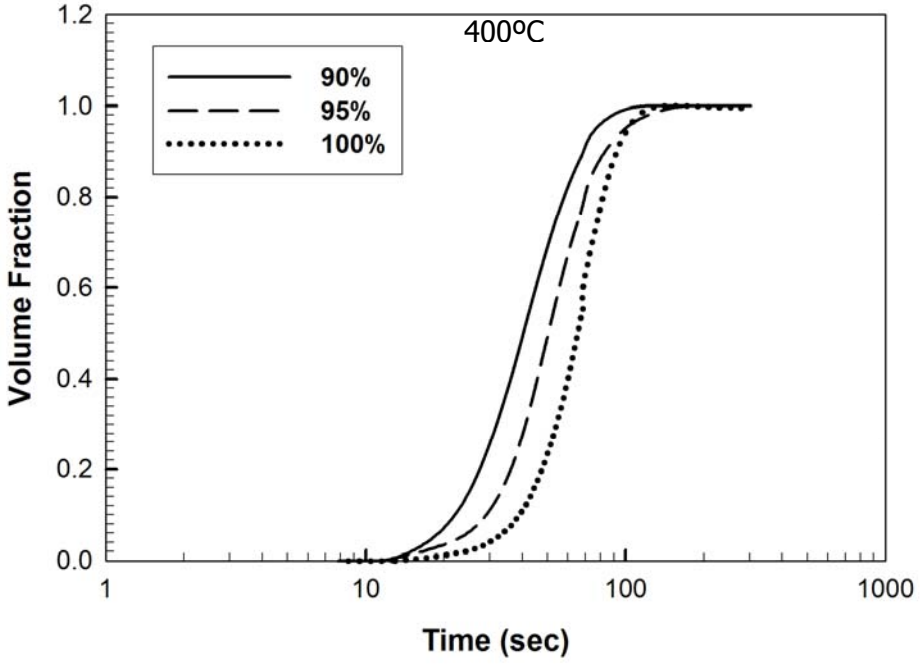
400ºC
90%
95%
100%
Volume Fraction
Time (sec)
0.0
0.2
0.4
0.6
0.8
1.0
1.2
1
10
100
1000

(c)

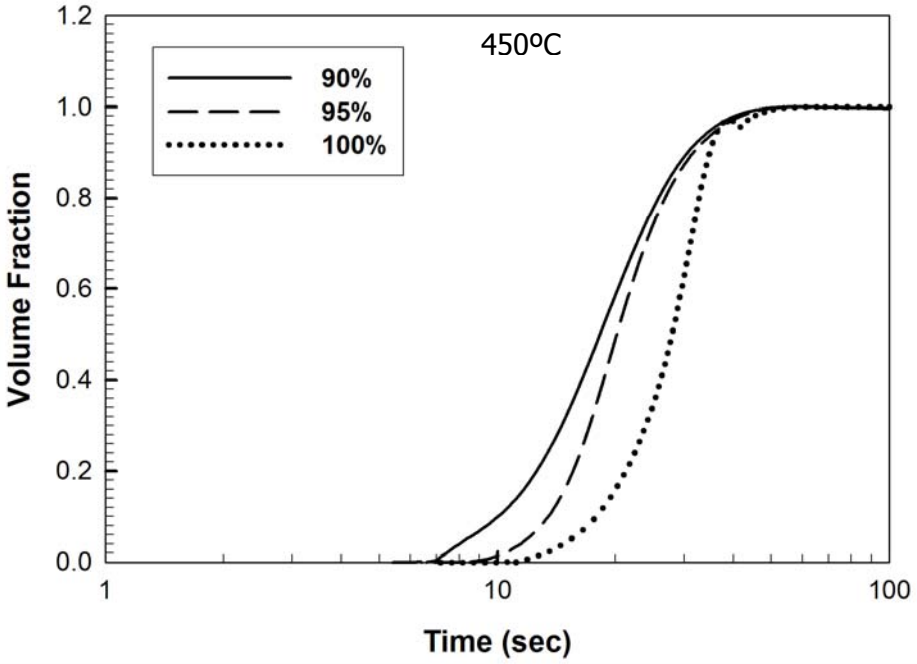
450ºC
90%
95%
100%
Volume Fraction
Time (sec)
0.0
0.2
0.4
0.6
0.8
1.0
1.2
1
10
100

(d)

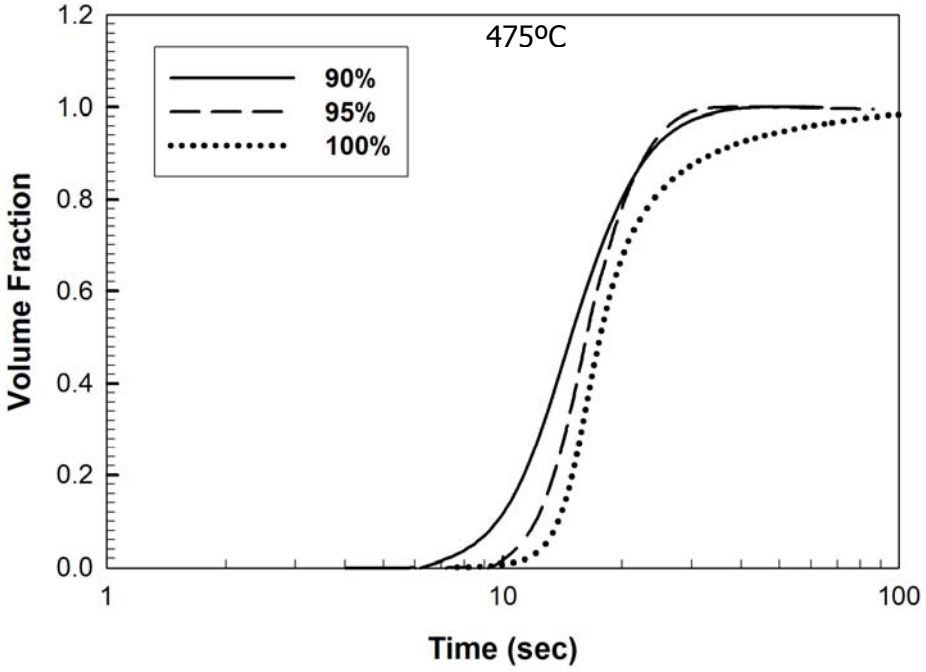
475ºC
90%
95%
100%
Volume Fraction
Time (sec)
0.0
0.2
0.4
0.6
0.8
1.0
1.2
1
10
100

(e)

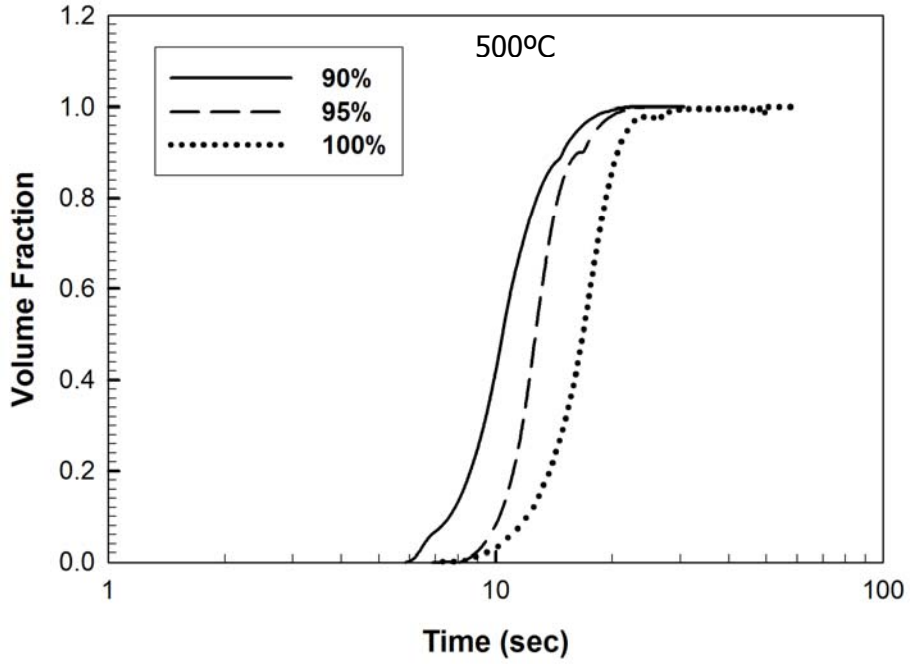

(f)

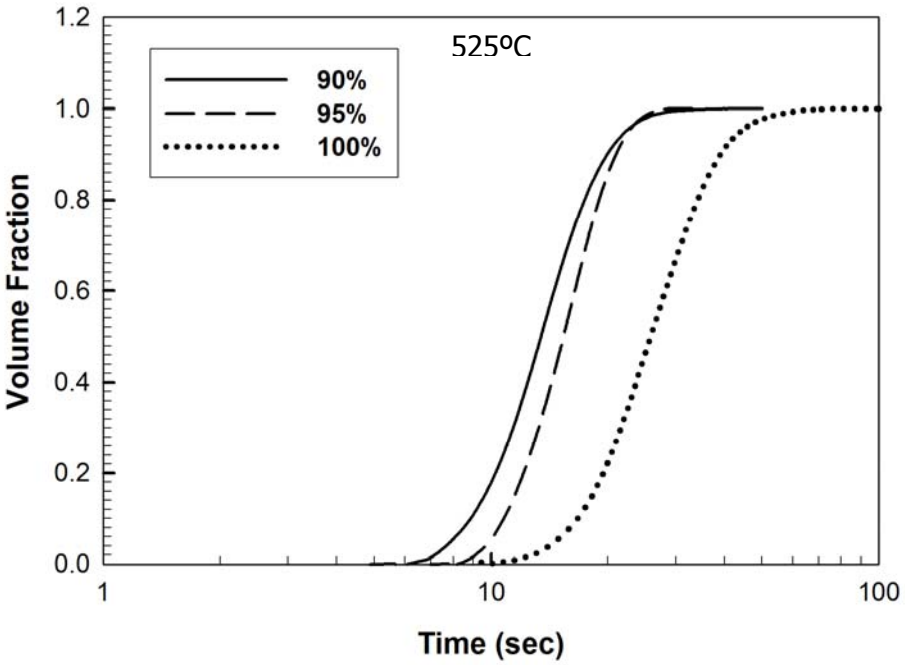

(g)

Figure 3: The change in volume fraction of bainite with isothermal holding time for specimens with 90%, 95% and 100% of theoretical density. (a) Specimen held at 300°C, (b) Specimen held at 350°C, (c) Specimen held at 400°C, (d) Specimen held at 450°C, (e) Specimen held at 475°C, (f) Specimen held at 500°C, (g) Specimen held at 525°C.

The incubation time for the austenite to bainite transformation was extracted from Figure 3 and is presented in Figure 4. The incubation time (t_o) was calculated as the time interval between the start of the cooling of the specimen from 850°C to the start of transformation. It is clear from Figure 4 that the incubation time for the austenite to bainite transformation becomes shorter with increased porosity at all transformation temperatures. This suggests that the presence of porosity in the steel lowers the thermodynamic stability of austenite and favors nucleation of bainite. The micrographs in Figure 5 show that the number of bainite laths that formed during isothermal holding, at 350 °C for 60 seconds, increases with the concentration of pores in the specimen, which also supports the hypothesis that the presence of porosity in the specimen increases the nucleation rate of bainite.

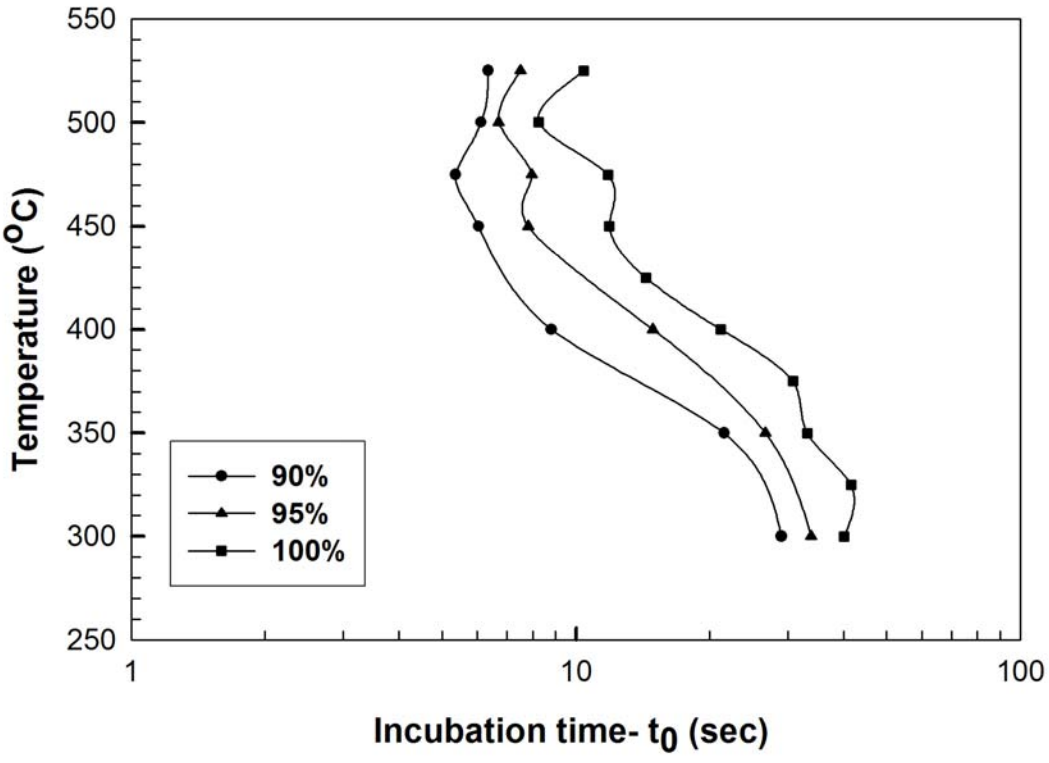

Figure 4: Variation of incubation time with isothermal holding temperature for specimens with 90%, 95%, and 100% of theoretical density.

Assuming that the isothermal transformation of austenite to bainite follows diffusive kinetics, an Avrami-type equation - Equation (2) - was applied to the measured data

$$\phi(t) = 1 - \exp\left[-b(T)(t - t_o)^n\right] \qquad (2)$$

In Equation (2), $\phi(t)$ is the fraction of bainite, n is the transformation mechanism exponent; $b(T)$ is a temperature-dependent parameter whose magnitude depends on the combined nucleation and growth characteristics of the material, and t_o is the incubation time [5]. The method suggested by Hawbolt et al. [6] was used to accurately determine the transformation start time. In this method, t_o is adjusted so as to produce the best fit possible for the parameters $b(T)$ and n. Using this procedure, it was found that n varies between 1.8 and 2.3 over the temperature range explored, and the average value of n is approximately 2, which is in agreement with values of n obtained by other researchers [4]. This finding suggests a constant nucleation rate and one-dimensional linear growth of bainite laths irrespective of the concentration of porosity in the specimen [4].

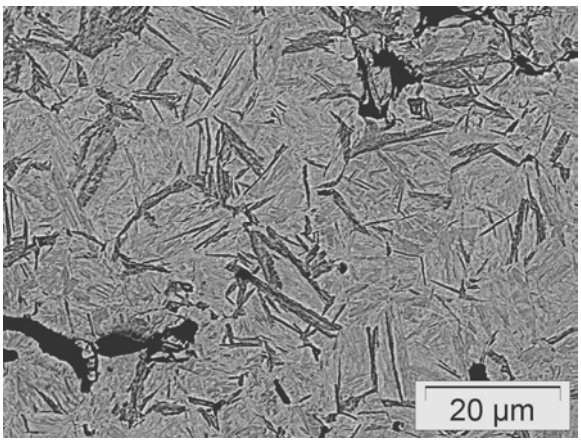

(a)

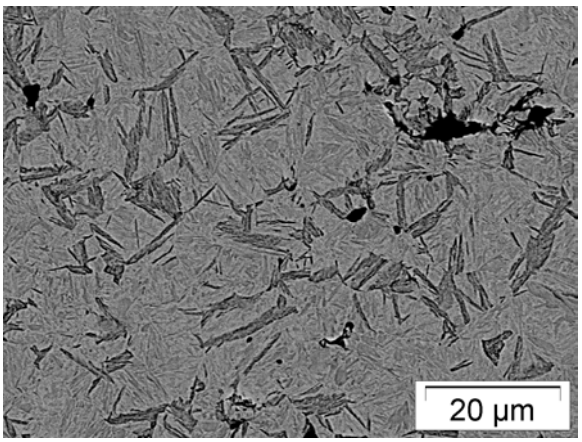

(b)

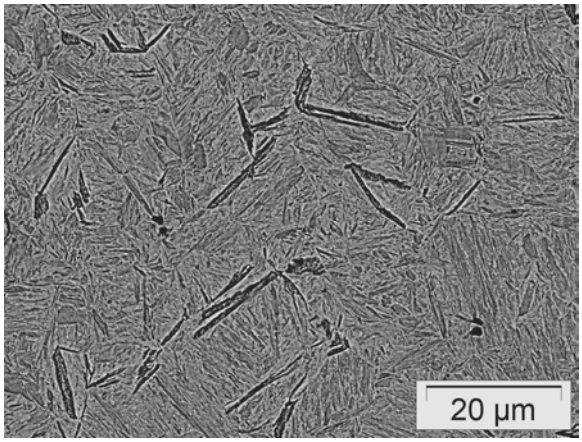

(c)

Figure 5: Backscattered scanning electron micrographs of specimens that were quenched after holding for 60 seconds at 350°C showing bainite laths (dark) with a martensitic background (light) for (a) 90% dense specimen, (b) 95% dense specimen, (c) 100% dense specimen.

In order to characterize the effect of porosity on $b(T)$, Equation (2) was re-fitted to the measured data, but this time while fixing n at $n = 2$. Figure 6 shows the variation of $b(T)$ with isothermal holding temperature for specimens with different density. It is clear from Figure 6 that for a particular transformation temperature, $b(T)$ increases with increasing porosity. Since the magnitude of $b(T)$ depends on the nucleation and growth characteristics of the material, Figure 6 suggests an increase in the bainite nucleation rate and/or bainite growth rate with increasing porosity.

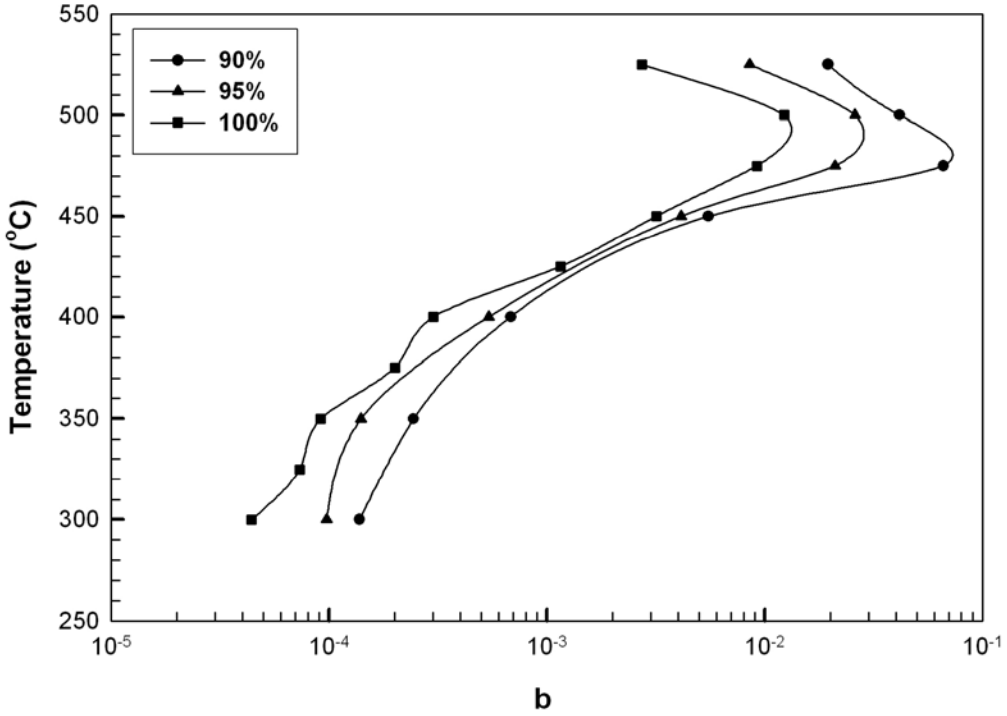

Figure 6: Variation of $b(T)$ with isothermal holding temperature for specimens with 90%, 95%, and 100% of theoretical density.

Table III shows the average length of the longest bainite laths that has grown in 60 seconds at 350°C in specimens with 90%, 95% and 100% of theoretical density. Every entry in Table III is an average of the longest laths measured in each of 25 images similar to those in Figure 5. Based on the measurements shown in Table III and the preceding discussion, it is assumed that porosity influences the nucleation rate of bainite from austenite but does not have a significant effect on its growth rate.

Table III: Average length of the longest bainite laths that grows in 60 seconds at 350°C.

Density (% of theoretical)	Length of the longest bainite laths (μm)		
	Average	Max.	Min.
90	16.29	21.26	10.41
95	16.46	26.60	12.27
100	16.56	21.42	12.04

In order to quantify the effect of porosity on the nucleation rate, Equation (2) is re-written in terms of the nucleation rate, $I(T)$, the growth rate, $G(T)$, and the average thickness of the bainite laths (d) as shown in Equation (3)[4]

$$\phi(t) = 1 - \exp\left(-\pi d^2 I(T) G(T) \left(t - t_o\right)^2\right) \tag{3}$$

Combining Equations (2) and (3) gives

$$b(T) = \pi d^2 I(T) G(T) \tag{4}$$

Rearranging the terms in Equation (4) gives the nucleation rate $I(T)$

$$I(T) = \frac{b(T)}{\pi d^2 G(T)} \tag{5}$$

Values of $b(T)$ from Figure 6 together with the measured values of d and measured growth rates from Quidort et al. [7] were used in Equation (5) to calculate the nucleation rate of bainite in austenite. Figure 7 shows the calculated nucleation rate at each of the isothermal transformation temperatures. Note that for all temperatures up to 475°C, the nucleation rate increases with increasing porosity.

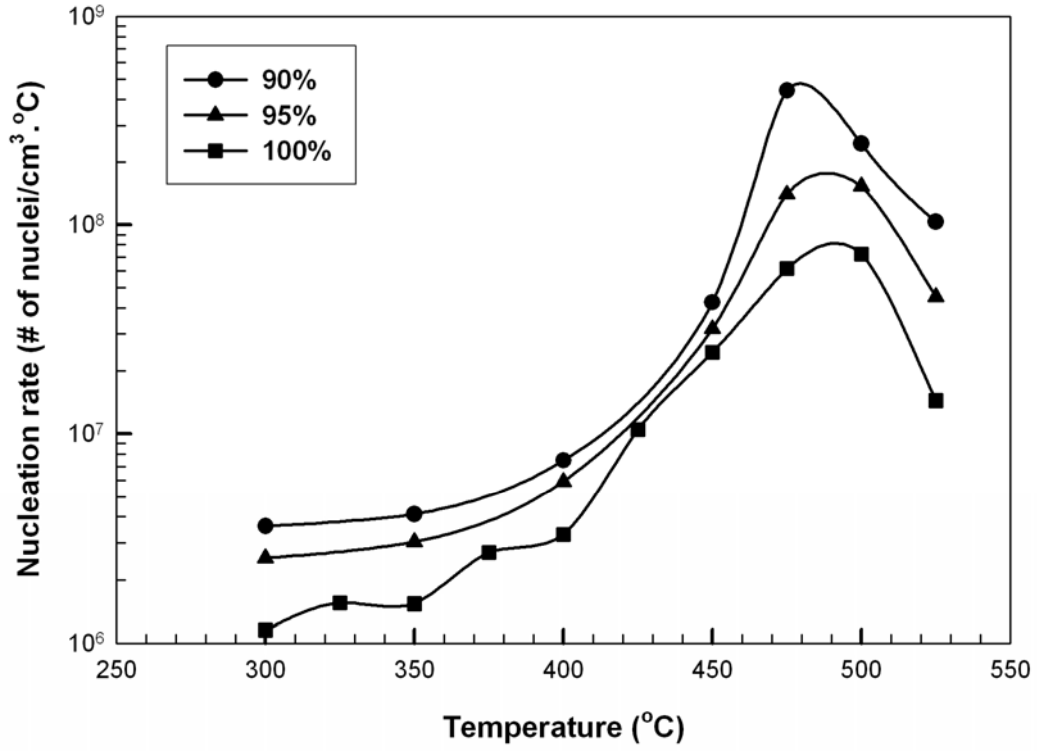

Figure 7: Variation of nucleation rate with isothermal holding temperature for specimens with 90%, 95%, and 100% of theoretical density.

Based on the classical nucleation theory [4], the nucleation rate, $I(T)$, is expressed as

$$I(T) = K \exp\left(-\frac{Q_D}{RT}\right)\exp\left(-\frac{\Delta G^*}{RT}\right) \tag{6}$$

In Equation (6), Q_D is the activation energy for diffusion of carbon atoms in austenite, ΔG^* is the critical free energy required to form a nucleus of bainite, K is a constant, and T is absolute temperature. The first exponential term in Equation (6) reflects the mobility of carbon atoms and the second exponential term reflects the driving force for the transformation. It is well known that at relatively low temperatures the nucleation rate is controlled predominantly by the mobility of carbon atoms [4]. Moreover, Quidort et al. [7] have shown that ΔG^* for the austenite to bainite transformation at any temperature is negligibly small compared to Q_D. Hence, at lower

transformation temperatures, the second exponential term in Equation (6) is assumed negligible to produce Equation (7), which allows calculation of the activation energy for diffusion of carbon atoms in austenite as shown in Figure 8.

$$I(T) \cong K \exp\left(-\frac{Q_D}{RT}\right) \tag{7}$$

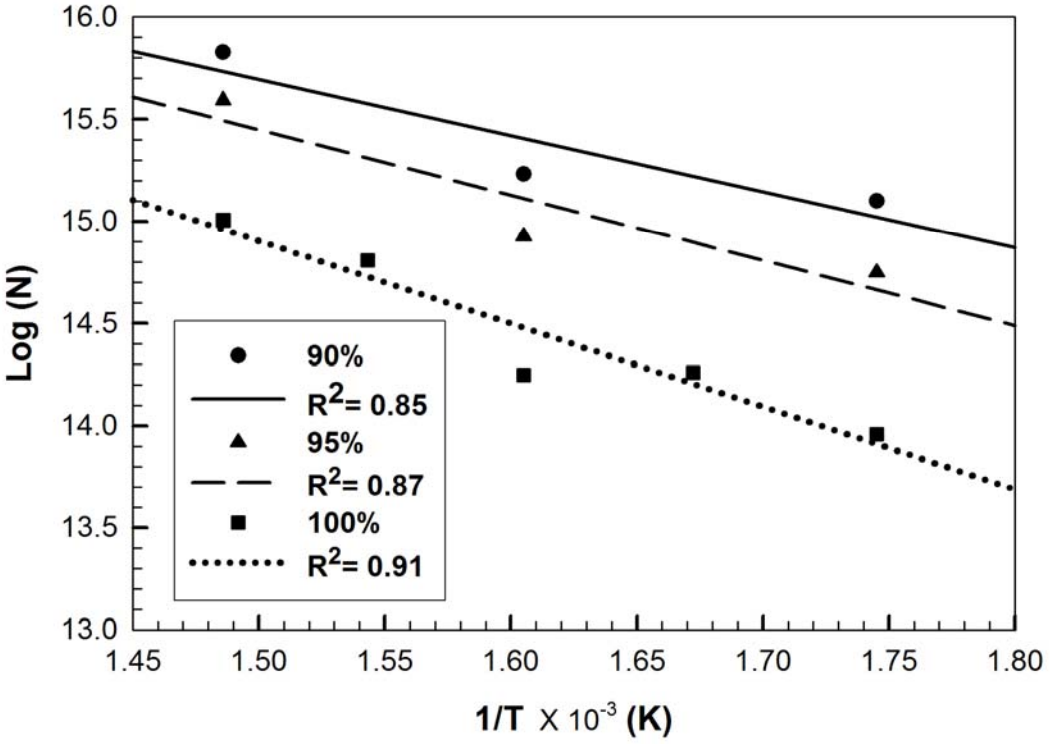

Figure 8: Nucleation rate vs. inverse temperature at low transformation temperatures in specimens with 90%, 95% and 100% of theoretical density.

Table IV shows the calculated activation energy for diffusion of carbon atoms in austenite together with the activation energy for grain boundary diffusion, and bulk diffusion of carbon in austenite. It is clear that porosity provides additional diffusion paths for carbon atoms during nucleation; hence, the overall activation energy for diffusion is reduced with increased porosity.

Table IV: Activation energy for diffusion of carbon in austenite.

	Activation Energy (KJ/mol)
90% of theoretical density	23
95% of theoretical density	27
100% of theoretical density	35
Grain boundary diffusion [8]	47
Bulk diffusion [4,9]	140

4.4 SUMMARY AND CONCLUSIONS

The effect of porosity on the kinetics of the austenite to bainite transformation in powder metallurgy steels was investigated using a high-speed quenching dilatometer. The measurements showed a reduction in the incubation time of the transformation with increased porosity, which suggests an increase in the number of bainite nucleation events with porosity.

Within the explored range of porosity, the dilatometry data nicely fits an Avrami-type equation with $n = 2$ irrespective of the concentration of pores in the material. However, the Avrami constant, $b(T)$, increases with increasing porosity, which suggests that porosity plays a role in the nucleation and/or growth of bainite. Metallographic measurements on quenched specimens showed that the change in the length of the longest bainite laths with porosity is insignificant, which indicates that the growth rate of bainite is independent of porosity.

Using measured growth rate data from Quidort et al. [7], the nucleation rate of bainite and the activation energy for diffusion of carbon atoms in austenite during low temperature isothermal austenite to bainite transformation were calculated for specimens with different concentrations of pores. It was found that the activation energy for diffusion of carbon atoms in austenite decreases with increasing porosity, which suggests that the presence of pores provides additional diffusion

paths for carbon atoms - over and beyond those provided by grain boundaries - and hence the presence of porosity increases the nucleation rate of bainite.

ACKNOWLEDGEMENTS

The authors gratefully acknowledge the member companies of the Powder Metallurgy Research Center of Worcester Polytechnic Institute for their support of this work. In addition, the authors gratefully acknowledge the High Temperature Materials Laboratory User Program, Oak Ridge National Laboratory managed by UT-Battelle, LLC for the U.S. Department of Energy under contract number DE-AC05-00OR22725 for providing assistance with the dilatometry measurements.

REFERENCES

6. Pustovoit V.N., Churyukin Yu. N., and Blinovskij V.A., *Izv AN SSSR Met*, 1991, **2**, 90.
7. Ermakov S.S., Kukushkin N.N., and Reznikov G.T., *Powder metallurgy materials (jounal,)* Kiev: IPM AN USSR, 1976, 56.
8. Ermakov S.S., *Powder metallurgy materials*, Kiev: IPM AN USSR, 1980, 150.
9. Quidort D., and Brechet Y.J.M., *ISIJ Intl.*, June 2002, 1010.
10. Porter, D.A. and Easterling K.E., *Phase Transformations in Metals and Alloys*, CRC press, 2nd edition, 2001.
11. Hawbolt E.B., Chau B. and Brimacombe J.K., *Metall. Trans.,* 1983, **14 A**, 1803
12. Quidort D. and Brechet Y.J.M., *Acta. Metall.*, 2001, **49,** 4161
13. Philibert J, *Diffusion et Transport de Matiere dans les Solides*, Ed. Physique, Paris, 1985, 247.
14. Kaufman L., Radcliffe S. V., and Cohen M., *Decomposition of Austenite by Diffusional Processes*, Interscience, 1962, NY, 313.

CHAPTER 5

A Model for Converting Dilatometric Strain Measurements to Fraction of Phase Formed during the Transformation of Austenite to Martensite in Powder Metallurgy Steels

Virendra S. Warke, Richard D. Sisson, Jr., and Makhlouf M. Makhlouf

ABSTRACT

Quench dilatometry is used extensively to study the transformation kinetics of steels. The method is based on the principle that during heating and cooling of steels, dimensional changes occur as a result of thermal expansion and phase transformation. Sensitive high-speed dilatometers detect and measure these changes in dimensions as functions of time and temperature during a defined thermal cycle. The changes in dimensions are then converted to strains, which in turn are used to determine the start and completion of a phase transformation. Models exist to relate the strain obtained from dilatometric measurements to volume fraction of phases formed. However these models are developed specifically for wrought steels and therefore they cannot account for the significant effect that porosity has on phase transformation. In this publication, we describe a model that allows converting dilatometric strains that occur during the continuous cooling transformation of austenite to martensite to volume fraction martensite formed in powder metallurgy steels. This model can accurately account for the observed decrease in the measured transformation strain with increased porosity.

5.1 INTRODUCTION

Quench dilatometry is used extensively to study the transformation behavior of steels, and the majority of the Time - Temperature - Transformation (TTT) and Continuous Cooling Transformation (CCT) diagrams that are available today were generated using quench dilatometry. The method is based on the principle that during heating and cooling of steels, dimensional changes occur as a result of thermal expansion and phase transformation. Sensitive high-speed dilatometers detect, measure, and record these changes in dimensions as functions of time and temperature during a defined thermal cycle. The changes in dimensions are then converted to strains, which in turn are used to determine the start and completion of phase transformations.

Historically, the conversion of the measured dilatometric strain to volume fraction of phase formed during a phase transformation was performed assuming a linear relationship between the transformation strain and volume fraction of phase formed. This model is often referred to as the Lever Rule model and implicitly assumes that the transformation is essentially complete when maximum strain is reached, usually when cooling has proceeded to room temperature [1]. However, most of the phase transformations that occur in commercial steels do not reach completion upon cooling to room temperature, and often a residual amount of austenite is retained in the steel. More accurate models for converting the transformation strain obtained from dilatometric measurements to volume fraction of phase formed have been recently developed [2-6]. Most of these models are based on converting the measured dilatometric strain to a volume change that is assumed to be caused entirely by the difference in crystal structure between the parent phase (e.g., FCC austenite - γ) and the product phase (e.g., BCT martensite - α'). These models, although more accurate than the Lever Rule model, were developed for the

transformation of γ to pro-eutectoid ferrite and/or pearlite, and specifically for wrought steels. Therefore they cannot account for the significant effect that porosity which may exist in powder metallurgy steels has on the magnitude of the measured dilatometric strain. In this publication, we describe a model that allows converting dilatometric strains that occur during the continuous cooling transformation of austenite to martensite to volume fraction martensite formed in powder metallurgy steels. This model can accurately account for the observed decrease in the measured transformation strain with increased porosity.

5.2 MATERIALS AND PROCEDURES

Production of the Bulk Material

Commercial AUTOMET 4601 steel powder* was admixed with powdered graphite to yield a powder with the chemical composition shown in Table I.

Table I: Composition of the alloy (in wt.%).

Carbon	Oxygen	Sulfur	Manganese	Molybdenum	Nickel	Iron
0.5	0.11	0.0093	0.196	0.549	1.812	Remainder

Bulk material was produced from this powder in three different densities corresponding to 90%, 95%, and 100% of theoretical density. In order to produce the 90% dense material, the powder was cold-compacted using 690 MPa pressure in a hydraulic press to produce green compacts that were then sintered at 1120°C for 30 minutes under a controlled atmosphere. In order to produce the 95% dense material, the powder was cold-compacted using 690 MPa pressure, but the green compacts were first pre-sintered at 850°C for 30 minutes and then they were re-pressed using

* AUTOMET 4601 steel powder is manufactured by Quebec Metal Powder, Ltd., Quebec, Canada.

690 MPa pressure and re-sintered at 1120°C for an additional 30 minutes. The 100% dense material was produced by warm-compacting the powder using 690 MPa pressure, heating the resulting compacts to 1150°C, and then forging them in a press using 760 MPa pressure for 10 seconds. Cylindrically shaped specimens for quench dilatometry measurements were machined from specific locations in these bulk materials using an electric discharge machine (EDM). The specimens were 8mm long and 3mm in diameter.

Generation of the Continuous Cooling Transformation Curves

The continuous cooling transformation curves were obtained by means of a high speed quench dilatometer. Each continuous cooling transformation thermal cycle in the dilatometer consisted of heating a specimen to an austenitizing temperature of 850±5°C at a nominal rate of 10°C/s. The specimen was held at the austenitizing temperature for 5 minutes and then cooled to room temperature at different cooling rates. Data was sampled and recorded at the rate of one dimension measurement per degree Celsius. Linear cooling rates were used to the maximum cooling rate possible.

5.3 RESULTS

Figure 1 shows the dilatometric strain measured in FL-4605 PM steel during its continuous cooling transformation from γ to α'.Each curve in Figure 1 reflects an average obtained from data generated at 3 different cooling rates, namely 40°C/s, 70°C/s, and 180°C/s.

It is important to note that the magnitude of the variation in the martensite start temperature (M_s) due to the different cooling rates is ±3°C, which is within the range of the statistical noise and is

significantly smaller than the magnitude of the variation in M_s caused by porosity, which is about 10°C [7].

The currently available models for converting measured dilatometric strains to volume fraction of phases formed [e.g., 2-6] cannot account for this significant effect of porosity. In the following section we describe a model that allows the accurate conversion of measured dilatometric strains that occur during the continuous cooling transformation of γ into α' to volume fraction α'formed in powder metallurgy steels.

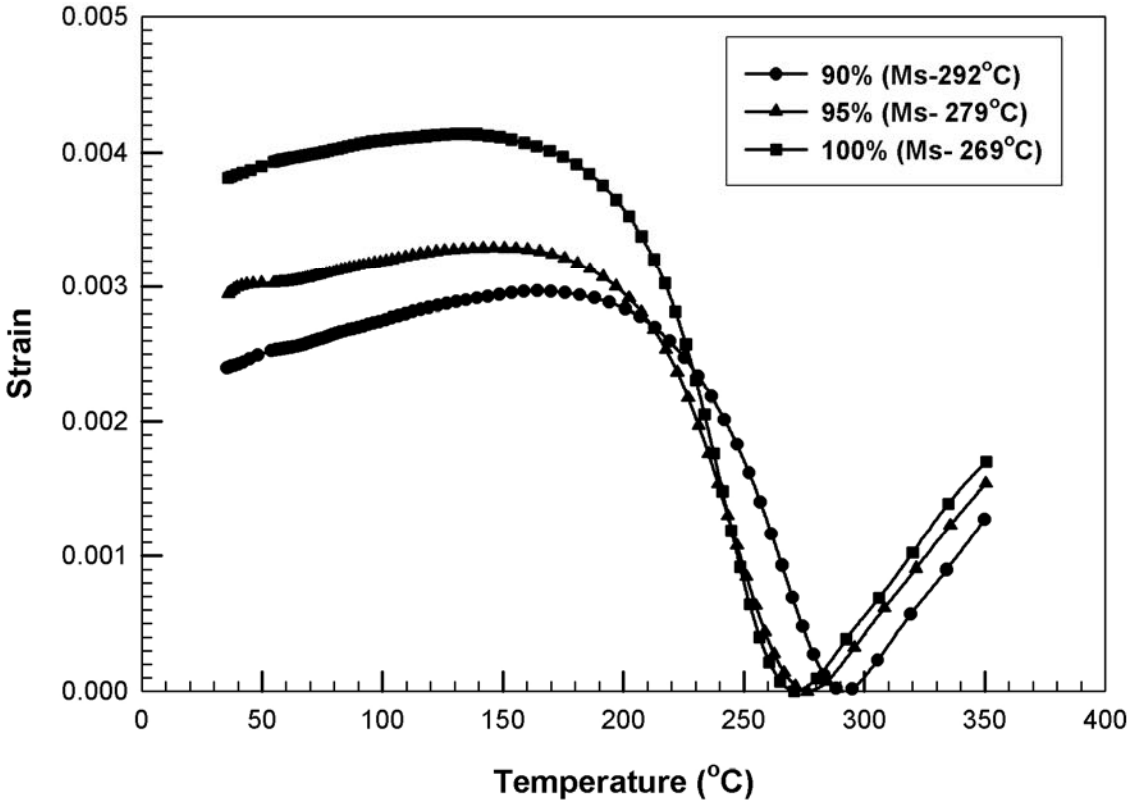

Figure 1: Measured dilatometric strain vs. temperature for FL-4605 PM steel specimens that were pressed and sintered to 90%, 95%, and 100% of theoretical density during the continuous cooling transformation of γ to α'.

5.4 MODEL DEVELOPMENT

The decomposition of γ with an initial atom fraction of carbon C_o into α'during a continuous cooling transformation can be expressed as

$$\gamma(C_o) \rightarrow \alpha'(C_{\alpha'}) + \gamma(C_\gamma) \quad (1)$$

In Eq. (1), $C_{\alpha'}$ and C_γ are atom fraction of carbon in α'and atom fraction of carbon in the remaining γ, respectively. It should be noted however that during the transformation of γ to α', the overall atom fraction of carbon in both phases remains unchanged and is equal to the initial atom fraction of carbon in the steel, namely C_o.

The relative volume change that is measured by the dilatometer during a phase transformation may be related to the specific volume change at the atomic level using the lattice parameters of the different phases that are involved in the transformation [2-6]. Two assumptions are made in order to simplify calculation of the specific volume change at the atomic level. These are: (1) The effect of substitutional alloying elements in the steel on the lattice parameters of γ and α'and on the change in the specific volume at the atomic level during the α' → γ transformation is negligible; and (2) Substitutional alloying elements in the γ and α' lattices can be replaced by iron atoms so that a mass balance can be set up by assuming that only iron and carbon atoms are present at the lattice sites of both γ and α'. The instantaneous specific volume change at the atomic level during the phase transformation may be given by

$$\frac{\Delta V}{V} = \frac{V_{instant} - V_{initial}}{V_{initial}} = \frac{\left(n_{\alpha'}^{Fe}\frac{V_{\alpha'}}{2} + n_{\gamma}^{Fe}\frac{V_{\gamma}}{4}\right) - \left(n_{\gamma_0}^{Fe}\frac{V_{\gamma_0}}{4}\right)}{\left(n_{\gamma_0}^{Fe}\frac{V_{\gamma_0}}{4}\right)} \quad (2)$$

In Eq. (2), $V_{\alpha'}$, V_{γ}, and V_{γ_0} are the unit cell volume for α', instantaneous γ, and initial γ, respectively. Also in Eq. (2), $n_{\alpha'}^{Fe}$, n_{γ}^{Fe}, and $n_{\gamma_0}^{Fe}$ are the number of iron atoms in α', the number of iron atoms in instantaneous γ, and the number of iron atoms in the initial γ, respectively. Expressions for $n_{\alpha'}^{Fe}$, n_{γ}^{Fe}, and $n_{\gamma_0}^{Fe}$ in terms of the initial atom fraction of carbon in the steel (C_o), the volume fraction of α' ($f_{\alpha'}$), and the total number of atoms in the unit cell (N) are given in Table II.

Table II: Expressions for the number of iron and carbon atoms in each phase.

Phase	Number of Fe atoms (n_i^{Fe})	Number of C atoms ($n_{\alpha'}^{Fe}$)
Martensite	$Nf_{\alpha'}(1-C_0)$	$Nf_{\alpha'}C_0$
Instantaneous austenite	$N(1-f_{\alpha'})(1-C_0)$	$N(1-f_{\alpha'})C_0$
Initial austenite	$N(1-C_0)$	NC_0

Substituting the expressions from Table II into Eq. (2) yields

$$\frac{\Delta V}{V} = \frac{2V_{\alpha'}f_{\alpha'} + V_{\gamma}(1-f_{\alpha'}) - V_{\gamma_0}}{V_{\gamma 0}} \tag{3}$$

Assuming that the change in specific length of the dilatometry specimen is one third the change in its specific volume, and replacing the volume of the unit cells by the respective lattice parameters yields

$$\frac{\Delta l}{l} = \frac{2a_{\alpha'}^2 c_{\alpha'} f_{\alpha'} + a_{\gamma}^3(1-f_{\alpha'}) - a_{\gamma_0}^3}{3a_{\gamma_0}^3} \tag{4}$$

From which,

$$f_{\alpha'} = \frac{3\left(\frac{\Delta l}{l}\right)a_{\gamma_0}^3 - a_\gamma^3 + a_{\gamma_0}^3}{2a_{\alpha'}^2 c_{\alpha'} - a_\gamma^3} \tag{5}$$

In Eq. (5), $a_{\alpha'}$ and $c_{\alpha'}$ are the lattice parameters for α', and a_γ and a_{γ_0} are the lattice parameters for γ. The lattice parameter for γ (i.e., a_γ) is given by Eq. (6a) and the dependence of the coefficient of thermal expansion of γ (i.e., β_γ) on porosity is given by Eq. (6b) [8, 9].

$$a_\gamma = (0.36306 + 7.83\times10^{-4} C_\gamma)\{1 + \beta_\gamma (T - 1000)\} \tag{6a}$$

$$\beta_\gamma = (24.9 - 0.5C_\gamma)\times10^{-6} \tag{6b}$$

In Eqs. (6a) and (6b) C_γ is the atom percent carbon in γ, T is absolute temperature, and ρ and ρ_T are the relative density and theoretical density of the steel, respectively. Similarly, the lattice parameters for α' (i.e., $a_{\alpha'}$ and $c_{\alpha'}$) are given by Eq. (7a) and the dependence of the coefficient of thermal expansion of α' (i.e., $\beta_{\alpha'}$) on porosity is given by Eq. (7b) [8, 9].

$$\begin{aligned} a_{\alpha'} &= (0.28610 + 0.0025855\, C_{\alpha'})\{1 + \beta_{\alpha'}(T - 273)\} \\ c_{\alpha'} &= (0.28610 - 0.0002898\, C_{\alpha'})\{1 + \beta_{\alpha'}(T - 273)\} \end{aligned} \tag{7a}$$

$$\beta_{\alpha'} = \left(14.9 - 1.9C_{\alpha'}\right)\times10^{-6} \tag{7b}$$

In Eqs. (7a) and (7b), $C_{\alpha'}$ is the atom percent carbon in α', T is absolute temperature, and ρ and ρ_T are the relative density and theoretical density of the steel, respectively.

In order to account for the decrease in measured dilatometric strain with increased porosity, the term $K(\phi)^{\frac{1}{3}} f_{\alpha'}$ is introduced into Eq. (4) to yield Eq. (8). $K(\phi)^{\frac{1}{3}} f_{\alpha'}$ is an empirically determined term that may be thought of as compensation for the loss of strain into the pores during the transformation of γ into α'.

$$\frac{\Delta l}{l} = \frac{2a_{\alpha'}^2 c_{\alpha'} f_{\alpha'} + a_{\gamma}^3 (1 - f_{\alpha'}) - a_{\gamma_0}^3}{3a_{\gamma_0}^3} - K\phi^{\frac{1}{3}} f_{\alpha'} \tag{8}$$

Eq. (8) may be rearranged to yield the volume fraction α', $f_{\alpha'}$

$$f_{\alpha'} = \frac{3\left(\frac{\Delta l}{l}\right)a_{\gamma_0}^3 - a_{\gamma}^3 + a_{\gamma_0}^3}{2a_{\alpha'}^2 c_{\alpha'} - a_{\gamma}^3 - 3Ka_{\gamma_0}^3 \phi^{\frac{1}{3}}} \tag{9}$$

In Eqs. (8) and (9), K is an empirical constant and ϕ is the percent porosity in the steel.

Determination of the Empirical Constant K

Most of the phase transformations that occur in commercial steels do not reach completion upon cooling to room temperature and a residual amount of γ often remains in the steel. The standard x-ray diffraction method for estimating the amount of retained austenite ($f_{\gamma\text{ - retained}}$) in quenched steels [10] is used to calculate the amount of $f_{\gamma\text{ - retained}}$ in specimens with varying degrees of porosity. Such data is shown in Table III for FL-4605 PM steel. The magnitude of K is obtained by an iterative process in which K in Eq. (9) is iteratively increased from an initial small value. At the end of each iterative step, the resulting $f_{\alpha'}$ is used to calculate $f_{\gamma\text{ - retained}}$. This computed $f_{\gamma\text{ - retained}}$ is then compared to $f_{\gamma\text{ - retained}}$ measured by x-ray diffraction and the process is repeated until the measured and calculated $f_{\gamma\text{ - retained}}$ converge.

Table III: Amount of retained austenite in FL-4605 PM steel specimens. $I_{\alpha'}$ and I_{γ} are the measured intensities of the 200-002 α' and 200 γ peaks, respectively.

Density (% of theoretical)	Measured Intensity		Calculated Intensity		$f_{\gamma\text{ - retained}}$ (%)
	$I_{\alpha'}$	I_{γ}	$R_{\alpha'}$	R_{γ}	
90	854	101	22.2468	35.4884	2.92
95	796	178	22.2468	35.4884	5.16
100	998	302	22.2468	35.4884	8.70

By using this method, the empirical constant K for FL-4605 PM steel is found to be 0.0009. This value of K is not obtained from the average curves presented in Figure 1, but rather from individual strain vs. temperature curves obtained by dilatometry measurements performed at each cooling rates for each porosity level. Hence, K is independent of porosity and cooling rate. Figure 2 is obtained using the data in Fig. 1 and Eq. (9) with $K = 0.0009$ and shows the volume fraction of α' as a function of temperature for FL-4605 PM steel.

Figure 3 is obtained also by using the data in Fig. 1, but instead of using Eq. (9), Eq. (5), which does not account for the effect of porosity, is used. Notice that in this case the correct effect of porosity on $f_{\gamma\text{ - retained}}$ is lost. Table IV shows that $f_{\gamma\text{ - retained}}$ calculated from dilatometric strain measurements using Eq.(5) is quite different from $f_{\gamma\text{ - retained}}$ measured using x-ray diffraction while $f_{\gamma\text{ - retained}}$ calculated using Eq. (9) is much closer to $f_{\gamma\text{ - retained}}$ measured using x-ray diffraction.

Table IV: Amount of retained austenite in FL-4605 PM steel specimens.

Density (% of theoretical)	Retained austenite (%)		
	Not corrected for effect of porosity	Corrected for effect of porosity	From x-ray diffraction
90	15.9	2.75	2.9
95	12.7	5.78	5.2
100	9.8	9.8	8.7

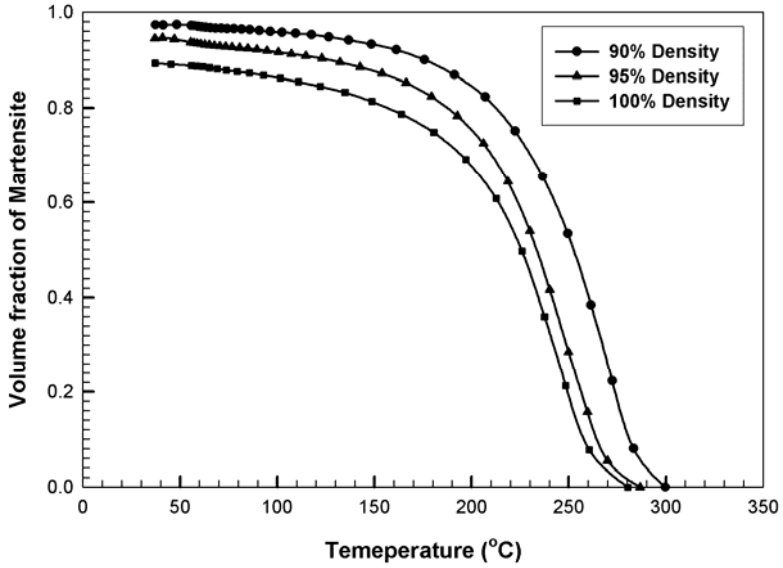

Figure 2: Volume fraction of α' vs. temperature for FL-4605 PM steel specimens during continuous cooling transformation of γ to α' calculated with correction for the effect of porosity on measured dilatometric strain.

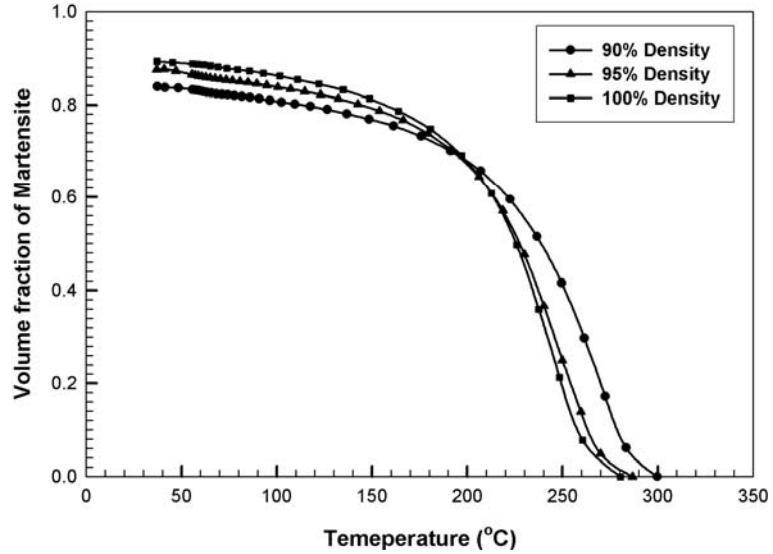

Figure 3: Volume fraction of α' vs. temperature for FL-4605 PM steel specimens during continuous cooling transformation of γ to α' calculated without correction for the effect of porosity on measured dilatometric strain.

5.5 SUMMARY AND CONCLUSIONS

Measurements during the continuous cooling transformation of austenite to martensite in powder metallurgy steels show a significant increase in the martensite start temperature (M_s) and a decrease in the measured dilatometric strain with increased porosity. The currently available models for converting dilatometric strains to volume fraction of transformed phase during continuous cooling transformations cannot account for these effects of porosity. A new model was thus developed to allow accurate conversion of measured dilatometric strain vs. temperature data to volume fraction of martensite vs. temperature. The term $K\phi^{\frac{1}{3}} f_{\alpha'}$ is introduced to account for the decrease in the measured strain with increased porosity. In this term, K is an empirically determined constant and ϕ is percent porosity. X ray diffraction measurements and data fitting routines allow determination of K for any given steel. As a demonstration, the model is used to accurately calculate the volume fraction of martensite formed during the continuous cooling transformation of austenite to martensite in FL-4605 PM steel.

ACKNOWLEDGEMENTS

The authors gratefully acknowledge the member companies of the Powder Metallurgy Research Center of Worcester Polytechnic Institute for their continued support. The authors also gratefully acknowledge the High Temperature Materials Laboratory User Program, Oak Ridge National Laboratory managed by UT-Battelle, LLC for the U.S. Department of Energy under contract number DE-AC05-00OR22725 for assistance with dilatometry measurements.

REFERENCES

1. Atkins M, "*Atlas for Continuous Cooling Transformation Diagrams,*" ASM International, 1980, 223-238.
2. Onink M et al., *Z. Metallkd.*, 1996, **87**, 24-32.
3. Choi S, *Material Science and Engineering A*, 2003, **363**, 72-80.
4. Kop TA, Sietsma J, and Van Der Zwaag S., *Journal of Materials Science*, 2001, **36**, 519-526.
5. Takahashi M, and Bhadeshia HK, *Journal of Materials Science Letters*, 1989, **8**, 477-478.
6. Lee SJ, Lusk M. T, and Lee YK, *Acta Mater.*, 2007, **55**, 875-882.
7. Warke VS, Ph.D. Thesis, Worcester Polytechnic Institute, Worcester, MA, 2007.
8. German RM, *Powder Metallurgy of Iron and Steel,* John Willey and Sons, Inc., 1998, 373-404.
9. German RM, *Powder Metallurgy Science,* Metal Powder Industries Federation, Princeton, NJ, 384.
10. ASTM Standard E975-84, "*Standard Practice for X-Ray Determination of Retained Austenite in Steel with Near Random Orientation,*" 1989.

CHAPTER 6

Effect of Porosity on the Quenching Heat Transfer Characteristics of Powder Metallurgy Steels

V.S. Warke, Md. Maniruzzaman, R.D. Sisson, Jr., and M.M. Makhlouf

ABSTRACT

The quenching heat transfer coefficient of FL-4605 PM steel with two different levels of porosity was measured and the role that porosity plays during quenching of powder metallurgy steels was characterized. It is found that surface pores tend to break the liquid vapor blanket that forms on the surface of the steel during nucleate boiling. In addition, pores act as sites for nucleation of bubbles during nucleate boiling, which agitate the liquid near the metal's surface. Moreover, if the pores become interconnected, quenching liquid may be absorbed through them into the bulk of the metal. These factors combine to enhance the overall rate of heat extraction from the steel and increase its average quenching heat transfer coefficient.

6.1 INTRODUCTION

Powder metallurgy (PM) components experience considerable changes during heat treatment that include changes in their mechanical properties, dimensions, magnitude and sense of residual stresses, and metallurgical phase composition. Since the quality assurances criteria that heat-treated PM components must meet include prescribed minimum mechanical properties and compliance with dimensional tolerances, it is necessary for PM producers to be able to

accurately predict these changes in order to take appropriate measures to prevent their harmful effects and insure the production of good quality parts. Towards that end, Warke et al [1] developed a finite element-based model that predicts the response of powder metallurgy steels to heat treatment. However, even the most sophisticated software uses fundamental laws of heat flow in order to numerically simulate the heat transfer process. Consequently, the accuracy of the model predictions depends on the accuracy of the boundary conditions, initial conditions and material property data that is used in the heat flow formulations. While the material property data is relatively easy to determine, and the initial conditions are usually known, the boundary conditions between a metal part and the quenching medium, i.e., the quenching heat transfer coefficients, are not - because they depend on many factors, including the initial conditions, the geometry and the surface condition of the part, as well as the chemical composition of the part and the quenching medium. Nevertheless, and because of the critical nature of the quenching heat transfer coefficient in computer simulations, a considerable amount of research has been devoted to determining its magnitude for many wrought metals and alloys [2-5]. However, quenching heat transfer coefficients for PM alloys and the effect of pores that invariably exist in PM components on the transfer of heat have not been addressed. Hence, the objective of this work has been to develop a method by which heat-transfer coefficients can be accurately calculated for use in simulations of industrial quenching of porous PM components, and to understand the effect of porosity on the heat transfer characteristics of these alloys during their quenching into cold liquids.

6.2 BACKGROUND

Heat transfer during quenching of a hot metal part in a relatively cold liquid is controlled by several distinct mechanisms that correspond to easily identifiable regions on a temperature vs. time plot similar to the one shown in Figure 1[4, 5]. Upon immersion into the cold liquid, the part becomes surrounded by a vapor film. Heat transfer in this range, which extends from point A to point B in Figure 1, occurs by "film boiling". During film boiling, the rate of heat transfer is small and heat is transferred from the part mainly by radiation. As the part cools between points B and C, the vapor film becomes unstable and "transition boiling" becomes the operative mechanism where the surface of the part becomes covered with alternating layers of vapor and liquid. The onset of this regime is known as the Leidenfrost point [6]. With further drop in temperature, the heat flux from the part steadily increases and eventually reaches a maximum, which is known as the critical heat flux (CHF). This is point C in Figure 1. Between points C and E heat transfer occurs by "nucleate boiling". With even further decrease in temperature, the partial vapor films break down into numerous bubbles and the liquid contacts the part directly. At this point, the liquid near the hot surface of the part becomes superheated and evaporates forming gas bubbles wherever there are nucleation sites on the surface of the metal, e.g., pits or scratches. The gas bubbles transport the latent heat of the phase change and increase heat transfer by agitating the liquid near the surface of the part. Accordingly, the rate of heat transfer in this region is relatively high. It is possible to further divide the nucleate boiling regime into two sub-regimes. These are the "bulk boiling" sub-regime, which happens in the region between points C and D, and the "local boiling" regime, which happens in the region between points D and E. Bulk boiling is in essence nucleate boiling in a saturated liquid where the gas bubbles do not collapse and leave the hot surface of the metal in the form of jets and columns of bubbles, and

local boiling is nucleate boiling in a sub-cooled liquid where the gas bubbles form at the hot metal surface and condense locally. Finally and when the part has cooled to below the boiling point of the liquid, it continues to cool by "natural convection" until its temperature equilibrates with that of the liquid. Obviously, the number and the average size of pores present on the surface of PM parts have an effect on heat transfer when these parts are quenched. For example, the surface pores may help break the liquid vapor film that forms on the surface of the metal thereby enhancing the heat extraction rate, also the presence of more and larger pores may increase heat extraction in the nucleate boiling regime.

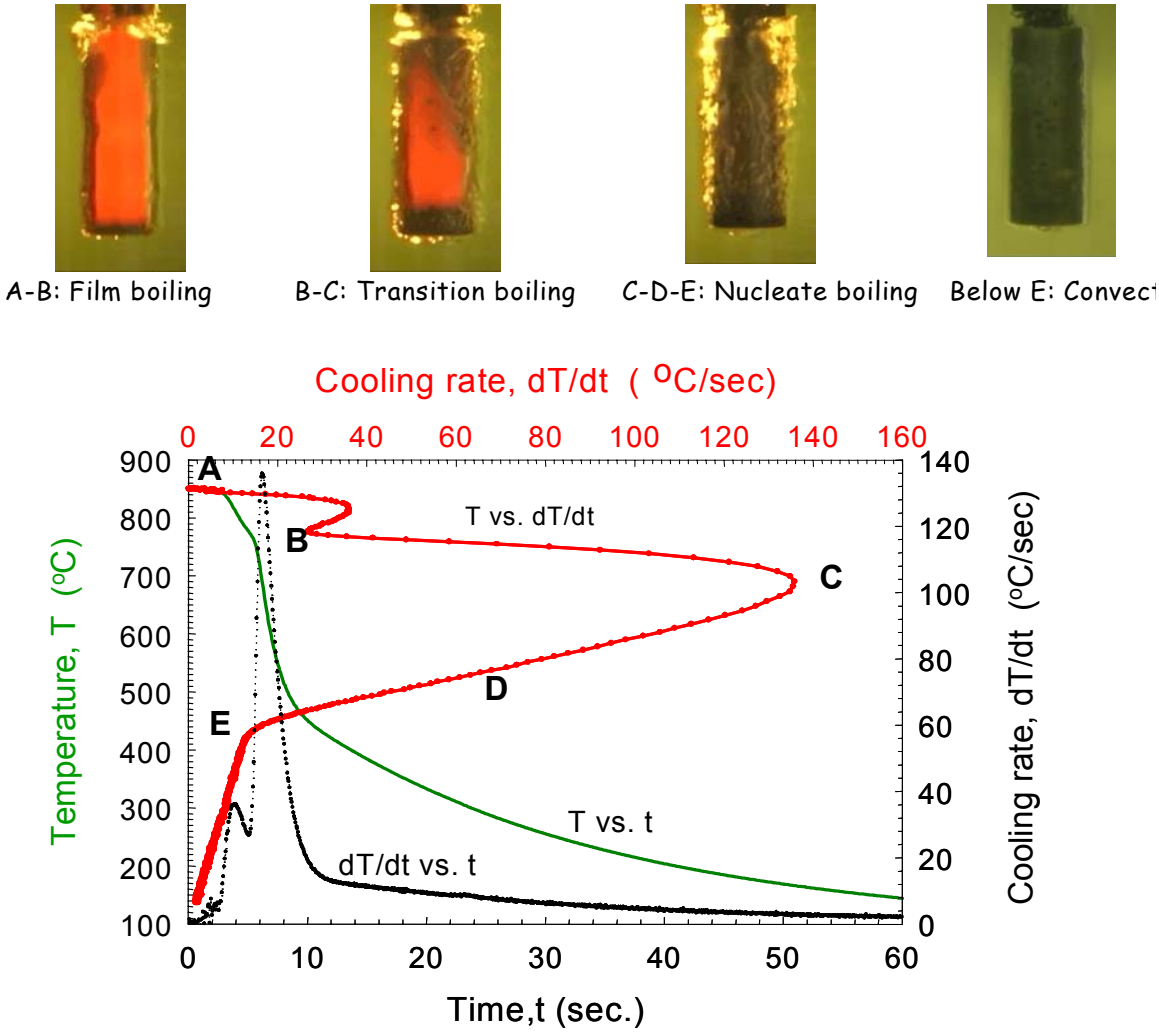

Figure 1: Temperature, cooling rate, time curves for 4140 steel quenched in mineral oil.

In order to characterize the effect of porosity on the quenching heat transfer coefficient of PM steels, the quenching heat transfer coefficient of FL-4605 PM steel samples with two significantly different levels of porosity was measured using the method developed by Sisson et al [5]. In addition, and in order to understand the role that pores play during quenching of PM steels, a "modified" Jominy end-quench test was performed on FL-4605 PM steel parts with similar levels of porosity to the parts used for measuring the quenching heat transfer coefficients.

6.3 MATERIALS AND PROCEDURES

Production of the Bulk Material

AUTOMET 4601 pre-alloyed steel powder[15] was admixed with powdered graphite to yield 0.5 wt. pct. carbon in the final product. Table I shows the chemical composition of the resultant powder.

Table I: Composition of the alloy (in wt.%).

Carbon	Oxygen	Sulfur	Manganese	Molybdenum	Nickel	Iron
0.5	0.11	0.0093	0.196	0.549	1.812	Remainder

Bulk material was produced from this powder in two different densities corresponding to 90% and 95% of the steel's theoretical density (7.81 g/cm^3). In order to produce the 90% dense material, the powder was cold-compacted using 690 MPa pressure in a hydraulic press to produce green compacts that were then sintered at 1120°C for 30 minutes under a controlled

[15] AUTOMET 4601 steel powder is manufactured by Quebec Metal Powders, Ltd., Quebec, Canada.

atmosphere where the carbon potential of the endothermic gas was fixed at 0.5 % Carbon. In order to produce the 95% dense material, the powder was cold-compacted using 690 MPa pressure, but the green compacts were first pre-sintered at 850°C for 30 minutes and then they were re-pressed using 690 MPa pressure and re-sintered at 1120°C for an additional 30 minutes. Table II summarizes the processing steps and dimensions of the bulk materials.

Table II: Processing steps and dimensions of the bulk material.

Density	Manufacturing Process	Dimensions (cm)
90 %	Pressed and sintered	$10.80 \times 10.80 \times 2.54$
95 %	Double pressed and double sintered	$10.80 \times 10.80 \times 2.54$

Procedure for Measuring the Quenching Heat Transfer Coefficient

The method employed for measuring the heat transfer coefficient involves quenching a heated cylindrical probe that is machined from the bulk material into the quenching medium and acquiring the temperature-time profile. The apparatus used for this purpose is shown in Figure 2 and consists of an electric box furnace for heating the probe, a connecting rod that joins the probe to a pneumatic cylinder that allows automatic quenching of the probe into a beaker that contains the quenching oil (in this case Houghton G mineral oil), and a computer connected to a fast data acquisition system. A k-type thermocouple inserted at the geometrical center of the probe continuously measures the temperature of the probe [2-5]. The probe dimensions are chosen such that the Biot number for the quenching process is < 0.1. This requirement insures that significant thermal gradients will not be present in the radial direction of the probe. Accordingly, a simple heat balance analysis (usually referred to as a lumped parameter analysis) can be performed on the system (probe + quenching medium) to yield the quenching heat

transfer coefficient. With Bi < 0.1, the error associated with such calculations of the quenching heat transfer coefficient is less than 5%. A heat balance applied to the probe results in Equation 1, which is used to calculate the average quenching heat transfer coefficient at the surface of the probe [7].

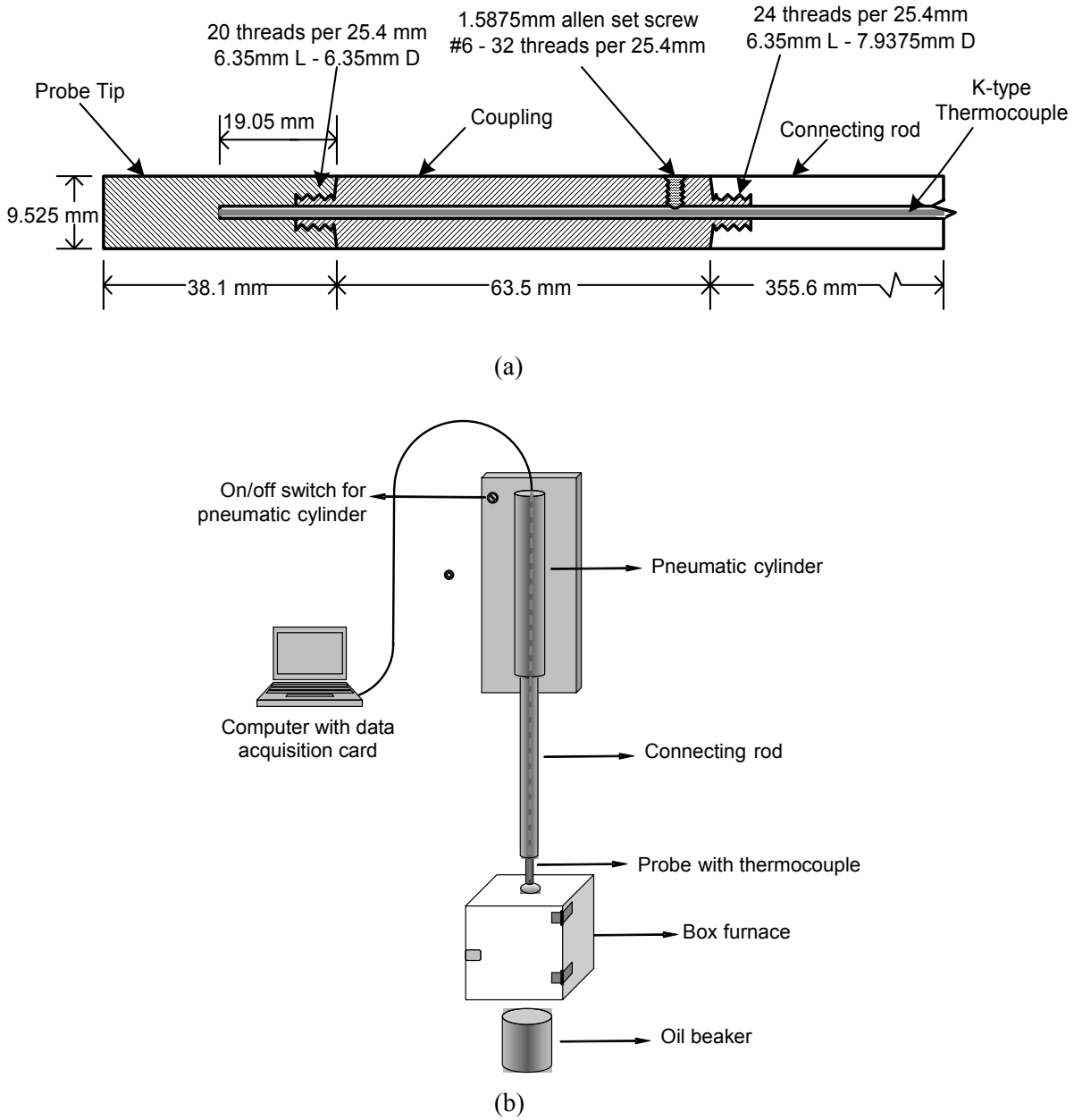

Figure 2: Schematic representation of the apparatus used in measuring the quenching heat transfer coefficient (a) the quenched probe, and (b) the quenching system.

$$\bar{h} = -\frac{\rho V C_p}{A_s\left(T_s - T_f\right)}\frac{dT}{dt} \tag{1}$$

In Equation (1), $\bar{h}$ is the average quenching heat transfer coefficient at the surface of the probe, ρ, V, C_p, and A_s are the density, volume, specific heat, and surface area of the probe, respectively. T_s is the temperature at the surface of the probe, which, because of the insignificant temperature gradient in the radial direction of the probe, is approximately equal to the measured temperature at the center of the probe, and T_f is the bulk temperature of the quenching medium. Two important parameters are needed by Eq. (1). These are the variation of the specific heat of the probe (C_p) with temperature, and the variation of the density of the probe with the amount of porosity, which can be calculated from Eq. (2) and Eq. (3), respectively [8, 9]

$$C_p = -3\times10^{-10}T^4 + 8\times10^{-7}T^3 - 8\times10^{-4}T^2 + 0.4991T + 440.25 \tag{2}$$

$$\rho = \left(1-\varepsilon\right)\rho_O \tag{3}$$

In Eq. (3), ρ_O is the density of the 100% dense steel and ε is the pore fraction.

Procedure for Performing the Modified Jominy End-Quench Test

Jominy end-quench bars that are 2.54 cm in diameter and 10.16 cm in length were machined from the bulk materials shown in Table II. Four holes were machined along the length of each bar as shown schematically in Figure 3 to allow insertion of thermocouples. Two sets of Jominy end-quench bars were prepared. The first set contained as-machined 90% and 95% dense bars, and the second set contained bars similar to those in the first set, but with a 1 mm thick coating of nickel plasma sprayed on the quenching end of each bar. The Ni coating minimizes penetration of water into the bottom of the bars during testing. All bars were polished with 180 grit SiC paper and had similar surface finish, and the Jominy end-quench tests were performed

according to SAE J406 and ASTM A255 standard methods for Jominy end-quench testing. [10-11]. Time vs. temperature data from all four thermocouples were recorded by a high-speed data acquisition system, and the cooling rate of each bar was computed by taking the first derivative of the time vs. temperature curve.

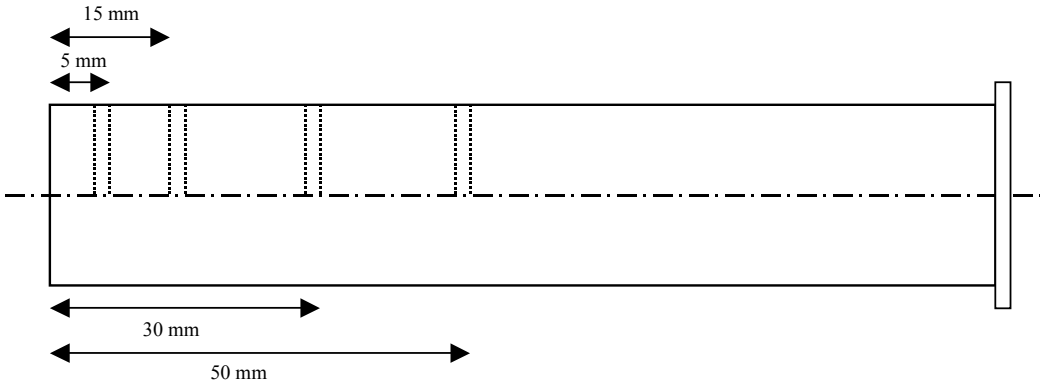

Figure 3: "Modified" Jominy end-quench bar.

6.4 RESULTS AND DISCUSSION

Figure 4 shows that there are more (and larger) pores on the surface of the 90% dense probe than on the surface of the 95% dense probe. Figure 5 shows typical cooling rate curves for the 90% and 95% dense probes. Notice that, in both probes the maximum cooling rate occurs at around 690°C also notice that the film boiling regime and the Leidenfrost point are not present in both curves.

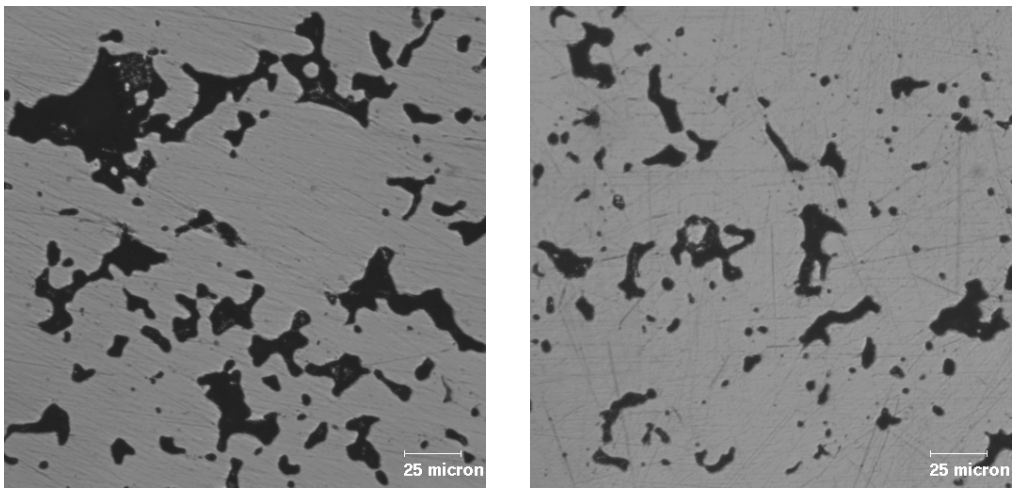

(a) (b)

Figure 4: Surface porosity in (a) 90% dense bars, and (b) 95% dense probes.

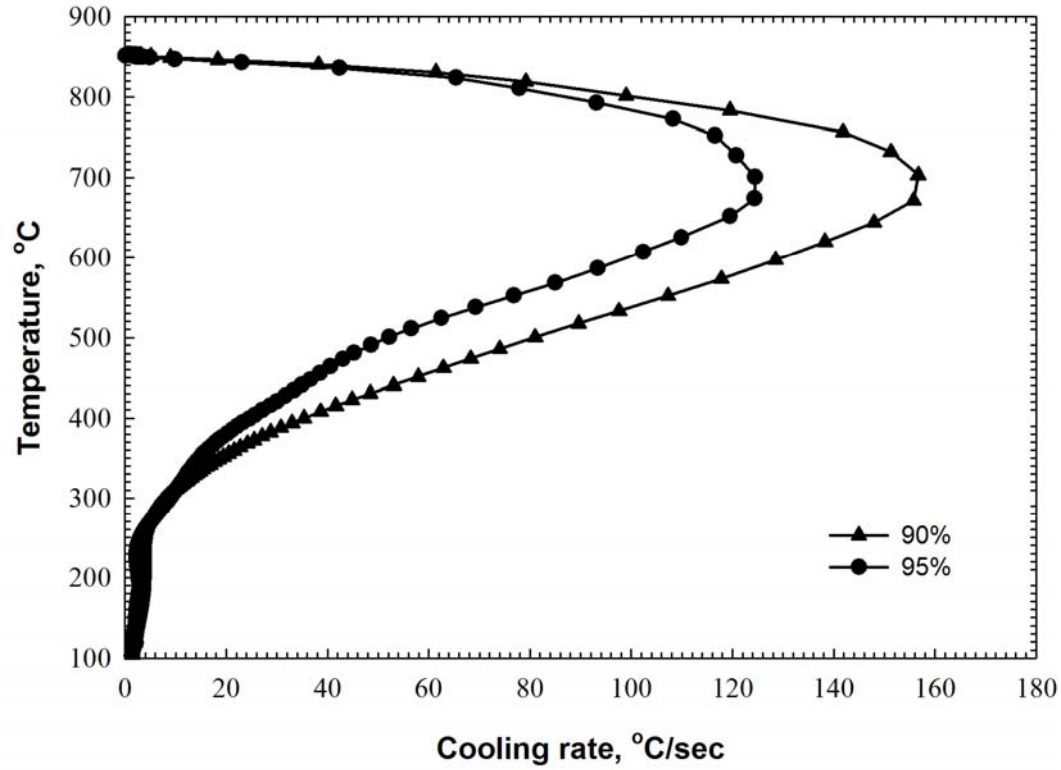

Figure 5: Typical cooling rate curves for 90% and 95% dense FL-4605 PM steel probes during quenching in Houghton G mineral oil.

It is believed that this is caused by the fact that pores on the surface of the probes break the oil vapor blanket and therefore "film boiling" is not prominent in porous PM materials. The presence of more and larger pores on the surface of the 90% dense probe also increases heat extraction from the surface of this probe over that from the surface of the 95% dense probe in the nucleate boiling regime. Since surface pores act as sites for nucleation of gas bubbles during nucleate boiling [12, 13], the 90% dense probe nucleates more bubbles during quenching, and since the bubbles transport the latent heat of the phase change and increase the convective heat transfer from the probe by agitating the oil near the surface of the probe, then the 90% dense probe loses heat to the quenching medium at a faster rate than the 95% dense probe. Moreover, the pores in the 90% dense material are most probably interconnected as shown in Table III. Therefore, during quenching, more oil is absorbed into the 90% dense probe, which helps to increase its rate of heat loss over that from the 95% dense probe. The combined effect of the above-mentioned factors makes the 90% dense probe exhibit a higher average quenching heat transfer coefficient than the 95% dense probe as shown in Figure 6.

Table III: Absorption of oil by FL-4605 PM steel during quenching.

	90% dense	95% dense
Weight before quenching (g)	16.98142	17.26612
Weight after quenching (g)	16.98816	17.26628
Weight gain (g)	0.00674	0.00016
Weight gain (%)	0.04%	0.001%

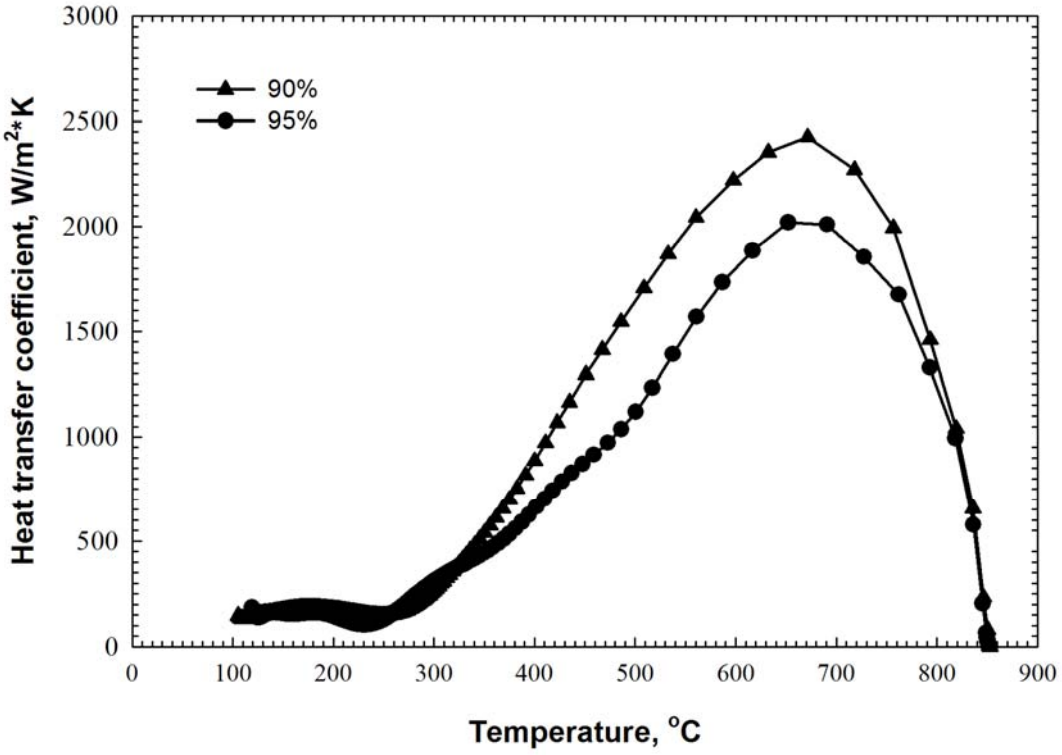

Figure 6: Variation of heat transfer coefficient with temperature for 90% and 95% dense FL-4605 PM steel probes during quenching in Houghton G mineral based oil.

Figure 7(a) shows the temperature vs. cooling rate curve at 5mm from the quenched end of the 90% and 95% dense as-machined Jominy end-quench bars. Similarly, Figure 7(b) shows the temperature vs. cooling rate curve at 5mm from the quenched end of the 90% and 95% dense Jominy end-quench bars with Ni coating on their quenched end. It is clear from Figure 7 that in both cases (as-machined vs. Ni coated bars); the 90% dense bars cool faster than the 95% dense bars. However, the difference in cooling rate between the 90% and the 95% dense bars with Ni-coating is smaller than the difference in cooling rate between their as-machined counterparts. The larger difference in cooling rate between the 90% and 95% dense as-machined bars is attributed to water penetration into the bars during the Jominy end quench test (See Table III). More water penetrates the 90% dense bars than the 95% dense bars. This does not happen with

the Ni-coated bars, and since from the quenched end of the bar up to 5 mm the thermal gradient along the bar is insignificant, and since the net thermal mass of the 90% dense bar is smaller than that of the 95% dense bar (because of porosity), then the 90% dense Ni-coated bar cools faster than the 95% dense bar.

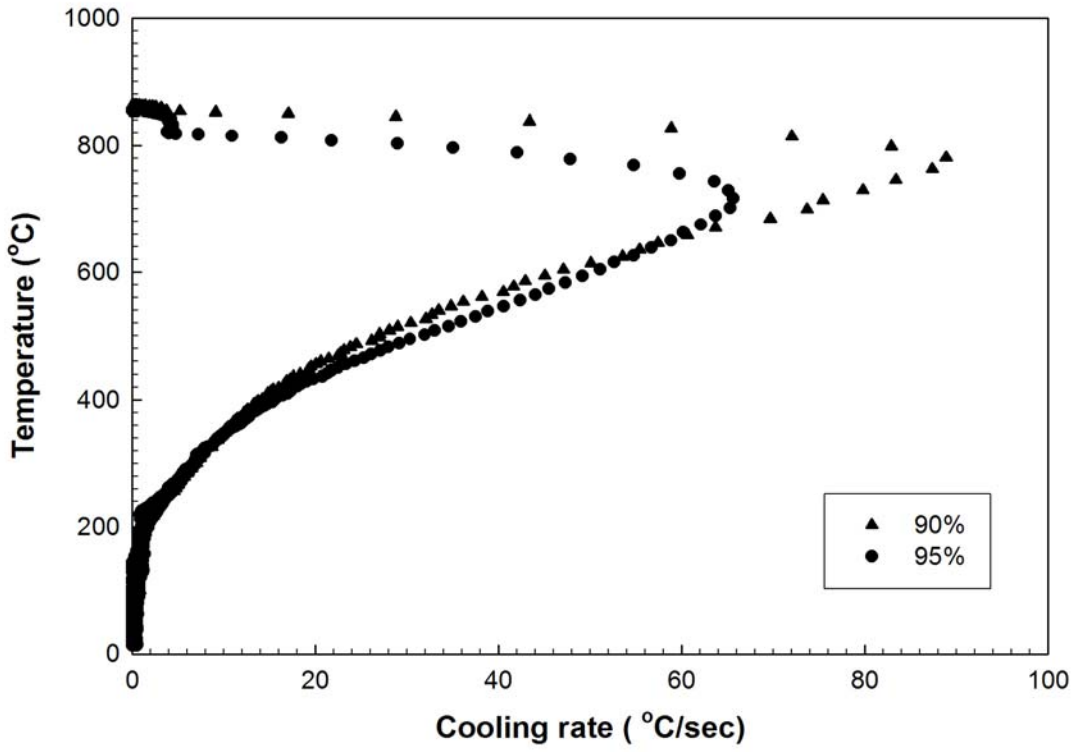

(a)

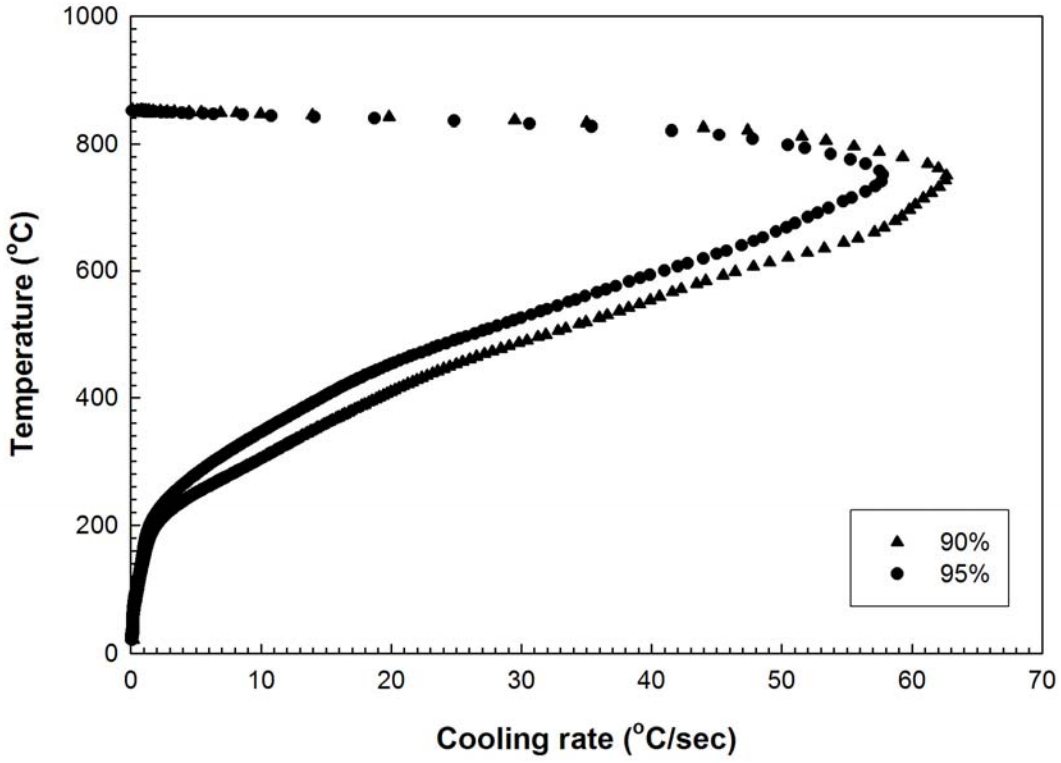

(b)

Figure 7: Temperature vs. cooling rate at 5 mm from the quenched end of (a) as-machined, and (b) Ni-coated Jominy end-quench bars.

However, beyond 5 mm from the quenched end of the bar, the thermal gradient along the bar becomes significant. Therefore, for distances beyond 5mm from the quenched end, one should expect a higher cooling rate in the 95% dense bar because of the higher thermal diffusivity. However, the measurements shown in Figures 8, 9, and 10 indicate that at distances beyond 5 mm from the quenched end, there is no significant difference in the cooling rate between the 90% and the 95% dense bars for both the as-machined bars (Figures 8(a), 9(a), and 10(a)), and the Ni-coated bars (Figures 8(b), 9(b), and 10(b)). This implies that porosity (5% vs. 10%) has an insignificant effect on the thermal diffusivity of the bars. This fact can be ascertained by making use of Eq. (4).

$$\alpha(\rho,T) = \frac{k(\rho,T)}{\rho(\gamma,T)\times C_p(T)} \tag{4}$$

In Eq. (4), α is thermal diffusivity in m^2/sec, k is thermal conductivity in W/m-K, ρ is density in kg/m^3, C_p is specific heat at constant pressure in J/Kg-K, and γ is volume expansion coefficient in m^3/m^3-K. The functional dependence of k, ρ, and C_p are given by Eqs. (5), (6), and (2), respectively [14, 15]

$$k = k_o \frac{1-\varepsilon}{1+\chi\varepsilon^2} \tag{5}$$

$$\rho(T) = \frac{\rho(25^oC)}{(1+\gamma T)} \text{ where } \gamma = \gamma_0\left(\frac{\rho}{\rho_T}\right)^{1/3} \tag{6}$$

So that Eq. (4) becomes

$$\alpha(\rho,T) = \frac{k_o(1-\varepsilon)}{1+\chi\varepsilon^2}\times\frac{1+\gamma_o T\left(\frac{\rho}{\rho_T}\right)}{C_P(T)\rho(25^\circ C)} \tag{7}$$

In Eq. (7), k_o is the thermal conductivity of the fully dense material, ε is the pore fraction, χ is a pore-sensitivity coefficient typically taken to be 11.0, γ_o is the volume coefficient of thermal expansion of the fully dense material, and ρ_T is the theoretical density of the material.

Figure 11 shows the variation of thermal diffusivity with temperature as calculated from Eq. (7) for 90% and 95% dense materials. It is clear from Figure 11 that the difference in thermal diffusivity between the 90% and 95% dense materials is indeed insignificant and therefore both materials should cool with approximately equal cooling rates at locations beyond 5 mm from their quenched end.

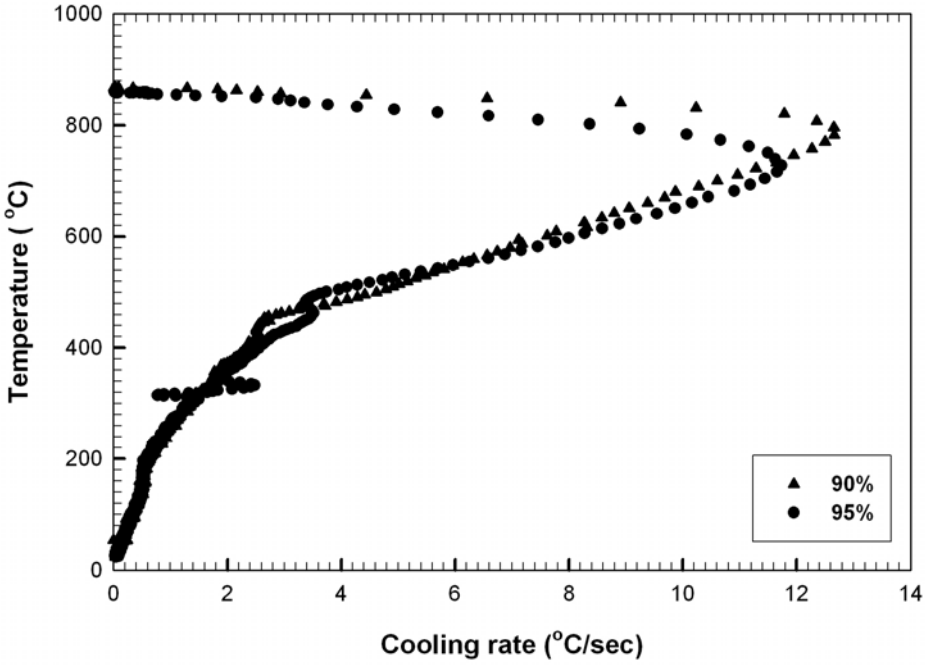

(a)

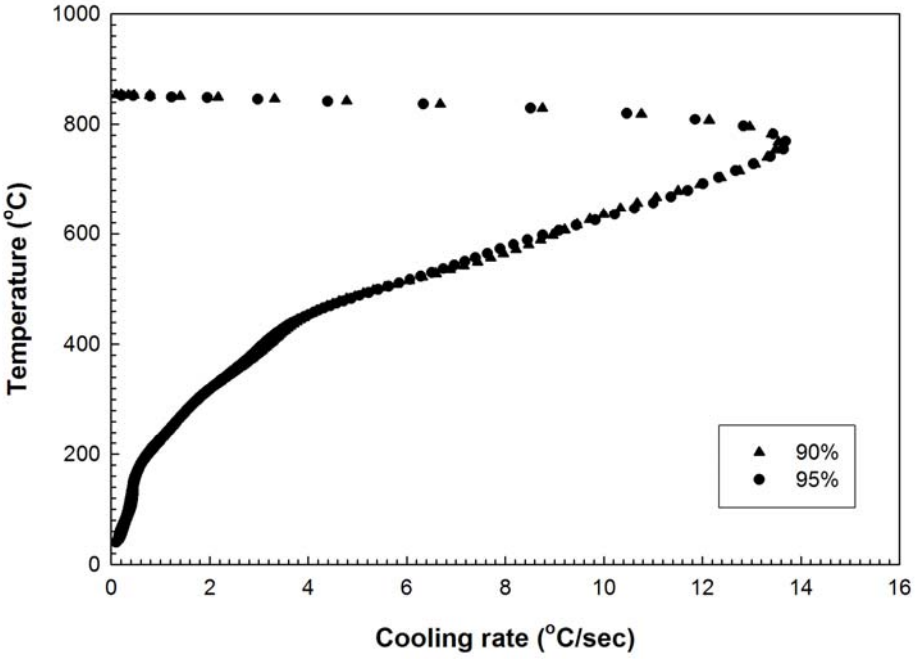

(b)

Figure 8: Temperature vs. cooling rate at 15 mm from the quenched end of (a) as-machined, and (b) Ni-coated Jominy end-quench bars.

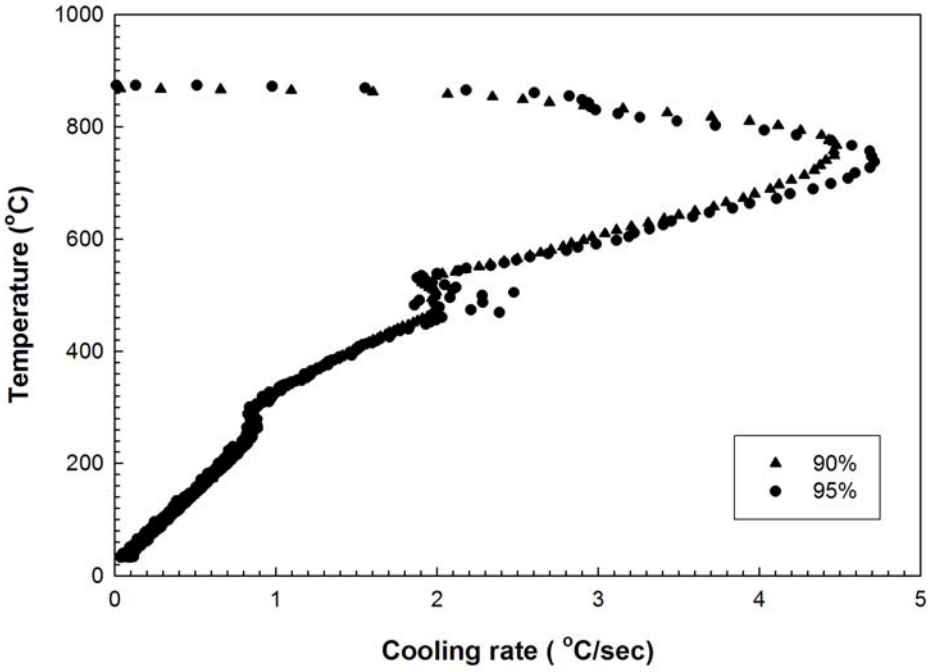

(a)

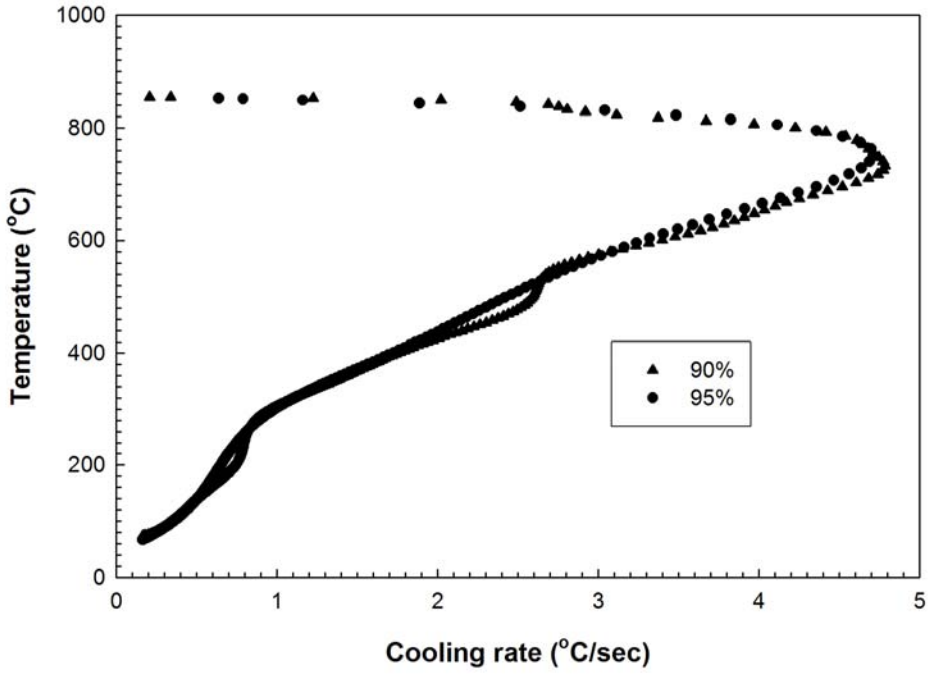

(b)

Figure 9: Temperature vs. cooling rate at 30 mm from the quenched end of (a) as-machined, and (b) Ni-coated Jominy end-quench bars.

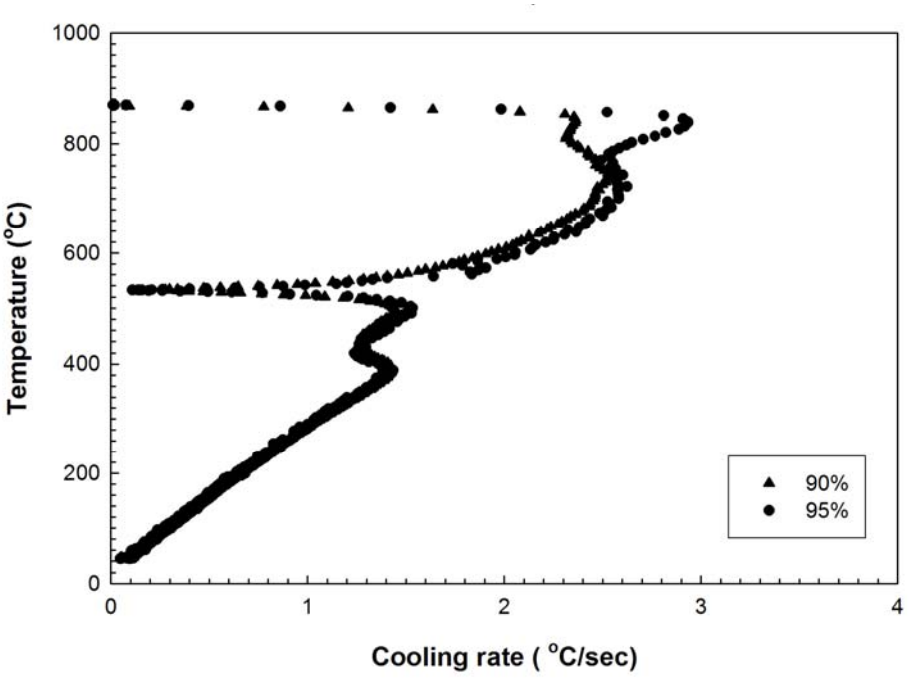

(a)

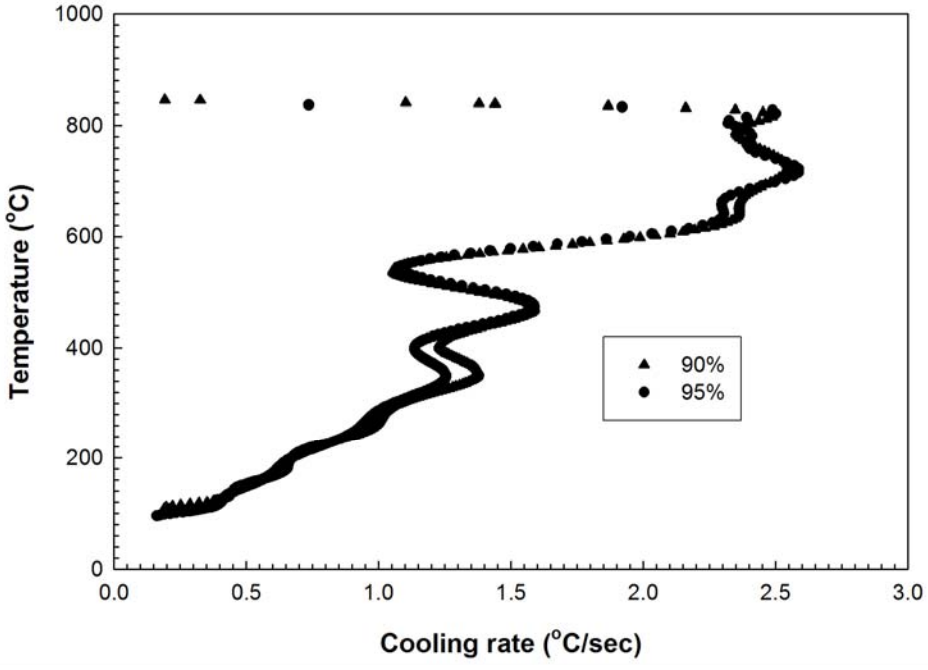

(b)

Figure 10: Temperature vs. cooling rate at 50 mm from the quenched end of (a) as-machined, and (b) Ni-coated Jominy end-quench bars.

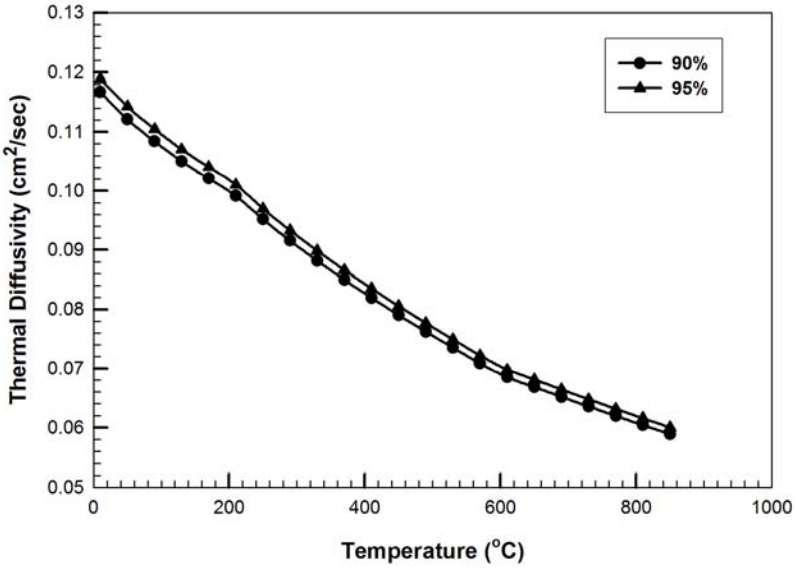

Figure 11: Effect of porosity on the thermal diffusivity of porous PM steel. Calculated from Eq. (7).

6.5 SUMMARY AND CONCLUSIONS

The quenching heat transfer coefficient of porous FL-4605 powder metallurgy steel was measured by quenching in mineral oil special probes that were machined from bulk material processed so as to contain pre-determined amounts of pores. In addition, the role that porosity plays during quenching of powder metallurgy steels was characterized by quenching in mineral oil "modified" quench-end Jominy bars that were machined from the same bulk material used to make the quenching probes.

It was found that

1. Surface pores tend to break the liquid vapor blanket that forms on the surface of the steel probes during nucleate boiling.
2. The 90% dense probes generate more gas bubbles than the 95% dense probes, and since these gas bubbles transport the latent heat of the phase change and increase the convective heat

transfer from the probe by agitating the liquid near the surface of the probe, then the 90% dense probes exhibited a higher quenching heat transfer coefficient than the 95% dense probes.

3. The 90% dense probes have a higher fraction of interconnected pores. These pores allow the quenching oil to be absorbed into the bulk of the probes thus cooling them faster than the 95% dense probes.
4. These factors combine to enhance the overall rate of heat extraction from the 90% dense probes and increase its average quenching heat transfer coefficient over that of the 95% dense probes.

ACKNOWLEDGEMENTS

The authors gratefully acknowledge the support of the member companies of the Particulate Materials Research Center at Worcester Polytechnic Institute.

REFERENCES

1. Warke V.S., Ph.D. Thesis, Worcester Polytechnic Institute, Worcester, MA, May 2008.
2. Maniruzzaman, M., Chaves, J.C., McGee, C., Ma, S. and Sisson, R.D., *Proceedings of the 5th International Conference on Frontiers of Design and Manufacturing (ICFDM 2002)*, Vol. 1, Dalian, China, pp. 619-625, 2002.
3. Chaves, J.C., Maniruzzaman, M. and Sisson, R.D., *Proceedings of the 21st Heat Treating Society Conference*, cdrom version, ASM International, Materials Park, OH, 2002.
4. Ma, S., Maniruzzaman, M. and Sisson, R.D., *Proceedings of the 1st ASM International Surface Engineering Congress and 13th International Federation for Heat Treatment and Surface Engineering (IFHTSE) Congress*, cdrom version, ASM International, Materials Park, OH, 2003.

5. Sisson, R.D.,Jr ,Maniruzzaman, M. D., Ma, S., Warke, V. S., and Makhlouf, M. M., *Proceedings of the 2004 International Conference On Powder Metallurgy & Particulate Materials*, Chicago, IL, June 2004, part-6, pp. 1-11
6. Totten, G.E., Bates, C.E. and Clinton, N.A. *Handbook of Quenchants and Quenching Technology*, ASM International, Materials Park, OH, 1993.
7. Mills, A.F. *Heat Transfer, 2nd ed.*, Prentice Hall Inc., Upper Saddle River, NJ, 1999.
8. Davis, J.R. *Metals Handbook*, ASM International, 1990, pp. 197-199 and 203.
9. Touloukian, Y.S. *Thermophysical Properties of Matter. TPRC Data Series. Vol. 4,* IFI Plenum, NY, 1970, pp 103-109.
10. ASTM Standard A 255, 2007, "Standard Test Methods for Determining Hardenability of Steel", *ASTM International, West Conshohocken, PA*, www.astm.org.
11. SAE Standard J406,1998, "Methods of Determining Hardenability of Steels", *SAE Internation, Warrendale, PA*, www.sae.org
12. Maniruzzaman, M. and Sisson, R.D., *Proceedings of the 21st Heat Treating Society Conference*, cdrom version, ASM International, Materials Park, OH, 2002.
13. Sisson, R.D., Chaves, J.C. and Maniruzzaman, M., *Proceedings of the 21st Heat Treating Society Conference*, cdrom version, ASM International, Materials Park, OH, 2002.
14. German R.M., *Powder Metallurgy of Iron and Steel,* John Willey and Sons, Inc., 1998, pp. 373-404.
15. German R.M., *Powder Metallurgy Science,* Metal Powder Industries Federation, Princeton, NJ, p. 384.

CHAPTER 7

SUMMARY AND SUGGESTED FUTURE WORK

SUMMARY

The work is presented in the form of a series of technical articles that describe the development of a mathematical model for predicting the response of PM steel components to heat treatment, and expand on the current understanding of the effect of porosity on phase transformation in steel during heat treatment. In addition, one article reports on the measurement of convective heat transfer in PM steels. The findings from the research are summarized in following sections.

1. **A Model for Predicting the Response of Powder Metallurgy Steel Components to Heat Treatment**

   - A model for predicting the response of PM steel components to heat treatment was developed.
   - The necessary database was created for FL-4605 PM steel with 90%, 95%, and 100% of theoretical density, and includes the following:
     - Quenching heat transfer coefficients
     - Transformation kinetics parameters
     - Transformation induced strains
     - Phase-specific, temperature dependent mechanical, physical, and thermal properties.
   - The model and database were used to simulate the response of a typical commercial PM component to a commercial heat treatment schedule.
   - The model predictions are in very good agreement with their measured counterparts.

2. The Effect of Porosity on the Austenite to Ferrite Transformation in Powder Metallurgy Steels

- Experimental measurements revealed shorter incubation time with increased porosity in the sample.
- Calculated Avrami exponent n = 1.45 suggested early site saturation during nucleation and diffusion controlled growth.
- Increase in the estimated Avrami constant $b(T)$ with increased porosity suggested an increase in the nucleation and/or growth rate of ferrite.
- Micrographs from interrupted quench samples showed an increase in the number of ferrite particles with increased porosity, hence the nucleation rate was found to be higher in lower porosity samples.
- Quantitative metallography showed an increase in the average equivalent diameter of the ferrite particles with decreased porosity. However, the transformation rate vs. fraction transformed plot showed highest initial transformation rate (growth rate) in lowest porosity sample.

3. The Effect of Porosity on the Austenite to Bainite Transformation in Powder Metallurgy Steels

- Experimental measurements revealed shorter incubation time with increased porosity in the sample.
- Estimated value of Avrami exponent n = 2 suggested a constant nucleation rate and one dimensional growth and found to be in agreement with estimated value from other researchers.

- Increase in the calculated Avrami constant $b(T)$ with increased porosity suggested an increase in the nucleation and/or growth rate of bainite.
- Quantitative metallography on interrupted quench samples show an insignificant change in the length of the largest bainite lath with porosity suggesting that porosity has no effect on the growth rate of bainite.
- Micrographs from interrupted quenched test samples revealed higher number of Bainite lathes in the lower porosity samples, implying increase of the nucleation rate of Bainite with the increase of the porosity in the sample.
- The calculated activation energy for carbon diffusion in the sample with 10% porosity was 23 KJ/mol which is half of the typical activation energy for grain boundary diffusion of carbon (49 KJ/mol)

4. A Model for Converting Dilatometric Strain Measurements to the Fraction of Phase Formed during the Transformation of Austenite to Martensite in Powder Metallurgy Steels

- Experimental measurements revealed that the M_s temperature increases and the overall strain decreases with increased porosity.
- This implies a decrease in the energy barrier for the nucleation of Martensite with increased porosity.
- The observed decrease in overall strain with increased porosity suggests the growth of Martensite into the pores.
- A new model is developed for converting dilatometry measurements to volume fraction Martensite that accounts for the loss of strain into the pores during the transformation.

- Calculations with the new model were compared to the measured amount of retained austenite and were found to be in good agreement.

5. Effect of Porosity on the Quenching Heat Transfer Characteristics of Powder Metallurgy Steels

- Quenching experiments on specially designed probes showed a higher cooling rate in the 90% dense samples compared to the 95% dense samples.
- Both as machined and Ni-coated Jominy bars showed higher cooling rates in the 90% dense samples than the 95% dense samples at 5mm from the quench end. This is attributed to the water penetration and the lower thermal mass of the 90% dense bars up to this location.
- At distances more than 5 mm from the quench end, there was no significant difference between the cooling rate of samples with 90% and 95% density for both as machined and Ni-coated samples.
- Although the thermal conductivity of the 90% dense samples is lower than that of the 95% dense samples, the difference in thermal diffusivities was found to be insignificant. Hence the cooling rates at distances more than 5 mm from the quench end were found to be independent of density.

SUGGESTED FUTURE WORK

The following is a list of research points that may be investigated in subsequent research efforts that build on this work.

- Pressed and Sintered PM components inherently exhibit a significant degree of directionality in mechanical properties caused by directional pressing of the powder

during manufacturing the parts. It will be worthwhile to characterize the effect of this directionality on the kinetics of phase transformation in these components.

- It is well known that the morphology of pores in PM components depends to a large extent on the sintering conditions, and that the morphology of the pores affects the mechanical properties of the components. It will be worthwhile to characterize the effect of pore morphology on the kinetics of phase transformation in these components.

- Only the static value of the component's density was used in the current model. It is suggested that the DANTE subroutines be modified in such a way as to include porosity into the state variable formulation of the subroutines thereby allowing the model to account for porosity gradients in the parts.

Appendix A

Determination of the Phase Transformation Kinetics by Quench Dilatometry

INTRODUCTION

Quench dilatometry is used extensively to study the transformation behavior of steels and the majority of Time Temperature Transformation (TTT) and Continuous Cooling Transformation (CCT) curves in handbooks are generated using quench dilatometry. The practice is based on the principle that during heating and cooling of steels, dimensional changes occur as a result of thermal expansion associated with temperature change and phase transformation. Sensitive high-speed dilatometer equipment is used to detect and measure the changes in dimension that occur as functions of both time and temperature during a defined thermal cycle. This information is then converted to discrete values of strain for specific values of time and temperature during the thermal cycle. Strain as a function of time or temperature (or both) can then be used to determine the beginning and completion of phase transformations. Quench dilatometry is also used to provide the phase transformation data required in numerical models for the prediction of microstructure, properties, and distortion during forging, casting, heat treatment, and welding operations. Additionally, quench dilatometry provides end-users of steel and fabricated steel products the phase transformation data that is required for selecting steel grades for a given application by determining the phase constituents that result from a prescribed thermal cycle.

MATERIALS AND PROCEDURES

This section describes sample preparation and the procedure for performing quench dilatometry measurements on FL-4605 PM steel with varying levels of porosity. Quench dilatometry measurements were performed at Oak Ridge National Laboratory, Oak Ridge, TN on an MMC high-speed quench dilatometer manufactured by Avanel. Inc.

Sample preparation

AUTOMET 4601 steel powder[16] was admixed with powdered graphite to yield 0.5-wt% carbon in the final product. Table I shows the chemical composition of the resultant powder.

Table I: Composition of the alloy (in wt.%).

Carbon	Oxygen	Sulfur	Manganese	Molybdenum	Nickel	Iron
0.5	0.11	0.0093	0.196	0.549	1.812	Remainder

Bulk material was produced from this powder in three different densities corresponding to 90%, 95%, and 100% of theoretical density. In order to produce the 90% dense material, the powder was cold-compacted using 690 MPa pressure in a hydraulic press to produce green compacts that were then sintered at 1120°C for 30 minutes under a controlled atmosphere. In order to produce the 95% dense material, the powder was cold-compacted using 690 MPa pressure, but the green compacts were first pre-sintered at 850°C for 30 minutes and then they were re-pressed using 690 MPa pressure and re-sintered at 1120°C for an additional 30 minutes. The 100% dense material was produced by warm-compacting the powder using 690 MPa pressure, heating the resulting compacts to 1150°C, and then forging them in a press using 760 MPa pressure for 10

[16] Manufactured by Quebec Metal Powder Ltd., Quebec, Canada.

seconds. Table II summarizes the process used to manufacture these blocks along with the dimensions. Samples shown in Figure 2 were machined from these blocks using wire EDM.

Table II: Dimensions and procedure used to produce the bulk material.

Density	Manufacturing Process	Dimensions
90 %	Pressed & Sintered	4.25" × 4.25" × 1"
95 %	Double pressed double sintered	4.25" × 4.25" × 1"
100 %	Pressed, sintered & powder forged	4" D × 2" L

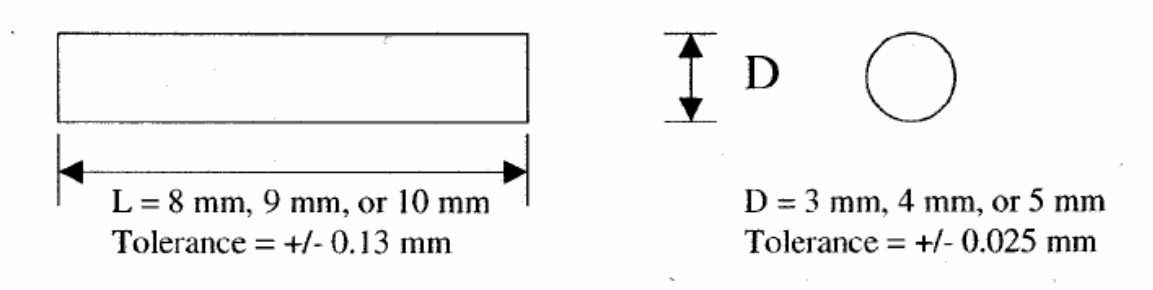

Figure 1: MMC quench dilatometry sample design.[1]

Procedure for Performing Quench Dilatometry

The sample shown in Figure 1 is heated by suspending it inside an induction-heating coil located between two platens as shown schematically in Figure 2. The setup is enclosed in a vacuum chamber and measurements are performed at 1×10^{-5} torr. Cooling is accomplished by a combination of controlled reduction in the heating current and injection of inert gas onto the sample. Dimensional change is measured along the longitudinal axis of the sample, and temperature is measured by means of a thermocouple welded to the surface of the sample midway along its length. Either Type R or Type S thermocouples are used.

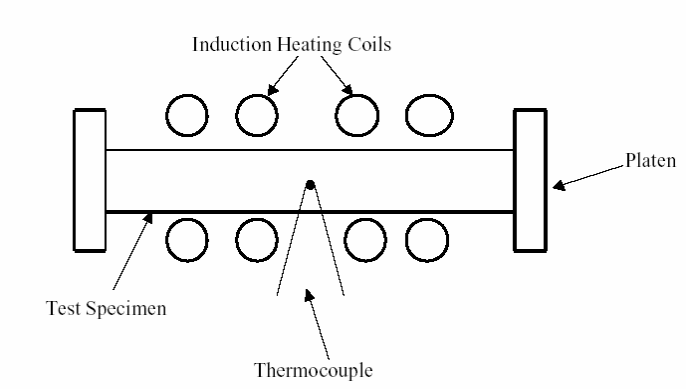

Figure 2: Schematic representation of the MMC high speed quench dilatometer.[1]

Prior to attaching the thermocouple, the sample was degreased using acetone, and in order to achieve proper connection of the thermocouple to the sample, the surface of the sample at the point of thermocouple attachment was lightly sanded using a 600 grit Silicon carbide paper to remove any surface oxide. Significant removal of metal was avoided. The length and diameter of the sample were measured with a micrometer and the diameter was measured at a point away from the sanded region in order to avoid error in measuring the actual sample diameter. These measurements are used to verify dimensional changes that occur during thermal cycling. Sheathed thermocouple wires with a nominal diameter of 0.13 mm were used. The thermocouple wires were individually welded to the specimen surface at the point of attachment and separated from each other by at least two wire diameters. The welding procedure resulted in a secure attachment of each wire while avoiding excessive melting of either wire. The sample was then placed between the holding platens in the dilatometer. For maximum accuracy, the length change measuring device, i.e., the linear variable differential transformer (LVDT), was adjusted so that it did not pass through its natural zero point during thermal cycling. Once the specimen was in place, the insulating sheaths on the thermocouple wires were moved along the thermocouple wires until they contacted the specimen surface. This prevents undesirable heat loss, and

prevents contact between the two thermocouple wires. Once the sample has been subjected to thermal cycling and has been removed from the apparatus, the thermocouple sheaths were moved away from the sample surface and the thermocouple leads were cut. The sample diameter and length were then re-measured.

Transformation Measurements

Sample Conditioning – Each sample was subjected to a conditioning run before testing in order to remove residual stresses and stabilize the position of the test specimen within the apparatus. This treatment consists of heating the sample to 850°C±5°C at a nominal rate of 10°C/s, holding the sample at 850°C for 5 minutes and then cooling it to room temperature at a cooling rate not exceeding 80°C/s. The sample was not removed from the apparatus prior to conducting dimensional measurements. This conditioning cycle is designed such that each sample has the same starting microstructure (Martensite in this case) before characterizing the actual transformation behavior.

Determining the Critical Temperatures – The critical temperatures: Ac_1 and Ac_3, were determined from samples separate from those used for other transformation measurements. The sample was heated to 600±5°C at the nominal rate of 10°C/s. Heating was then continued at a nominal rate of 28°C/hr while strain was continuously measured until the Ac_1 and Ac_3 temperatures were identified.

Generating the Isothermal Transformation Data Sets – Each isothermal transformation thermal cycle consists of heating a sample to an austenitizing temperature of 850°C ± 5°C at a nominal

rate of 10°C/s. The sample was held at this austenitizing temperature for 5 minutes and then quenched to the isothermal hold temperature. A cooling rate of at least 175°C/s was employed. During the quench, the temperature of the sample did not undershoot the isothermal hold temperature by more than 20°C and stabilized at the isothermal hold temperature within 2 seconds. The temperature of the sample was maintained within ±5°C of the isothermal hold temperature during dimension measurement. The sample was held at the isothermal hold temperature and its dimensions continuously measured until transformation was 100% complete[17]. The sample was then quenched to room temperature. Data was sampled and recorded at a rate of at least 5 dimension measurements per second, and a different sample was used for each thermal cycle. Table III shows the experiment matrix for isothermal tests for the temperature range between Ac_3 and M_s. This test matrix will be repeated for samples with the three levels of porosity.

Generating the Continuous Cooling Transformation Data Sets – Each continuous cooling transformation thermal cycle consists of heating a sample to an austenitizing temperature of 850±5°C at a nominal rate of 10°C/s. The sample was held at the austenitizing temperature for 5 minutes and then cooled to room temperature at the cooling rates specified in Tables IV and V. Data was sampled and recorded at the rate of one dimension measurement per degree Celsius. Linear cooling rates were used to the maximum cooling rate possible. For cooling rates where linear control was not possible, the rate at 700°C was reported along with the cooling time between 800°C and 500°C. A different sample was used for each thermal cycle. The tests depicted in Tables IV and V will be repeated for each porosity level.

[17] Complete transformation is defined as the time at which maximum dimensional change has occurred.

Table III: Test Matrix for generating the isothermal transformation data sets.

Phases	Isothermal hold temperature (°C)	Number of tests
Ferrite	700	1
	675	3
Ferrite + Pearlite	650	3
	625	1
	600	3
	575	2
	550	2
Bainite	500	2
	475	2
	450	1
	425	2
	400	2
	375	1
	350	1
	325	1
	300	1

Table IV: Test matrix for Martensitic transformation.

Cooling rate (°C/s)	Number of tests
8	1
16	1
54	2

Table V: Test matrix for generating the continuous cooling transformation datasets.

Cooling rate (°C/s)	Number of tests
0.05	1
0.1	1
0.2	1
0.35	2
0.5	2
1	1
4	1

Determination of the Kinetics Parameters

Kinetics Parameter Fitting

The data generated from the isothermal and continuous cooling measurements is used to fit the kinetics parameters for the Austenite to Ferrite, Austenite to Pearlite, Austenite to Bainite, and Austenite to Martensite transformations. The phase transformation model based on internal state variable approach is discussed in subsequent section. Figure 3 shows the flow chart of the fitting routine developed by Deformation Control Technology, Inc., Cleveland, OH. This routine requires the following:

- Measured strain vs. time data for all isothermal tests. Figure 4 shows measured data for the Bainite transformation at different isothermal holding temperatures.
- Measured strain vs. temperature data for all continuous cooling tests. Figure 5 shows the data acquired during continuous cooling at different cooling rates.
- Measured time vs. temperature data for all continuous cooling tests. Figure 6 shows the cooling curves for all continuous cooling tests conducted.
- Coefficient of thermal expansion for Austenite, Bainite, Pearlite, and Martensite. This can be obtained by fitting data to the linear portion of the strain vs. temperature curve provided that only the phase of interest exists over that linear portion of the curve. Figures 7, 8, 9, and 10 show the fitted linear coefficient of thermal expansion as a function of temperature for Austenite, Bainite, Pearlite, and Martensite, respectively.

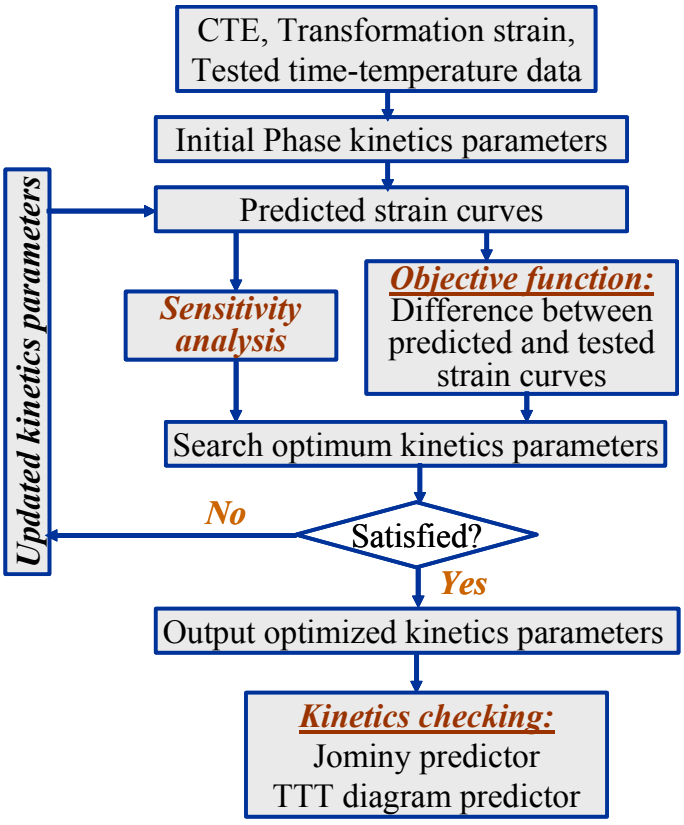

Figure 3: Flow chart of the kinetics parameters fitting routine developed by Deformation Control Technology, Inc.

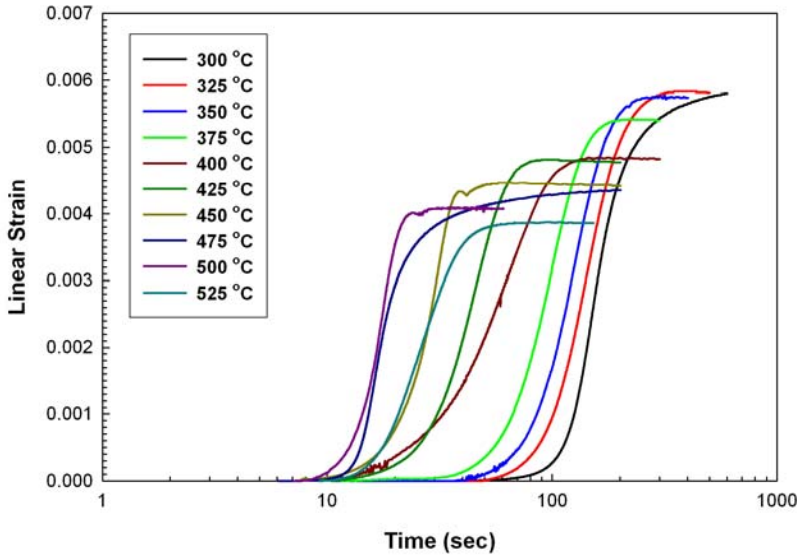

Figure 4: Measured strain vs. time data for Bainite transformation at different isothermal holding temperatures.

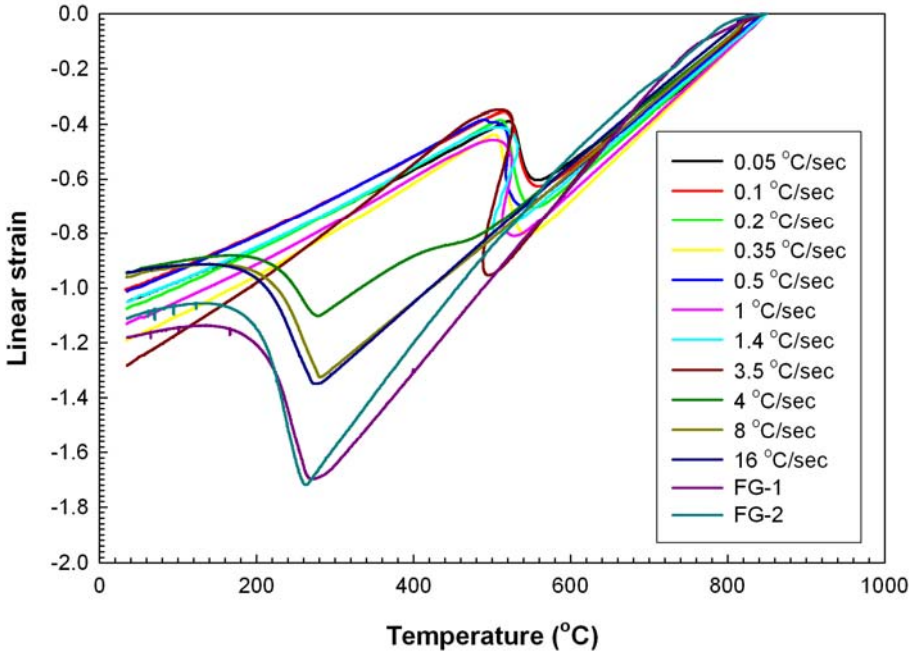

Figure 5: Measured strain vs. temperature data at different cooling rates during continuous cooling transformation tests.

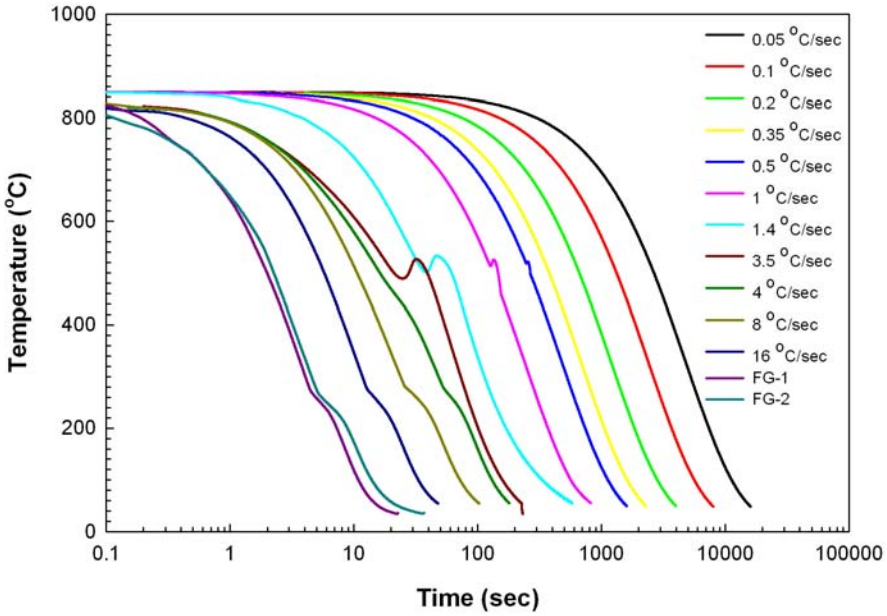

Figure 6: Measured cooling curves during continuous cooling transformation tests.

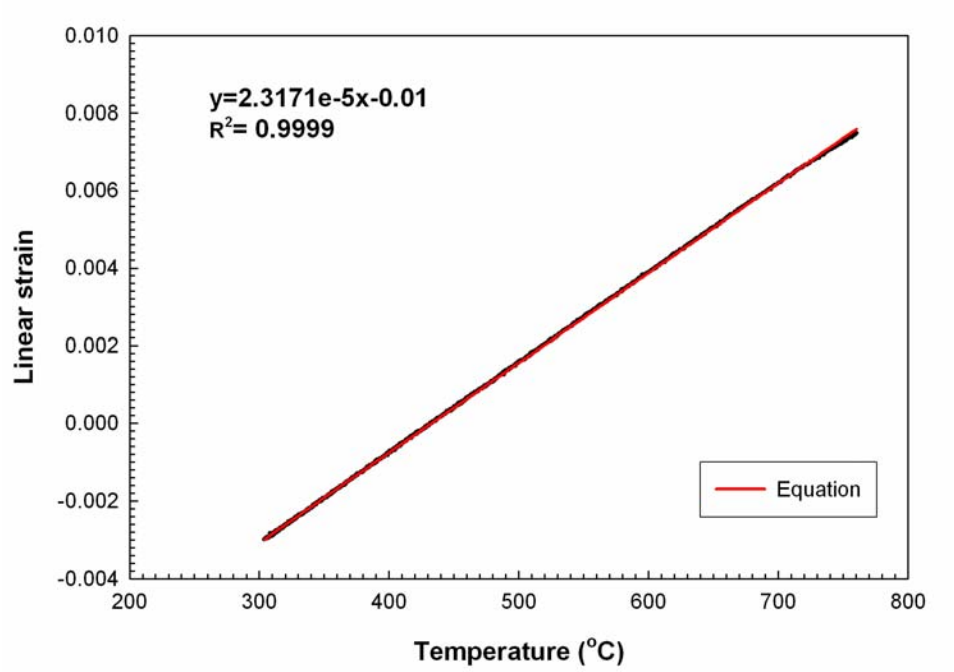

Figure 7: Data fitting to estimate coefficient of thermal expansion as a function of temperature for 100% dense Austenite sample.

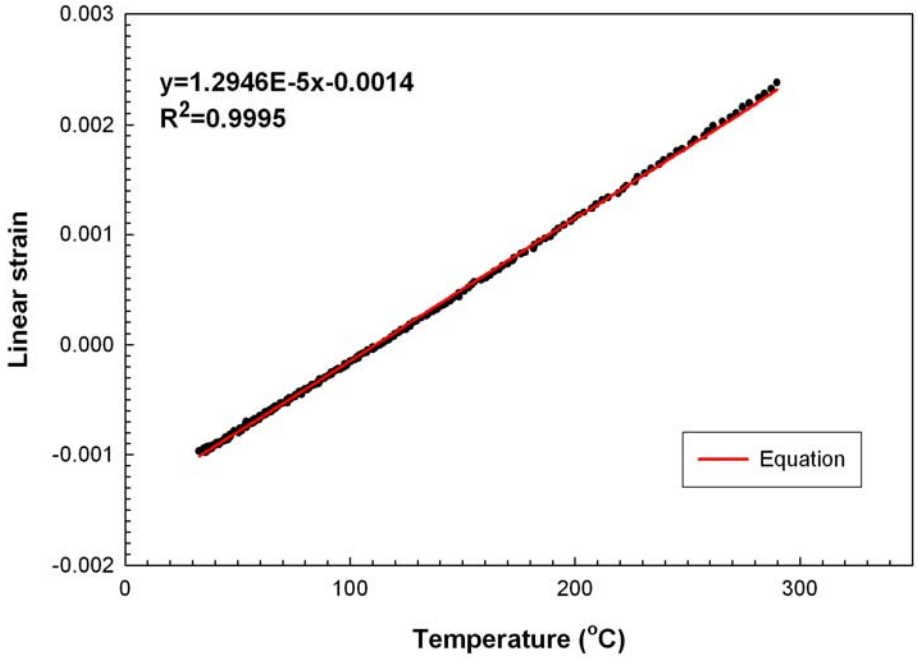

Figure 8: Data fitting to estimate coefficient of thermal expansion as a function of temperature for 100% dense Bainite sample.

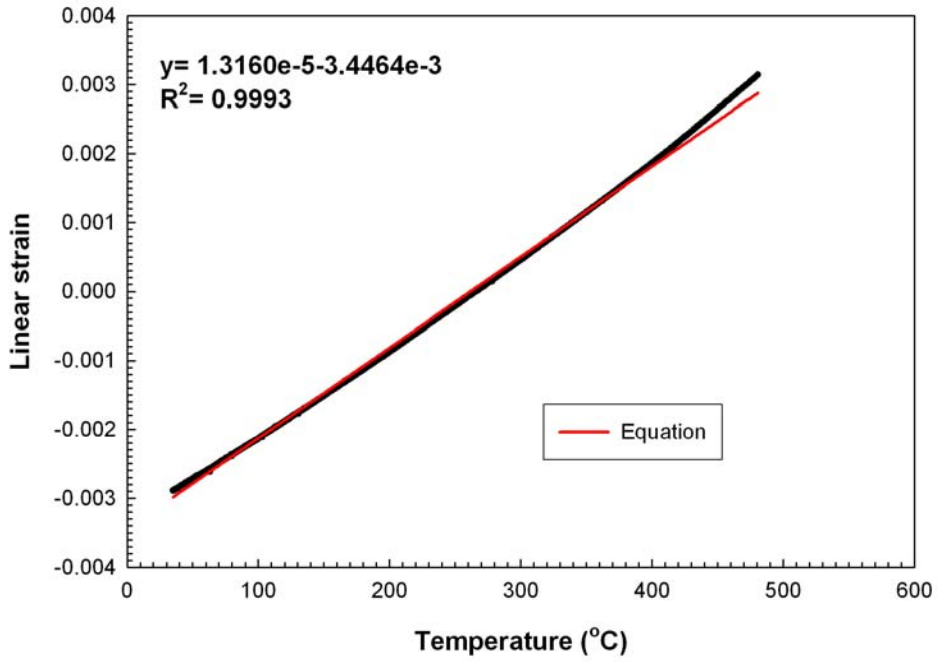

Figure 9: Data fitting to estimate coefficient of thermal expansion as a function of temperature for 100% dense Pearlite sample.

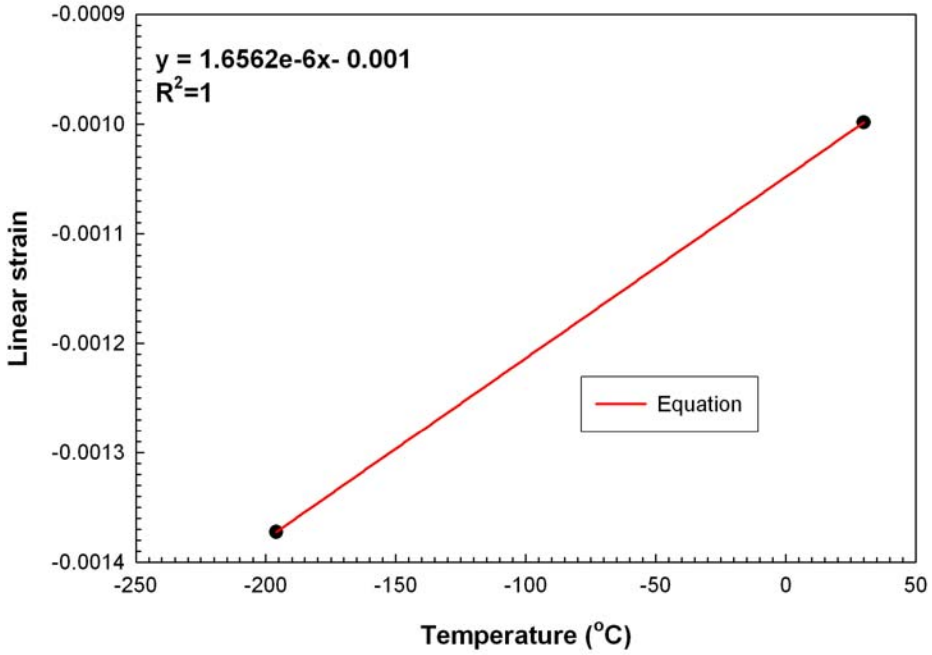

Figure 10: Data fitting to estimate coefficient of thermal expansion as a function of temperature for 100% dense Martensite sample.

Phase Transformation Kinetics Model

Equations 1 though 4 give the transformation kinetics model where the volume fraction of each phase is tracked as a function of time. The volume fraction of a phase is denoted by ϕ, with the subscripts a, f, p, b, and m referring to Austenite, Ferrite, Pearlite, Bainite, and Marteniste, respectively. The terms k_f, k_p, and k_b are temperature dependent mobility functions and are given by Equations 1a through 3a for Ferrite, Pearlite, and Bainite, respectively [2-4]. The first derivative with respect to time is denoted by a dot on the symbol. In Equations 1-3, $\phi_{f,eq}$ is the temperature dependent equilibrium volume fraction of ferrite. The expression $\phi_{En,b} = \gamma_b(\phi_f + \phi_p)$ reflects the influence of existing Ferrite and Pearlite on the rate of formation of Bainite. The influence parameter γ_b is typically set to 0.2, and the initial volume fraction of each phase is usually set to 0.0001.

$$\dot{\phi}_f = k_f 2^{2a_f} \phi_{f,eq}^{1-2a_f} \phi_f^{a_f} <\phi_{f,eq} - \phi_f> \phi_a^{a_f-1} \tag{1}$$

$$\dot{\phi}_p = k_p 2^{2a_p} (1-\phi_{f,eq})^{1-2a_p} \phi_p^{a_p} (1-\phi_p) \phi_a^{a_p-1} \tag{2}$$

$$\dot{\phi}_b = k_b 2^{2a_b} (1-\phi_{f,eq})^{1-2a_b} (\phi_b + \phi_{En,b})^{a_b} \phi_a^{a_b} \tag{3}$$

$$k_f = e^{-\alpha_f} 2^{0.41g} e^{-Q_f/R(T+273)} (A_{e3} - T)^{n_f}, A_{cm} < T \le A_{e3} \;\&\; k_f > k_b \tag{1a}$$

$$k_p = e^{-\alpha_p} 2^{0.32g} e^{-Q_p/R(T+273)} (A_{e1} - T)^{n_p}, B_s < T \le A_{e1} \tag{2a}$$

$$k_b = e^{-\alpha_b} 2^{0.29g} e^{-Q_b/R(T+273)} (B_s - T)^{n_b}, M_s < T \le B_s \tag{3a}$$

In Equations 1a-3a, Q_f, Q_p, and Q_b are the effective thermal activation energies, g is the ASTM grain size of the Austenite, and n_f, n_p, and n_b are the critical exponents that relate the driving force for the transformation to the degree of undercooling. The mobility parameters, α_f, α_p, and α_b, as well as the activation energies and the critical exponents are algebraic functions of alloy

chemistry. The fitting subroutine sets these twelve parameters to some preset value and the stain vs. time and/or stain vs. temperature curves are predicted iteratively. These parameters are optimized until the predicted and measured strain vs. temperature curves match to within a prescribed tolerance value. Once the optimum values for these parameters are calculated, the subroutine writes this data as a kinetics database. Figures 11 and 12 show examples of data fitted to the measured curves for the formation of Pearlite and Bainite, respectively.

Equation 4 represents the kinetics of Martensite formation. Although the Martensitic transformation is athermal, the kinetics equation written in the rate form has explicit dependence on cooling rate.

$$\dot{\phi}_m = \nu_m(\phi_m + \phi_{En,m})^{\alpha_m}(1-\phi_m)^{\beta_m - 1}\phi_a \frac{dT}{dt} U(Min(T_{\min}, M_s) - T) \tag{4}$$

In Equation 4, $U(x) = 0$, $x < 0$ and $U(x) = 1$, $x \geq 0$, T_{min} = Lowest temperature attained, and

$$\begin{aligned} \alpha_m &= \alpha_{m0} + \alpha_{m1} C \\ \beta_m &= \beta_{m0} + \beta_{m1} C \\ \nu_m &= \nu_{m0} + \nu_{m1} C + \nu_{m2} C^2 + \nu_{m3}{}^3 \end{aligned} \tag{4a}$$

In Equation 4, *Ms* is the Martensite start temperature and the expression $\phi_{En,b} = \gamma_b(\phi_f + \phi_p + \phi_b)$ reflects the influence of the existing diffusive phases (Ferrite, Pearlite, and Bainite) on the rate of formation of Martensite. The parameter γ_m is typically set to 0.2. The carbon content of the alloy in weight percent is denoted as *C*. The effect of the carbon content of the alloy on the transformation is reflected in the kinetics equation while the effect of the other alloying elements are assumed to only influences the Martensite start temperature. Figure 13 shows the fitted data for the kinetics parameters of Martensite formation.

Once the optimum values for all the parameters for the diffusive transformations kinetics and the Martensitic transformation kinetics equations are found, the fitting routine generates a database

with all these values and the TTT diagram can be generated using another routine. Figure 14 shows the TTT diagram for the 100% density FL-4605 PM steel.

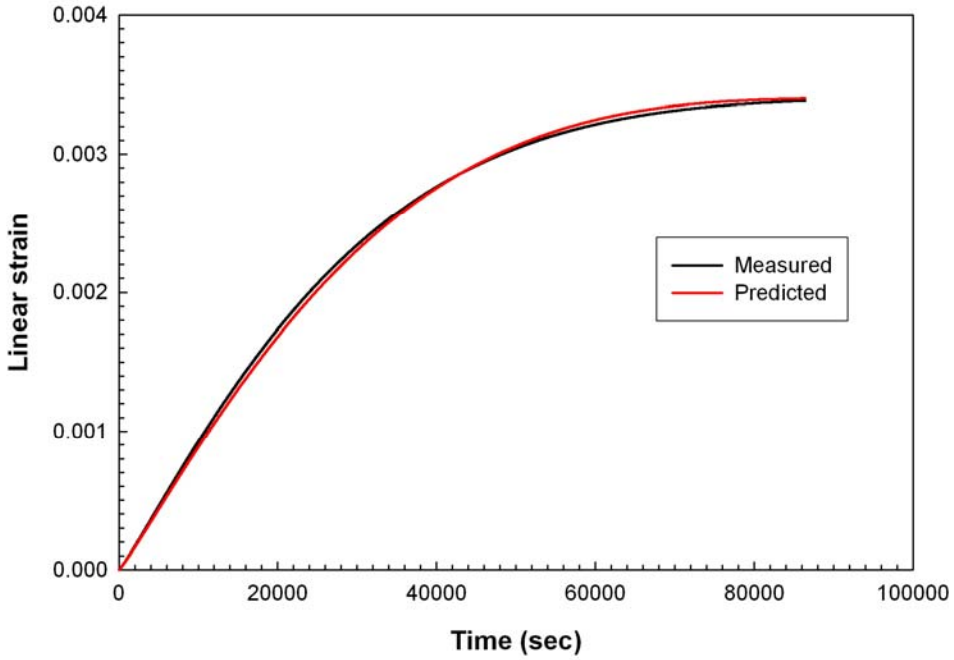

Figure 11: Kinetics parameter fitting for the formation of Pearlite in 100% dense sample at 675°C.

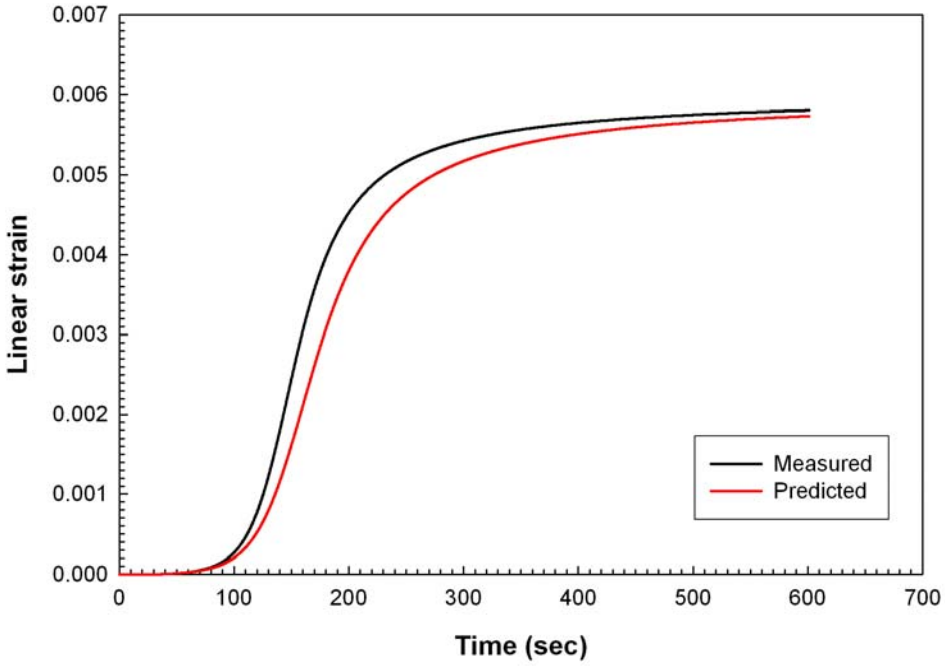

Figure 12: Kinetics parameter fitting for the formation of Bainite in a 100% dense sample at 350°C.

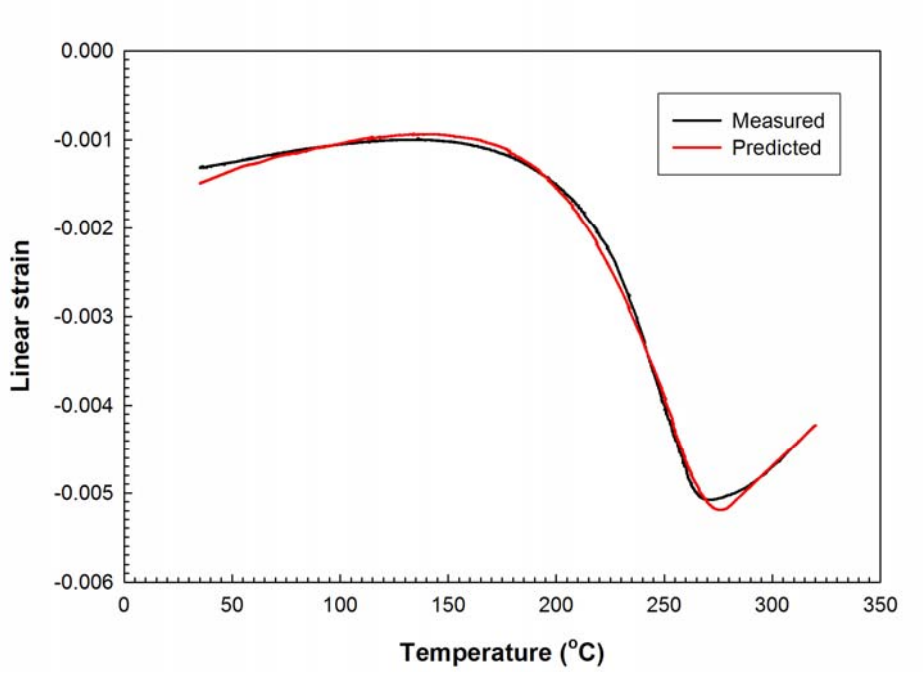

Figure 13: Kinetics parameter fitting for the formation of Martensite during continuous cooling test.

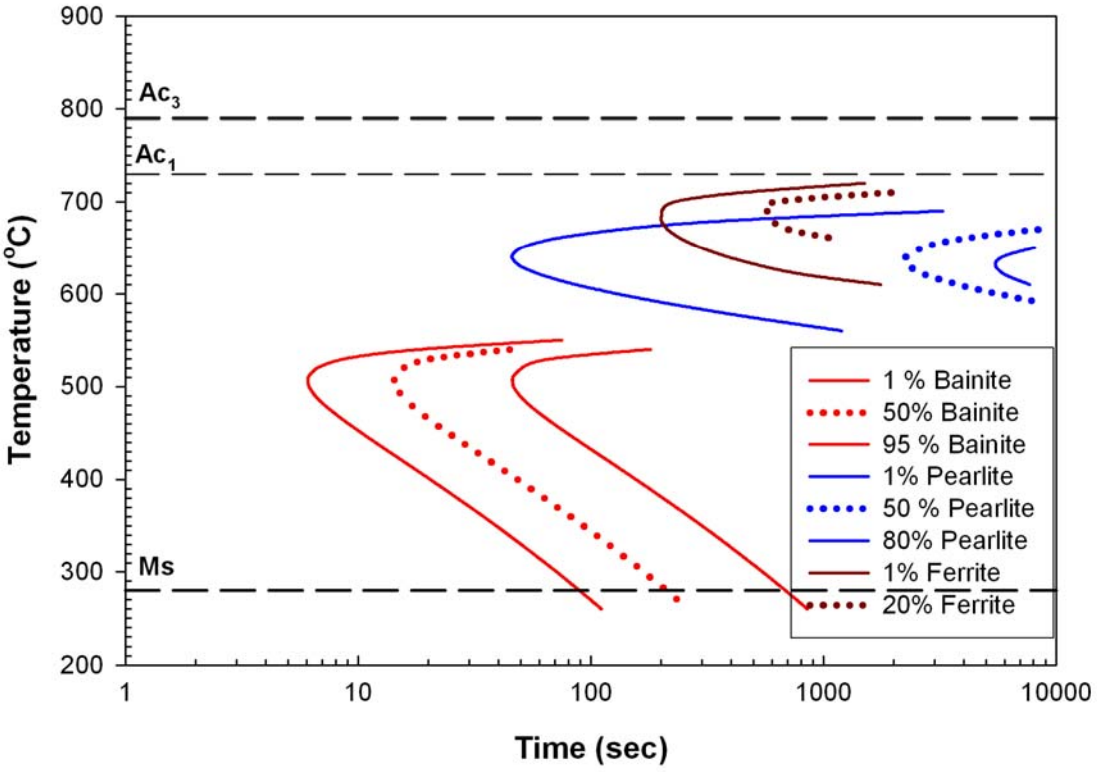

Figure 14: TTT diagram for 100% dense FL-4605 PM steel generated using the fitting routine.

REFERENCES

1. "Recommended Practice for the Quantitative Measurement and Reporting of Hypo- Eutectoid Carbon and Low-Alloy Steel Phase Transformations," *ASTM Standard*, A1033-04.
2. Lusk M.T. , and Lee Y.K., *Proceedings of the Seventh International Seminar on Heat Treatment and Surface Engineering of Light Alloys,* 1999, pp. 273-282.
3. Ferguson B.L., Petrus G.J., and Pattok T., *Proceedings of the Third International Conference on Quenching and Control of Distortion*, 1999, pp. 188-200.
4. Prantil, V.C. et al., *Trans. Of ASME*, vol. 125, April 2003, pp. 116-124.

Appendix B

Determination of the Phase Specific, Temperature and Porosity Dependent Mechanical Properties

INTRODUCTION

The intent of the phase specific, temperature and porosity dependent mechanical property testing is to determine the elastic and plastic behavior of each phase over a range of temperatures and strain rates. This data is primarily used by the mechanics model in DANTE to compute the stresses developed in the part undergoing heat treatment. These stresses are of two types, stress due to change in phase fraction and stresses due to plastic flow arising from thermal shocks. The tables below indicate temperatures and strain rates for each phase to be tested. The phase specific temperature, porosity and strain rate dependent tension and compression tests were performed using Gleeble 3500 thermo-mechanical simulator machine at The Ohio State University.

MATERIALS AND PROCEDURES

This section describes sample preparation and the procedure for performing mechanical testing to generate phase specific, temperature and porosity dependent flow curves for FL-4605 PM steel alloy.

Materials

AUTOMET 4601 steel powder[18] was admixed with powdered graphite to yield 0.5-wt% carbon in the final product. Table I shows the chemical composition of the resultant powder.

Table I: Composition of the alloy (in wt.%).

Carbon	Oxygen	Sulfur	Manganese	Molybdenum	Nickel	Iron
0.5	0.11	0.0093	0.196	0.549	1.812	Remainder

Bulk material was produced from this powder in three different densities corresponding to 90%, 95%, and 100% of theoretical density. In order to produce the 90% dense material, the powder was cold-compacted using 690 MPa pressure in a hydraulic press to produce green compacts that were then sintered at 1120°C for 30 minutes under a controlled atmosphere. In order to produce the 95% dense material, the powder was cold-compacted using 690 MPa pressure, but the green compacts were first pre-sintered at 850°C for 30 minutes and then they were re-pressed using 690 MPa pressure and re-sintered at 1120°C for an additional 30 minutes. The 100% dense material was produced by warm-compacting the powder using 690 MPa pressure, heating the resulting compacts to 1150°C, and then forging them in a press using 760 MPa pressure for 10 seconds. Table II summarizes the process used to manufacture these blocks along with the dimensions. Samples for the mechanical testing are machined from these blocks.

Table II: Dimensions and procedure used to produce the bulk material.

Density	Manufacturing Process	Dimensions
90 %	Pressed & Sintered	4.25” × 4.25” × 1”
95 %	Double pressed double sintered	4.25” × 4.25” × 1”

[18] Manufactured by Quebec Metal Powder Ltd., Quebec, Canada.

100 %	Pressed, sintered & powder forged	4” D × 2” L

Measurement Procedures

Sample Conditioning – Each sample was subjected to a conditioning run before testing in order to remove residual stresses and stabilize the position of the test specimen within the apparatus. This treatment consists of heating the sample to 850°C±5°C at a nominal rate of 10°C/s, holding the sample at 850°C for 5 minutes and then cooling it to room temperature at a cooling rate not exceeding 80°C/s. The sample was not removed from the apparatus prior to conducting dimensional measurements. This conditioning cycle is designed such that each sample has the same starting microstructure (martensite in this case) before characterizing the actual mechanical behavior.

Mechanical Testing – In a Gleeble machine with both heating and cooling capability, the test piece is austenitized at 850°C±5°C and then cooled to the required test temperature. If austenite is being characterized, the test is conducted immediately once the test temperature has been reached. If a diffusive phase is being tested, the test sample is held at temperature until the phase transformation at that temperature has been completed, and then the sample is tested.
For martensite, compression is used because of the brittle nature of the as-quenched martensite. Test pieces for martensite are heated and quenched using a box furnace and a small quench bath. These as-quenched pieces are then compressed at room temperature, or after heating to a low temperature. The test matrix is given in Tables III and IV.

Table III: Matrix for mechanical testing of austenite and martensite.

Relative Density	Austenite (tension)				Martensite (compression)	
	Temp., ºC	0.001/s	0.1/s	1.0/s	Temp. ºC	0.1/s
1.00 (Full Density)	900	*	*	*	290	*
	700		*		240	*
	575	*	*	*	120	*
	350		*	*	RT	*
0.95	900	*	*	*	290	*
	700		*		240	*
	575	*	*	*	120	*
	350		*	*	RT	*
0.90	900	*	*	*	290	*
	700		*		240	*
	575	*	*	*	120	*
	350		*	*	RT	*

Table IV: Matrix for mechanical testing of ferrite/pearlite and bainite

Relative Density	Ferrite/Pearlite (tension)				Bainite (tension)		
	Temp. ºC	0.001/s	0.1/s	1.0/s	Temp. ºC	0.1/s	1.0/s
1.00 (Full Density)	675	*	*	*	500	*	*
	650	*	*	*	450	*	*
	600		*		375	*	*
					300	*	*
0.95	675	*	*	*	500	*	*
	650	*	*	*	450	*	*
	600		*		375	*	*
					300	*	*
0.90	675	*	*	*	500	*	*
	650	*	*	*	450	*	*
	600		*		375	*	*
					300	*	*

Determination of Materials Mechanics Parameters

The Internal State Variable Model – In the formulation of this model, there are internal state variables associated with underlying micro-mechanisms that are assumed to dominate micro-mechanical response during thermal and phase transformation cycle. At the microscopic level, the introduction of these variables results in the prediction of strain rate, temperature, and materials mechanical response. In the ISV model, [1, 2, 3] hypo-elastic relation governs the Cauchy stress in each phase, *i*, in a manner consistent with an assumption of linear elasticity giving Eq. 1

$$\overset{o}{\sigma}^{(i)} = \overset{\bullet}{\sigma}^{(i)} - W_e^{(i)}\sigma^{(i)} + \sigma^{(i)}W_e^{(i)} = 2\mu D_e^{'(i)} \tag{1}$$

Where (^{o}) denotes the co-rotational derivative, $D_e^{'(i)}$ is the elastic symmetric part of the deviatoric velocity gradient, μ is the temperature dependent shear modulus, assumed to be same for all phases, $W_e^{(i)}$ is the skew part of elastic velocity gradient for each phase, and is given by Eq. 2

$$W_e^{(i)} = W - W_p^{(i)} \tag{2}$$

The elastic deformation rate of the material, $D_e^{(i)}$, is given by Eq. 3

$$D_e^{(i)} = D - D_{trip} - D_p^{(i)} - D_{th}^{(i)} - D_{PT}^{(i)} \tag{3}$$

Where, D is the total deformation rate, $D_{th}^{(i)}$,is the thermal deformation rate, $D_{PT}^{(i)}$, is the phase transformation strain rate, $D_p^{(i)}$, is the plastic deformation rate , and D_{trip}, transformation induced plastic strain rate.

The effective stress acting on each phase to cause plastic deformation is then given by Eq. 4

$$\left|\sigma_{eff}^{(i)}\right| = \left|\sigma^{'(i)} - \alpha^{(i)}\right| - \kappa^{(i)} \tag{4}$$

Where, $\alpha^{(i)}$, and $\kappa^{(i)}$, are tensor and scalar internal state variables representing directional and isotropic resistance to plastic flow, respectively. The tensorial internal state variable, $\alpha^{(i)}$, is often referred as back stress or kinematic hardening variable, and it results in the smooth transition from elastic to elastic plastic response in a uni-axial stress-strain curve, and controls materials softening upon unloading, this phenomena is also referred as Bauschinger effect. The scalar internal state variable, $\kappa^{(i)}$, is an isotropic hardening variable that predicts no change in flow stress upon reverse loading. This variable is a scalar measure of dislocation density and responsible for the prediction of continued hardening at large strains. These two variables are given in the form of classical hardening vs. recovery formulation, given by Eq. 5, and Eq. 6 below:

$$\dot{\alpha}^{(i)} = h^{(i)}(T,C)D_p^{(i)} - \{(r_s(T) + r_d(T)\left|D_p^{(i)}\right|)\left\|\alpha^{(i)}\right\|\alpha^{(i)}\} \tag{5}$$

$$\dot{\kappa}^{(i)} = H^{(i)}(T,C)\left\|D_p^{(i)}\right\| - \{(R_s(T) + R_d(T)\left\|D_p^{(i)}\right\|)\kappa^{(i)^2}\} \tag{6}$$

Where, the scalar functions, $r_s(T)$ and $R_s(T)$ describe the diffusion controlled static or thermal recovery, and, the scalar functions, $h_s(T)$, and $H_s(T)$ describe dynamic recovery. $h^{(i)}(T,C)$, and $H^{(i)}(T,C)$ are the isotropic hardening modulus as a function of temperature and carbon content. These hardening and recovery parameters as a function of temperature are given as

$$r_d^{(i)}(T) = C_7 \exp(-C_8 / T) \tag{7}$$

$$h^{(i)}(T) = C_9 - C_{10}T \tag{8}$$

$$r_s^{(i)}(T) = C_{11} \exp(-C_{12} / T) \tag{9}$$

$$R_d^{(i)}(T) = C_{13} \exp(-C_{14} / T) \tag{10}$$

$$H^{(i)}(T) = C_{15} - C_{16}T \tag{11}$$

$$R_s^{(i)}(T) = C_{17}\exp(-C_{18}/T) \tag{12}$$

$$h^{(i)}(C) = C_{22} - C_{23}C \tag{13}$$

$$H^{(i)}(C) = C_{24} - C_{25}C \tag{14}$$

The plastic flow rule describing non-linear dependence of plastic strain on the effective stress is given by Eq. 15 below:

$$D_p^{(i)} = f^{(i)}(T)\frac{\sigma'^{(i)} - \alpha^{(i)}}{\left|\sigma'^{(i)} - \alpha^{(i)}\right|}\sinh\left(\frac{\left|\sigma_{eff}^{(i)}\right| - Y^{(i)}(T)}{V^{(i)}(T)}\right) \tag{15}$$

Where, $Y^{(i)}(T)$, is rate-independent yield stress of the material, $f^{(i)}(T)$, is a function that defines cutoff strain rate below which the material exhibits strain rate independent yielding, and, $V^{(i)}(T)$, is a function that determines magnitude of strain rate dependence on yielding. These three functions can be determined from the isothermal tension/compression mechanical tests and are given by Eq. 16 , Eq. 17, and Eq. 18 below:

$$Y^{(i)}(T) = \frac{C_3}{2}\exp(C_4/T)(1+\tanh(C_{19}(C_{20}-T))) \tag{16}$$

$$f^{(i)}(T) = C_5\exp(-C_6/T) \tag{17}$$

$$V^{(i)}(T) = C_1\exp(-C_2/T) \tag{18}$$

The materials constant $C_1 - C_{27}$ are fitted to the uni-axial tension/compression test data using non-linear regression fitting routine. The detail procedure to fit these parameters is described in the following section.

Mechanics Parameter Fitting – The engineering stress vs. displacement data, shown in Figure 1, generated from the mechanical tests is converted to true stress and true strain. Specialized optimization fitting routine is used to fit 27 ISV model parameters representing plastic behavior

of each phase for a given density at all test temperatures and strain rates. Figure 2 shows the flow chart of the fitting routine developed by Deformation Control Technology, Inc., Cleveland, OH.

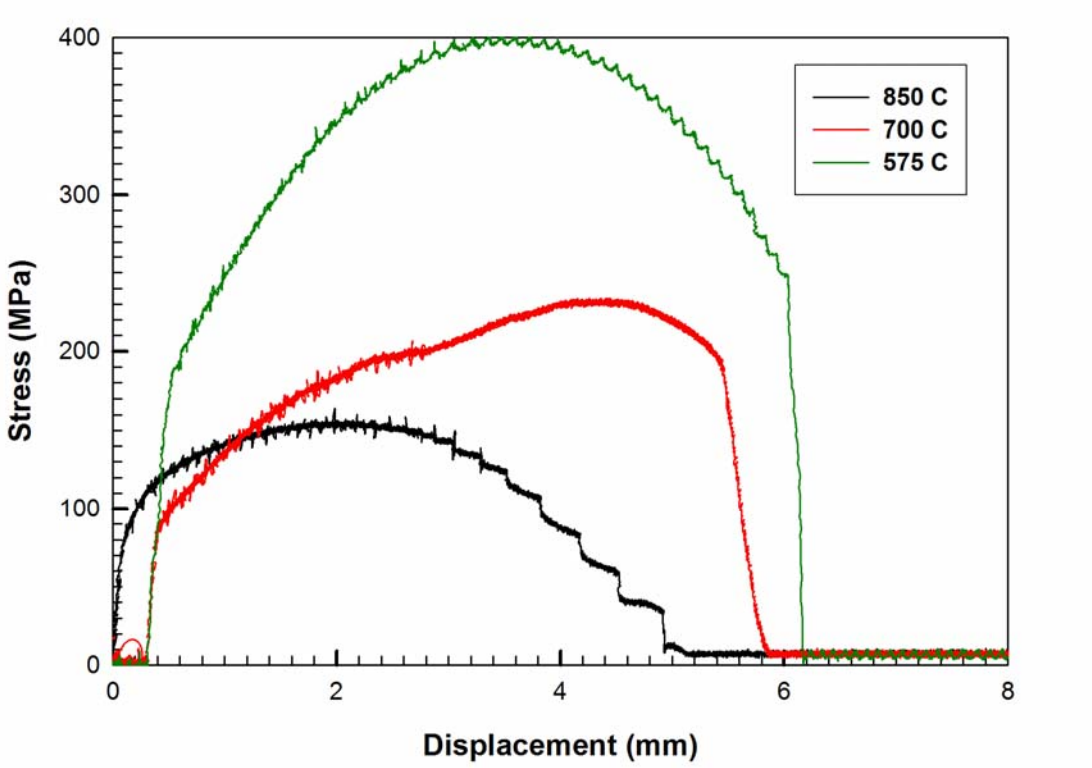

Figure 1: Measured Engineering stress vs. displacement during tension test of Austenite in 100% dense samples at three temperatures.

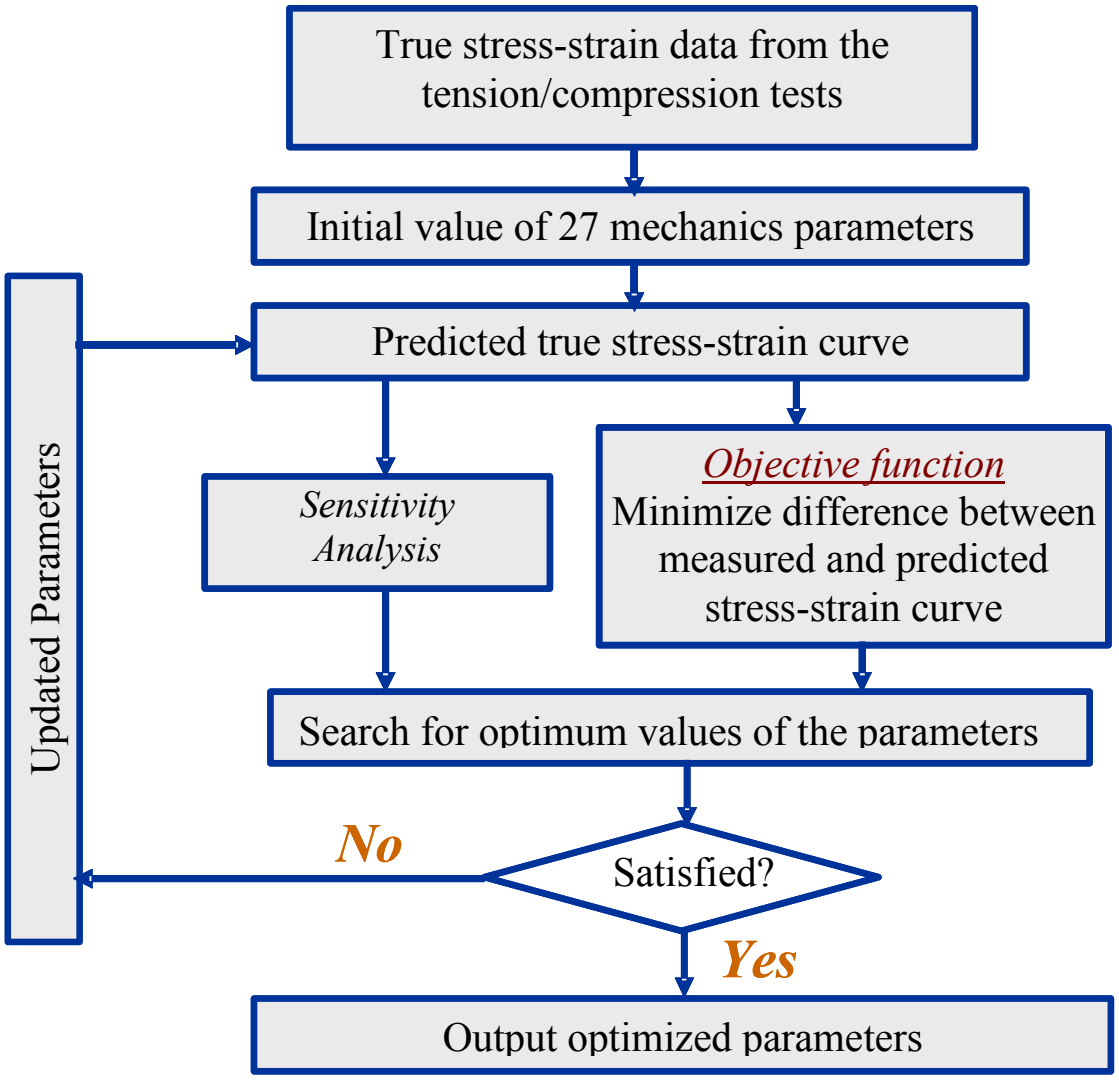

Figure 2: Flow chart of the mechanics parameters fitting routine developed by Deformation Control Technology, Inc.

Figure 3 shows, comparison of measured stress-strain curves with the ones that are generated by fitting routine. The fitting routine writes 27 mechanics parameters into the mechanics database for each phase.

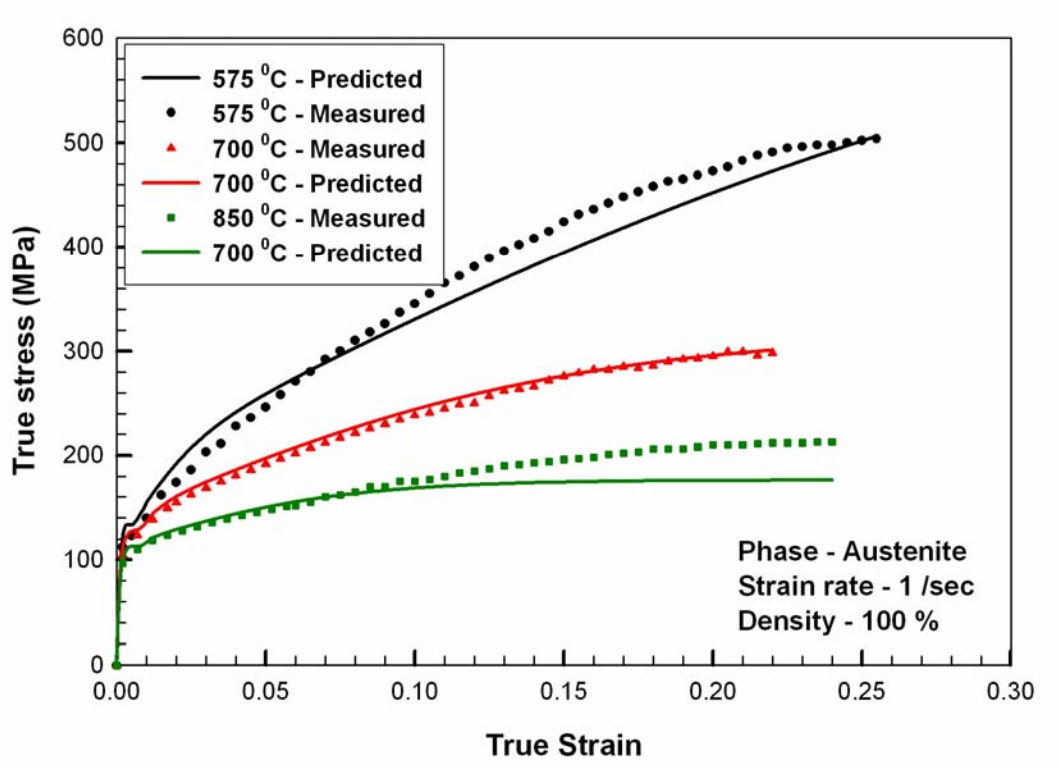

Figure 3: Comparison of measured vs. fitted true stress-strain curve of Austenite at strain rate 1 sec^{-1} for 100% density samples.

REFERENCES

1. Bammann, D.J., Chiesa, M.L., and Johnson, G.C., *Proceedings of 19th International Congress of Theoretical and Applied Mechanics,* Kyoto, Japan, pp. 359-376.
2. Bammann, D.J., and Ortega, A.R., *Welding and Advanced Solidification Processes- VI*, TMS, pp. 543-545.
3. Prantil, V.C. et al. , *Trans. Of ASME*, vol. 125, April 2003, pp. 116-124.

Appendix C

Determination of Transformation-Induced Plasticity in PM Steels by Low Stress Dilatometry

INTRODUCTION

When steel alloys are cooled from the austenitization temperature, a solid state phase transformation occurs, resulting in a product phases that are larger in volume and harder than the parent austenite phase. Hence during the decomposition of parent austenite, due to the higher volume and strength of the product phase produce microscopic plastic flow as the transformation proceed. This phenomenon is known as Transformation Induced Plasticity. The transformation induced plastic strain must be included in modeling the final residual stresses during the thermal cycle of a steel alloy, as omission of this parameter not only can lead to erroneous stress values, but also may generate wrong signs of the residual stresses predicted by the model.. This article describes test matrices and measurement procedure for dilatometry measurements to determine the transformation induced plasticity in FL-4605 PM steel alloy. Low Stress Dilatometry is used to determine the transformation-induced plasticity by applying external compressive static load just before the start of the transformation. In this appendix, the detailed procedure for assessing transformation plasticity caused by the austenite-to-martensite transformation and the austenite-to-bainite transformation is described. These measurements were performed at Oak Ridge National Laboratory, Oak Ridge, TN.

MATERIALS AND PROCEDURES

This section describes sample preparation and the procedure for performing dilatometry measurements on FL-4605 PM steel with varying levels of porosity. Dilatometry measurements under static compressive stress were performed at Oak Ridge National Laboratory, Oak Ridge, TN using a Gleeble 3500 thermo-mechanical simulator machine.

Sample preparation

AUTOMET 4601 steel powder[19] was admixed with powdered graphite to yield 0.5-wt% carbon in the final product. Table I shows the chemical composition of the resultant powder.

Table I: Composition of the alloy (in wt.%).

Carbon	Oxygen	Sulfur	Manganese	Molybdenum	Nickel	Iron
0.5	0.11	0.0093	0.196	0.549	1.812	Remainder

Bulk material was produced from this powder in three different densities corresponding to 90%, 95%, and 100% of theoretical density. In order to produce the 90% dense material, the powder was cold-compacted using 690 MPa pressure in a hydraulic press to produce green compacts that were then sintered at 1120°C for 30 minutes under a controlled atmosphere. In order to produce the 95% dense material, the powder was cold-compacted using 690 Mpa pressure, but the green compacts were first pre-sintered at 850°C for 30 minutes and then they were re-pressed using 690 Mpa pressure and re-sintered at 1120°C for an additional 30 minutes. The 100% dense material was produced by warm-compacting the powder using 690 Mpa pressure, heating the resulting compacts to 1150°C, and then forging them in a press using 760 Mpa pressure for 10

[19] Manufactured by Quebec Metal Powder Ltd., Quebec, Canada.

seconds. Table II summarizes the process used to manufacture these blocks along with the dimensions. Samples shown in Figure 1 were machined from these blocks using wire EDM.

Table II: Dimensions and procedure used to produce the bulk material.

Density	Manufacturing Process	Dimensions
90 %	Pressed & Sintered	4.25" × 4.25" × 1"
95 %	Double pressed double sintered	4.25" × 4.25" × 1"
100 %	Pressed, sintered & powder forged	4" D × 2" L

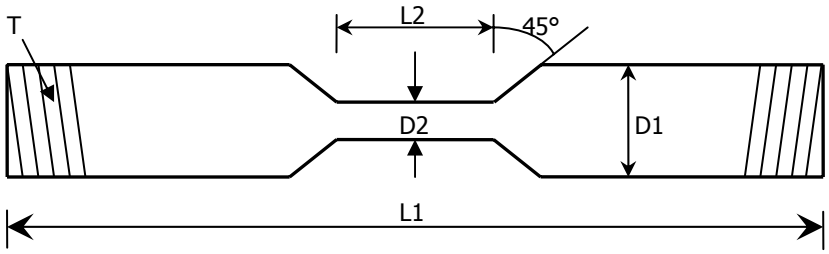

L1 (mm)	L2 (mm)	D1 (mm)	D2 (mm)	T
90	6	10	5	10 mm × 1.5

Figure 1: Schematic of sample used for Transformation induced plasticity measurements.

Measurement of Transformation Induced Plastic Strain (TRIP)

Low Stress Dilatometry is used to characterize the transformation-induced plasticity in the alloy. The procedure entails applying an axial compressive static load to a standard sample (shown in Figure 1) in a dilatometer just before the start of the transformation. While the transformation is in progress under the applied axial load, the change in diameter of the sample is measured. The levels of applied load are chosen such that the magnitude of applied stress is less than the flow stress of austenite at the temperature of application of the load. The transformation induced plastic strain for two different transformations (namely, (1) austenite to Martensite and (2) austenite to bainite) is measuring in a Gleeble 3500 machine, as follows:

Sample Conditioning – Each sample was subjected to a conditioning run before testing in order to remove residual stresses and stabilize the position of the test specimen within the apparatus. This treatment consists of heating the sample to 850°C±5°C at a nominal rate of 10°C/s, holding the sample at 850°C for 5 minutes and then cooling it to room temperature at a cooling rate not exceeding 80°C/s. The sample was not removed from the apparatus prior to conducting dimensional measurements. This conditioning cycle is designed such that each sample has the same starting microstructure (martensite in this case) before characterizing the actual transformation plasticity measurements.

Austenite to Martensite Transformation – For each test listed in Table II, a test specimen is heated to an austenitizing temperature of (Ac3 + 50°C) ±5°C at a nominal rate of 10°C/s. The test specimen is held at the austenitizing temperature for 5 minutes, and then it is cooled to room temperature at a rate of 175°C/s under the applied compressive stress. The axial compressive stress (Table III) is applied on the specimen just before the start of transformation (at about 300°C), and kept constant until the sample cools to room temperature. The change in diameter of the sample is measured, and this data is sampled and recorded at the rate of one dimension measurement per degree Celsius. Tests listed in Table III are repeated at least twice to ensure consistency of the results.

Table III: Stress levels for austenite to martensite transformation.

Test Number	Sample Density	Stress (MPa)*
1	Fully dense	-120
2		-90
3		-60
4	95% of theoretical density	-120
5		-90
6		-60
7	90% of theoretical density	-120
8		-90
9		-60

*A negative sign indicates a compressive stress.

Austenite to Bainite Transformation – For each test listed in Table IV, a test specimen is heated to an austenitizing temperature of (Ac3 + 50°C)±5°C at a nominal rate of 10°C/s. The test specimen is held at the austenitizing temperature for 5 minutes, and then quickly cooled to the isothermal hold temperature (425 °C). A cooling rate of at least 175°C/s shall be employed. During the quench, the temperature of the specimen must not undershoot the isothermal hold temperature by more than 20°C, and must be stabilized at the isothermal hold temperature within 2 seconds. The temperature of the specimen must be maintained within ±5°C of the isothermal hold temperature during dimension measurement. The test specimen is held at the isothermal hold temperature and the axial compressive stress (Table IV) is applied just before the start of the transformation and is kept constant until the test is complete. The specimen is then quenched to room temperature. The change in diameter during the progress of the transformation is measured and this data is sampled and recorded at a rate of at least 5 dimension measurements per second. Tests listed in Table IV are repeated at least twice to ensure consistency of the results.

Table IV: Stress levels for austenite to bainite transformation.

Test Number	Density	Stress (MPa)*
1	Fully dense	-90
2		-60
3		-30
4	95 % dense	-90
5		-60
6		-30
7	90 % dense	-90
8		-60
9		-30

*A negative sign indicates a compressive stress.

Determination of the Transformation Plasticity Parameters

Transformation Plasticity Model – In their research work, Leblond and co-worker [1-4] have outlined an extensive theoretical treatment to evaluate transformation plasticity, where the transformation plastic strain is given by

$$\dot{\varepsilon}_{trip} = \frac{K}{\sigma_y^A}\left(\frac{\Delta V}{V}\right)\Psi(\Phi)\dot{\Phi}\sigma' \tag{1}$$

Where, the transformation plastic strain rate is proportional to the applied stress deviator, σ', the rate of change of volume fraction of the phase during transformation, $\dot{\Phi}$, the volume misfit, $\left(\frac{\Delta V}{V}\right)$, and is inversely proportional to the yield strength of the austenite, σ_y^A.

Based on the theoretical treatment of Leblond et al [1-4], Prantil et al [5] proposed a purely phenomenological model where the trip strain rate is proportional to Weibull probability distribution function for $\Psi(\Phi)$ in Eq. 1. This model (Eq. 2 below) is implemented in the internal state variable formulation presented in previous Appendix.

$$\dot{\varepsilon}_{trip} = \frac{Am}{B}\left(\frac{\Phi}{B}\right)^{m-1}\exp\left(-\left(\frac{\Phi}{B}\right)^{m}\right)\dot{\Phi}\,\sigma' \qquad (2)$$

Where, A, m, and B are material parameters which are fitted from the low stress dilatometry data. The fitting of these parameters will be discussed in following section in detail. Also, In Eq.2, $\Psi(\Phi)$ is chosen such that the total integrated TRIP strain is zero at zero volume fraction of the product phase. Furthermore, this function approached zero when the volume fraction of product phase approaches one.

TRIP Parameters fitting – Figure 1 shows data from low stress dilatometry measurements during austenite to bainite transformation at 425 °C at four levels of applied static uni-axial compressive stress. This data is used as an input to the non-linear regression fitting routine developed, by Deformation Control Technology, Inc., based on model presented in the previous section. This optimization routine fits 4 model parameters into the measured data. Figure 2 shows the comparison of the measured dilatation curves with the ones predicted by the fitting routine.

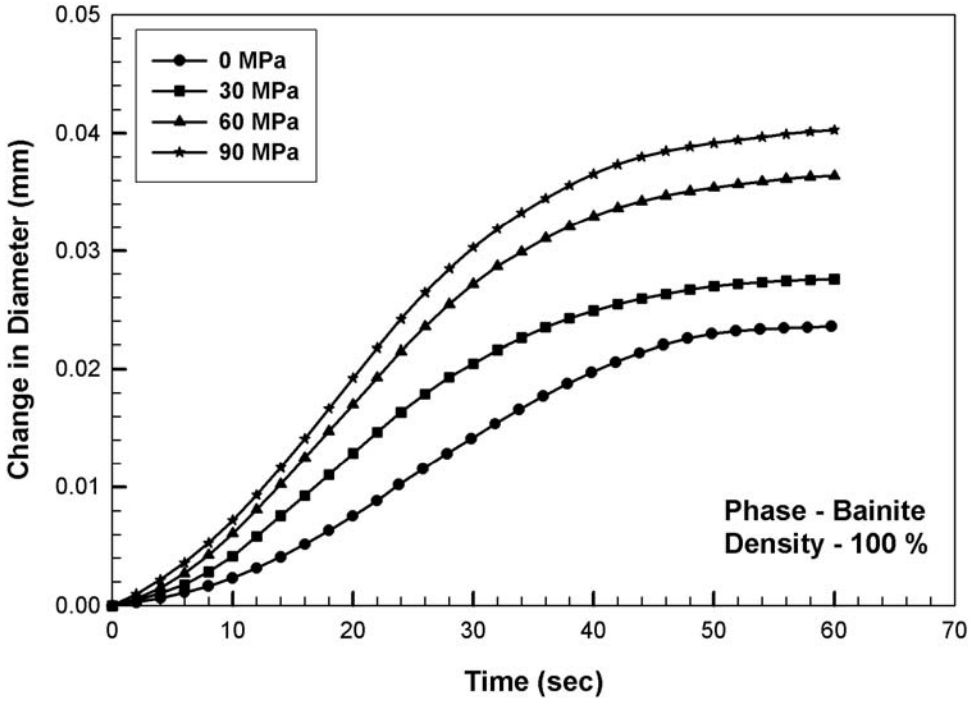

Figure 1: Measured dilatation curves for four levels of applied static uni-axial compressive stress during austenite to bainite transformation at 425 °C.

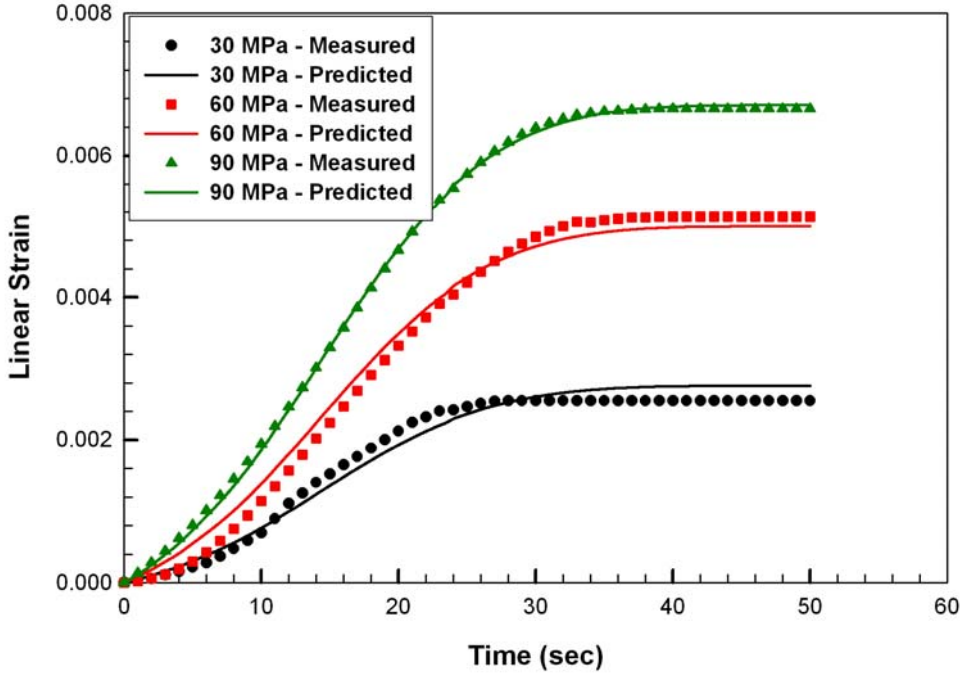

Figure 2: Comparison of measured dilatation with the one predicted by the fitting routine.

REFERENCES

1. Leblond, J.B., Mottet, G., and Devaux, J.C., *J. Mech. Phys. Solids,* vol. 34, No. 4, 1986, pp. 395-409.
2. Leblond, J.B., Mottet, G., and Devaux, J.C., *J. Mech. Phys. Solids,* vol. 34, No. 4, 1986, pp. 411-432.
3. Leblond, J.B., Devaux, J., and Devaux, J.C., *Int. J. of Plasticity,* vol. 5, 1989, pp. 551-572.
4. Leblond, J.B., Devaux, J., and Devaux, J.C., *Int. J. of Plasticity,* vol. 5, 1989, pp. 573-591.
5. Prantil, V.C. et al. , *Trans. Of ASME*, vol. 125, April 2003, pp. 116-124.

Appendix D

Determination of Quenching Heat Transfer Coefficients of Powder Metallurgy Alloys

INTRODUCTION

One of the challenges in modeling the thermal response of materials is the heat transfer coefficient. Even the most sophisticated software uses fundamental laws of heat flow to numerically model the heat transfer process. As a result, the accuracy of the model predictions invariably depends on the accuracy of the boundary conditions, initial conditions and material property data used in the heat flow equations. While the material property data is relatively easy to determine and the initial conditions are usually known, the boundary conditions between the metal part and the quenching medium, i.e., the heat transfer coefficient, are dependant on many factors including the initial conditions, the geometry of the part, the chemistry of the part and the quenching medium, and the surface condition of the part. Moreover, some of these factors may interact with one another. Because of the critical nature of the heat transfer coefficient in computer modeling, an effort is made to provide a system and procedure for accurately determining this parameter. The method involves quenching a heated cylindrical probe machined from the material under consideration and equipped with a thermocouple connected to a fast data acquisition system into the quenching medium and acquiring the temperature-time profile. The probe dimensions are so chosen such that the Biot number for the quenching process is <0.1. [1] This insures that significant thermal gradients will not be present in the radial direction in the probe. Accordingly, a simple heat balance analysis (usually referred to as a

lumped parameter analysis) can be performed on the system (probe + quenching medium) to yield the heat transfer coefficient. Since the Bi < 0.1, the error associated with the calculation of the heat transfer coefficient is less than 5%. [1,2] Conversely, an "inverse" heat transfer analysis may be performed on the temperature-time data whereby the heat equation is solved in reverse numerically (knowing the temperature–time profile and the heat equation, work backwards to obtain the heat transfer coefficient). The inverse heat transfer method can yield more accurate values of the heat transfer coefficient than the lumped parameter analysis method.

EXPERIMENTAL SETUP AND MEASUREMENT PROCEDURE

This section describes sample preparation and the procedure for measuring heat transfer coefficients for FL-4605 PM alloy with varying levels of porosity. These measurements were performed on a CHTE probes (Figure 1) made from FL-4605 PM steel with 90% and 95% theoretical density, using CHTE quench system as shown schematically in Figure 2.

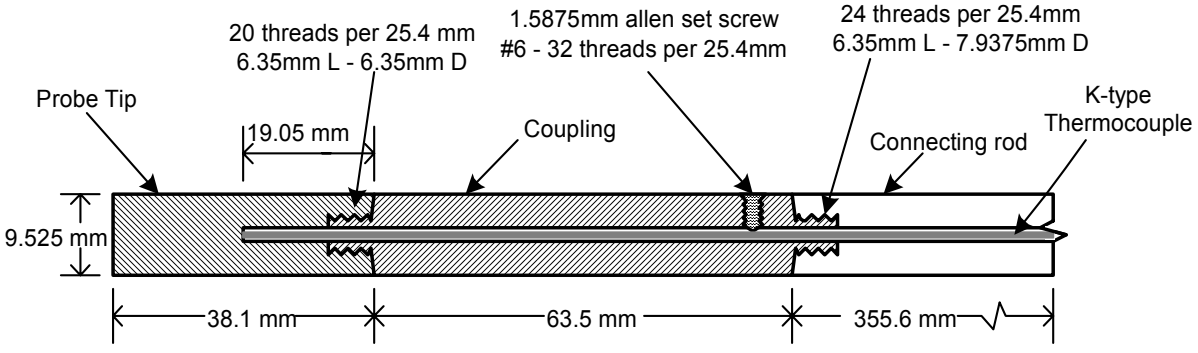

Figure 1: CHTE quench probe-coupling-connecting rod assembly [2]

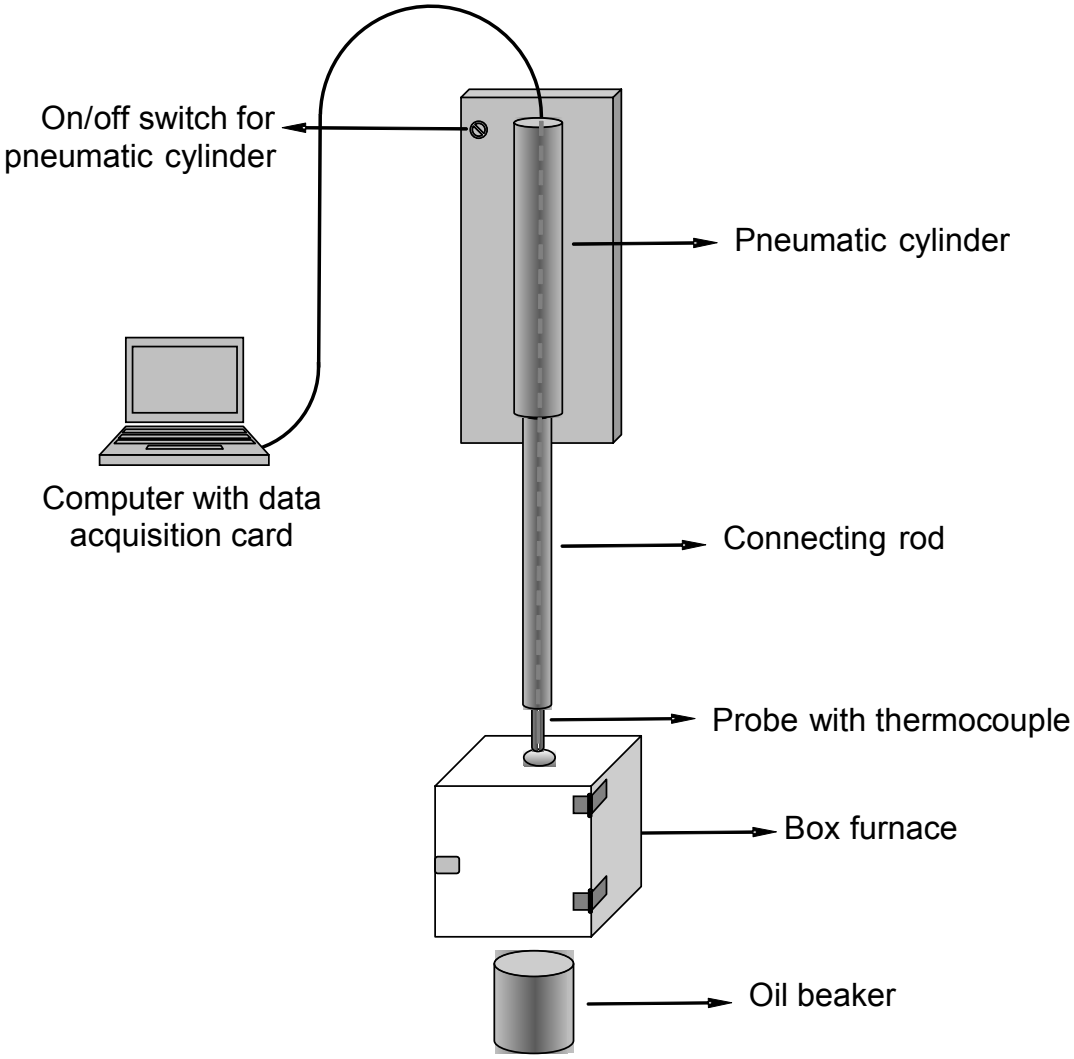

Figure 2: Schematic of CHTE quench system [1, 3].

Sample P reparation

AUTOMET 4601 steel powder manufactured by Quebec Metal Powder Limited, Quebec, Canada was admixed with powdered carbon to yield 0.5 wt% carbon in the final product. Table I shows the chemical composition of the resultant powder.

Table I: Composition of the alloy in wt.%.

Carbon	Oxygen	Sulfur	Manganese	Molybdenum	Nickel
0.5	0.11	0.0093	0.196	0.549	1.812

Samples were produced from the powder with the chemical composition shown in Table I to yield three levels of density, namely 90%, 95% and 100% of theoretical density. Bulk material was produced from this powder in three different densities corresponding to 90%, 95%, and 100% of theoretical density. In order to produce the 90% dense material, the powder was cold-compacted using 690 MPa pressure in a hydraulic press to produce green compacts that were then sintered at 1120°C for 30 minutes under a controlled atmosphere. In order to produce the 95% dense material, the powder was cold-compacted using 690 Mpa pressure, but the green compacts were first pre-sintered at 850°C for 30 minutes and then they were re-pressed using 690 Mpa pressure and re-sintered at 1120°C for an additional 30 minutes. The 100% dense material was produced by warm-compacting the powder using 690 Mpa pressure, heating the resulting compacts to 1150°C, and then forging them in a press using 760 Mpa pressure for 10 seconds. Table II summarizes the process used to manufacture these samples along with the sample dimensions.

Table II: Dimensions and procedure used to produce the bulk material.

Density	Manufacturing Process	Dimensions
90 %	Pressed & Sintered	4.25” × 4.25” × 1”
95 %	Double pressed double sintered	4.25” × 4.25” × 1”
100 %	Pressed, sintered & powder forged	4” D × 2” L

A small cylindrical probe 9.5 mm in diameter and 38mm long is are machined from the steel blocks . A hole is drilled down to the geometrical center of this probe, and a thermocouple is inserted for measuring the time-temperature data.

Measurement procedure

Graphite powder was packed into the hole before the thermocouple was inserted in order to ensure intimate contact between the probe and the thermocouple. The probe was heated to 850° C, and held at that temperature for 20 min after equilibration in order to ensure the completion of transformation. Subsequently, the probe was quenched into Houghton-G oil maintained at room temperature. Figure 2 shows a schematic representation of the CHTE quench system. During the quenching , the time-temperature from the thermocouple in the probe was acquired using a very fast data acquisition system with the scan rate of 1000 scans/sec.

Calculation of the heat transfer coefficients using the lumped parameter analysis

A heat balance applied to the probe results in Equation 1 [3], which can be used directly to calculate the heat transfer coefficient at the surface of the probe.

$$\overline{h} = -\frac{\rho V C_p}{A_s\left(T_s - T_f\right)}\frac{dT}{dt} \tag{1}$$

In Equation (1), $\overline{h}$ is the average quenching heat transfer coefficient at the surface of the probe, ρ, V, C_p, and A_s are the density, volume, specific heat, and surface area of the probe, respectively. T_s is the temperature at the surface of the probe, which, because of the insignificant temperature gradient in the radial direction of the probe, is approximately equal to the measured temperature at the center of the probe, and T_f is the bulk temperature of the quenching medium. Two important parameters are needed by Eq. (1). These are the variation of the specific heat of

the probe (C_p) with temperature, and the variation of the density of the probe with the amount of porosity, which can be calculated from Eq. (2) and Eq. (3), respectively [8, 9]

$$C_p = -3\times10^{-10}T^4 + 8\times10^{-7}T^3 - 8\times10^{-4}T^2 + 0.4991T + 440.25 \quad (2)$$

$$\rho = (1-\varepsilon)\rho_O \quad (3)$$

The cooling rate as function of temperature is determined by taking first derivative of the time temperature data collected from the quenching experiments. Figure 1 shows typical plot of cooling rate vs. temperature from the measured data. Using Eq. 1, heat transfer coefficient at the surface of the probe is estimated. Figure 2 shows, heat transfer coefficient estimated using Eq. 1 for 90% and 95 % dense probes quenched in Hougton-G mineral oil.

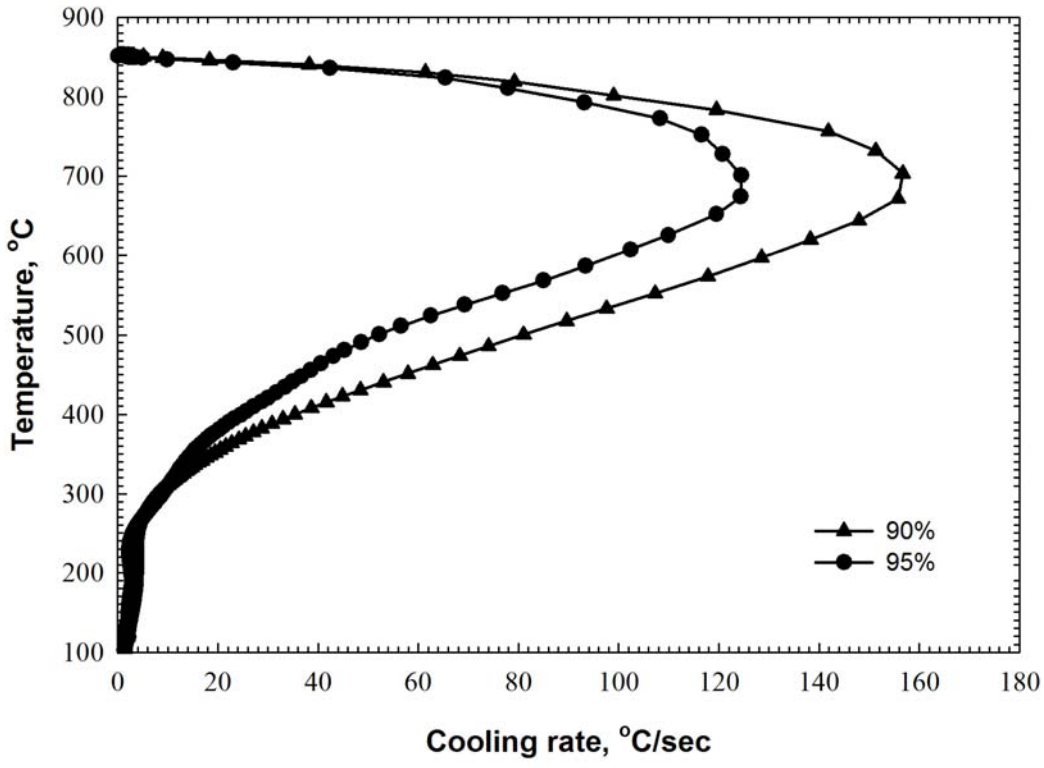

Figure 1: Typical cooling rate curves for 90% and 95% dense FL-4605 PM steel probes during quenching in Houghton G mineral oil.

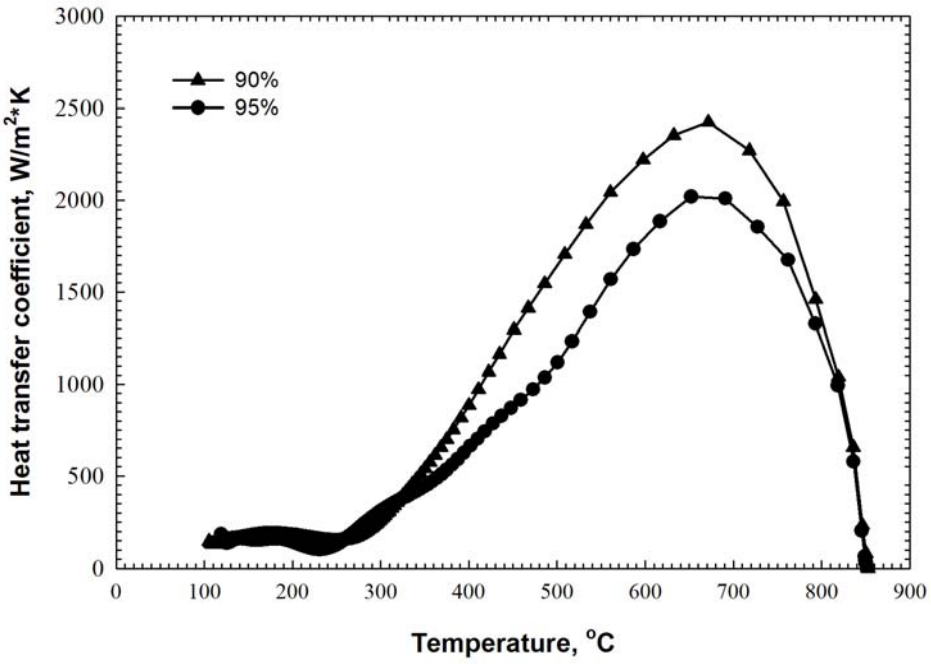

Figure 2: Variation of heat transfer coefficient with temperature for 90% and 95% dense FL-4605 PM steel probes during quenching in Houghton G mineral based oil.

REFERENCES

1. M. Maniruzzaman et al., "CHTE Quench Probe System – a New Quenchant Characterization System", *Proceedings of the 5th International Conference on Frontiers of Design and Manufacturing (ICFDM 2002)*, Dalian, China ,Vol. 1, July 10-12, 2002, , pp. 619-625.
2. Sisson R., Maniruzzaman M., Ma S., Warke V., Makhlouf. M, "Quenching Powder Metallurgy Product", *International Conference on Powder Metallurgy and Particulate Materials*, Chicago, IL , June 2004, part-6,pp.1-11.
3. Ma, S., Maniruzzaman, M. and Sisson, R.D. "Characterization of Mineral Oil Based Quenchants Using CHTE Quench Probe System", *Proceedings of the 1st ASM International Surface Engineering Congress and 13th International Federation for Heat Treatment and Surface Engineering (IFHTSE) Congress*, CDrom version, ASM International, Materials Park, OH, 2003.